ANL/ACTV-95/1

APSTNG:
ASSOCIATED PARTICLE SEALED-TUBE NEUTRON GENERATOR STUDIES FOR ARMS CONTROL

-FINAL REPORT ON NN-20 PROJECT ST220

BY

E. RHODES, C. E. DICKERMAN,
T. BRUNNER*, A. HESS*, AND S. TYLINSKI*

December 1994

Reactor Engineering Division
ARGONNE NATIONAL LABORATORY
9700 South Cass Avenue
Argonne, Illinois 60439

This work was sponsored by the U.S. Department of Energy Office of Nonproliferation and National Security.

---

*Cooperative Student Assistant, Purdue University.

Argonne National Laboratory, with facilities in the states of Illinois and Idaho, is owned by the United States government, and operated by The University of Chicago under the provisions of a contract with the Department of Energy.

DISCLAIMER

ANL/ACTV-95/1

APSTNG:
ASSOCIATED PARTICLE SEALED-TUBE NEUTRON GENERATOR STUDIES FOR ARMS CONTROL

-FINAL REPORT ON NN-20 PROJECT ST220

BY

E. RHODES, C. E. DICKERMAN,
T. BRUNNER*, A. HESS*, AND S. TYLINSKI*

December 1994

Reactor Engineering Division
ARGONNE NATIONAL LABORATORY
9700 South Cass Avenue
Argonne, Illinois 60439

This work was sponsored by the U.S. Department of Energy Office of Nonproliferation and National Security.

*Cooperative Student Assistant, Purdue University.

Table Of Contents

List of Figures

List of Figures (continued)

List of Tables

List of Acronyms and Abbreviations

ADC	Analog-to-digital converter
ALARA	As low as reasonably achievable (radiation-exposure guideline)
ANL	Argonne National Laboratory
APSTNG	Associated particle sealed-tube neutron generator
CFD	Constant-fraction discriminator
CW	Chemical warfare
DOE	Department of Energy
EGRIS	Emissive gamma-ray imaging and spectroscopy
ENIS	Emission-neutron imaging and spectroscopy
ESH	Environmental Safety and Health
FIFO	First in, first out
FNTI	Fast-neutron transmission imaging
GB	A volatile nerve gas
HD	Mustard gas
HE	High explosive
HPGe	High-purity germanium
HV	High voltage
IAEA	International Atomic Energy Agency
INEL	Idaho National Engineering Laboratory
LCD	Liquid-crystal display
LN	Liquid nitrogen
MCA	Multi-channel analyzer
MSDS	Material Safety Data Sheet
NAD	Nuclear accident dosimeter
NDS	Nuclear Diagnostic Systems Corporation
PC	Personal computer
PGRS	Passive gamma-ray spectroscopy (neutron generator off)
PINS	Portable isotopic neutron spectrometer (developed at INEL)
PNAA	Prompt-neutron activation analysis
RE	Reactor Engineering (Division at ANL)
ROI	Region of interest
RWMC	Radioactive Waste Management Center (at INEL)
SNM	Special nuclear materials (i.e., fissile materials)
SWEPP	Stored Waste Examination Pilot Plant (at INEL)
TAC	Time-to-amplitude converter
UGRS	Uncorrelated gamma-ray spectra (neutron generator on)
VX	A persistent nerve gas

APSTNG: Associated Particle Sealed-Tube Neutron Generator Studies for Arms Control

-Final Report on NN-20 Project ST220

E. Rhodes, C. E. Dickerman,
T. Brunner, A. Hess, and S. Tylinski

Abstract

Argonne National Laboratory has performed research and development on the use of Associated Particle Sealed-Tube Neutron Generator (APSTNG) technology for treaty verification and non-proliferation applications, under funding from the DOE Office of Nonproliferation and National Security. Results indicate that this technology has significant potential for nondestructively detecting elemental compositions inside inspected objects or volumes. The final phase of this project was placement of an order for commercial procurement of an advanced sealed tube, with its high-voltage supply and control systems. Procurement specifications reflected lessons learned during the study.

The APSTNG interrogates a volume with a continuous 14-MeV neutron flux. Each neutron is emitted coincident with an "associated" alpha-particle emitted in the opposite direction. Thus detection of an alpha-particle marks the emission of a neutron in a cone opposite to that defined by the alpha detector. Detection of a gamma ray coincident with the alpha indicates that the gamma was emitted from a neutron-induced reaction inside the neutron cone: the gamma spectra can be used to identify fissionable materials and many isotopes having an atomic number larger than that of boron. The differences in gamma-ray and alpha-particle detection times yield a coarse measurement of the distance along the cone axis from the APSTNG emitter to each region containing the identified nuclide. A position-sensitive alpha detector would permit construction of coarse three-dimensional images.

The source and emission-detection systems can be located on the same side of the interrogated volume. The neutrons and gamma rays are highly penetrating. A relatively high signal-to-background ratio allows the use of a relatively small neutron source and conventional electronics. No collimators or personnel radiation shielding are required, and a complete APSTNG inspection system could be transported in an automotive van.

Measurements have been performed to study the system stability, reliability, spatial depth resolution of identified elements along the cone axis, element composition ratios, discrimination between items of different composition, and the characteristic signature of prompt gamma rays from uranium fission. Proof-of-principle experiments and analyses have been conducted related to weapons dismantlement, detection of uranium and plutonium smuggling, radioactive waste characterization, detecting cocaine in propane tanks, and identifying chemical and high-explosive munitions. The table on the next page summarizes proposed APSTNG applications mentioned in this report. They have been grouped into six categories: Monitoring warhead dismantlement, monitoring at checkpoints for smuggled fissionable material, miscellaneous arms-control and nonproliferation, detecting contraband explosives, detecting illicit drugs, and waste remediation. These items illustrate the range of potential use of this technology, but not necessarily its limits.

Summary of APSTNG Applications

As described in the text, APSTNG systems, operated in various modes, have the potential to be useful for the following purposes:

Monitoring warhead dismantlement

Input stream

- Assay the fissionable and fissile material
- Check for undeclared neutron and gamma-ray shielding
- Assay the chemical high explosive inside the incoming weapon
- Check that the configuration inside the weapon is acceptable

Fissionable output stream

- Check for moderator that might be there for concealment
- Assay fissionable material
- Assay fissile material
- Confirm declared changes in geometry

Nonfissionable output stream

- Check for hidden shielding
- Check for fissionable material
- Check for fissile material

Monitoring at checkpoints for smuggled fissionable material

Check for unshielded fissionable material
Check for shielding
Do extended counting of shielded items

Miscellaneous arms-control and nonproliferation

Inspect cruise missiles for undeclared warheads
Production control at SNM-producing facilities
IAEA use in monitoring reactor facilities
Fixed-portal monitoring of SNM at points of entry
Challenge inspections
Detect neutron shielding
Detect CW munitions
Detect HE munitions

Detecting contraband explosives

At airport and embassy portals
In hand-carried luggage
In vehicles
Behind walls; beneath floors; above ceilings

Detecting illicit drugs

Cocaine—concealed, for example, in propane tanks, luggage, or large cargo containers

Waste remediation

Characterizing waste by detecting

- Plutonium and uranium, even when heavily shielded
- Water
- Toxic, nonradioactive chemicals
- Coarse distribution of the above

1.0 INTRODUCTION

Argonne National Laboratory has conducted an R&D program (ST220) to study the potential of the Associated Particle Sealed Tube Generator (APSTNG) technology for arms control treaty verification and non-proliferation applications, under funding from the DOE Office of Nonproliferation and National Security. The project operated an APSTNG system commercially procured from the Advanced Systems Division of Nuclear Diagnostic Systems (NDS). This project was an outgrowth of an ANL Arms Control Advanced Concepts project, in which joint proof-of-concept studies were performed with NDS, using an NDS APSTNG system. Key results of this phase were reported in Reference 1, which is included as Appendix A to this final report. This final report summarizes the status of the project as of October 1994, after the initial APSTNG sealed tube had been replaced, field measurements at the Radioactive Waste Management Center (RWMC) at Idaho National Engineering Laboratory (INEL) had been conducted and analyzed, and after placement of an order with MF Physics for procurement of an advanced sealed tube unit with its high voltage (HV) and control systems. The procurement specifications incorporated lessons learned during the course of the project.

The nuclear physics of the Associated Particle technique was developed with laboratory research apparatus unsuitable for field use in arms control applications; and, further, was subject to operational concerns and constraints due to the use of tritium in conventional accelerator technology. The next-generation metal-ceramic sealed tube APSTNG technology[2] developed by C. W. Peters (head of the Advanced Systems Division of NDS at the time of ANL procurement of the system), appears to have significant potential for arms control applications, as a means of nondestructively detecting the elemental composition inside inspected objects or volumes.

The APSTNG interrogates inspection objects with a continuous low-intensity flux of 14-MeV neutrons generated by the deuterium-tritium reaction. Gamma rays emitted from resulting neutron reactions inside the object are detected; their spectra can identify fissionable materials (from the fission gamma rays) and many elements (nuclides) from inelastic scattering. Chemical substances can be identified by comparing relative spectral line intensities with ratios of elements in reference compounds (although molecular bonds are not identified). Potentially detectable items include nuclear weapons, special nuclear materials (SNM), explosives, narcotic drugs, and toxic chemicals.

Each neutron is coincident with an alpha particle emitted in the opposite direction with respect to the neutron in the center-of-mass coordinate system. An alpha particle detector is incorporated in the APSTNG. Detection of a gamma ray in time-coincidence with the alpha indicates that the gamma ray was generated in the cone defined by the solid angle opposite to that of the alpha detector. By exploiting the difference between the velocities of 14-MeV neutrons and gamma rays (5 cm/nsec and 30 cm/nsec, respectively), the APSTNG system can determine the approximate distance of the gamma ray source from the neutron source. If the alpha detector is position-sensitive, thus defining a manifold of pixel cones, the APSTNG data can be analyzed to provide coarse 3-D images. Because the present ANL APSTNG has an alpha detector that is not position-sensitive, no ANL 3-D data are available.

The existing ANL APSTNG system is sufficiently compact that it could be van-mounted without significant miniaturization. No studies have been performed on component durability

under van-transportation conditions in the field, however. Measurements have been performed to study the system stability, reliability, spatial resolution of identified elements along the cone axis, measurement of element composition ratios, discrimination between items of different composition, and the characteristic signature of prompt gamma rays from uranium fission.

The APSTNG principles of operation are described in Section 2.0. Section 3.0 describes the ANL APSTNG system. Section 4.0 summarizes representative data obtained to characterize APSTNG capabilities. A discussion of the results and potential applications and suggestions for near-term future work is given in Section 5.0.

2.0 PRINCIPLES OF APSTNG OPERATION

2.1 Fundamental EGRIS Detection Mode

The basic operation of the APSTNG neutron probe in its fundamental detection mode is presented in Fig. 1, which provides a simplified sketch of a generic system. This mode is designated as the emissive gamma-ray imaging and spectroscopy (EGRIS) mode. The object to be interrogated is placed in the inspection position and irradiated with neutrons from the APSTNG tube. Neutrons are emitted approximately isotropically in the laboratory coordinate system. Each neutron is associated with an alpha-particle emitted at the same time, travelling in the direction opposite to that of the neutron in the center-of-mass coordinate system (~ 4° offset in the laboratory system). The gamma-ray detectors are time-gated by pulses from the alpha detector, thus detection of a gamma-ray indicates that it was emitted from a location in the neutron cone directed opposite to that defined by the alpha detector. In the flight-time electronics, detector pulses are time-resolved by a constant-fraction discriminator (CFD), and flight times are determined by a time-to-amplitude converter (TAC), digitized by an analog-to-digital converter (ADC), and recorded on a personal computer (PC).

When a gamma ray from a prompt reaction in the neutron cone is detected, the time delay between the alpha pulse and the gamma pulse yields the spot on the cone axis where the reaction occurred, because the geometry and the velocities of the neutron and gamma ray are known (5 cm/nsec and 30 cm/nsec, respectively). If the APSTNG has a two-dimensional position-sensitive multi-pixel alpha detector, each individual alpha pulse defines the reaction position with respect to coordinates transverse to the cone axis. Thus, a coarse 3-D image of reaction densities can be generated from measurements taken at a single orientation. (The ANL APSTNG has a single-pixel alpha detector, but 3-D data can be approximately simulated by placing a optical mask in front of the alpha scintillation detector to restrict the volume of the time-resolved neutron cone and mechanically scanning the alpha detector or inspected object horizontally and vertically.)

Fig. 2 is a schematic view of the cross-section of the sealed neutron tube. Shown is a single-pixel alpha detector, such as used in the ANL system, having the alpha window coated with a scintillator on the inside, with photons detected by a photomultiplier. In the case of a 2-D position-sensitive alpha detector, the photomultiplier might be replaced by a lens or fiber-optic interface to a microchannel plate having a fast delay-line readout and an analog position computer that would give the x and y alpha transverse position values, as indicated in Fig. 1.

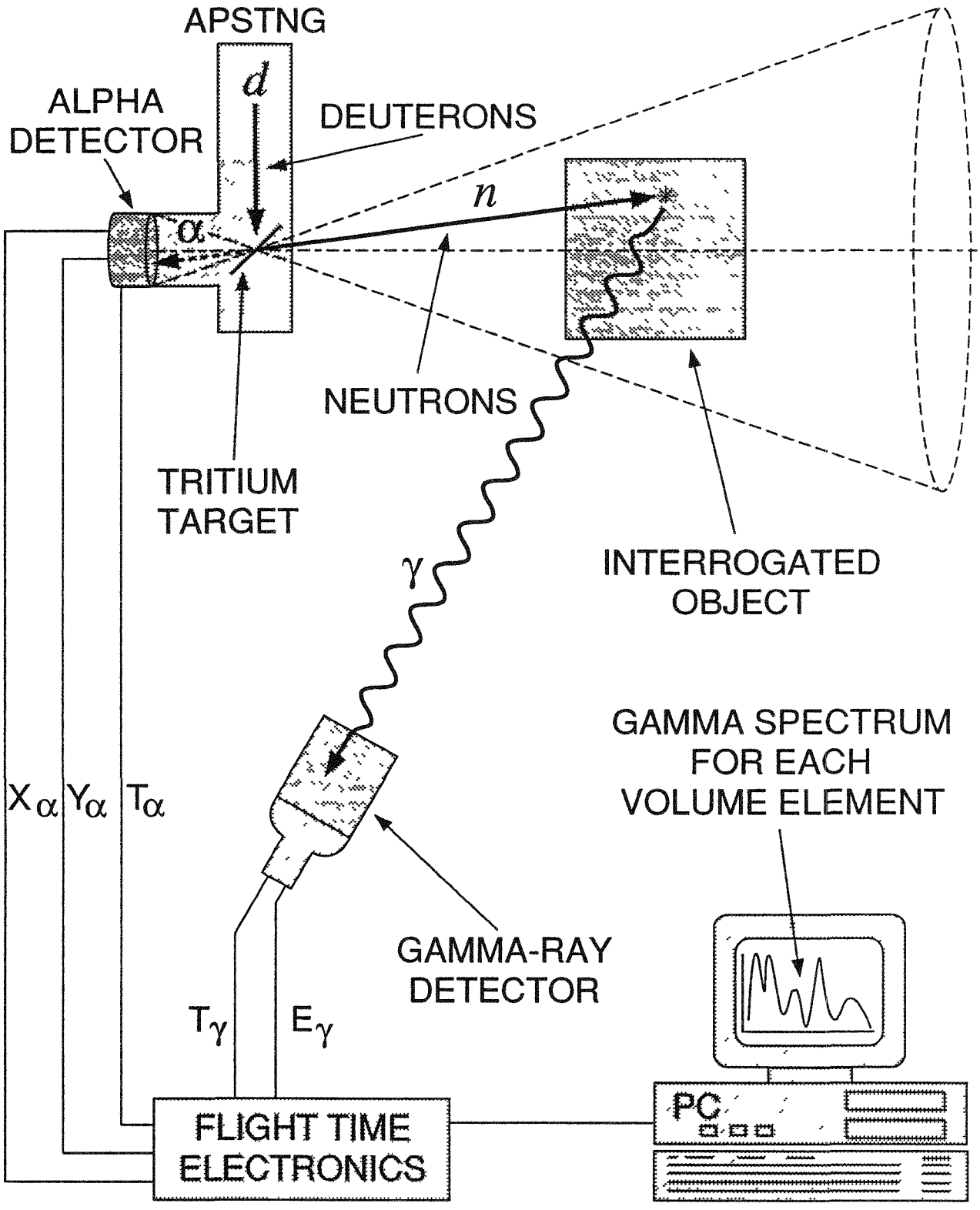

Figure 1. APSTNG Principle of Operation.

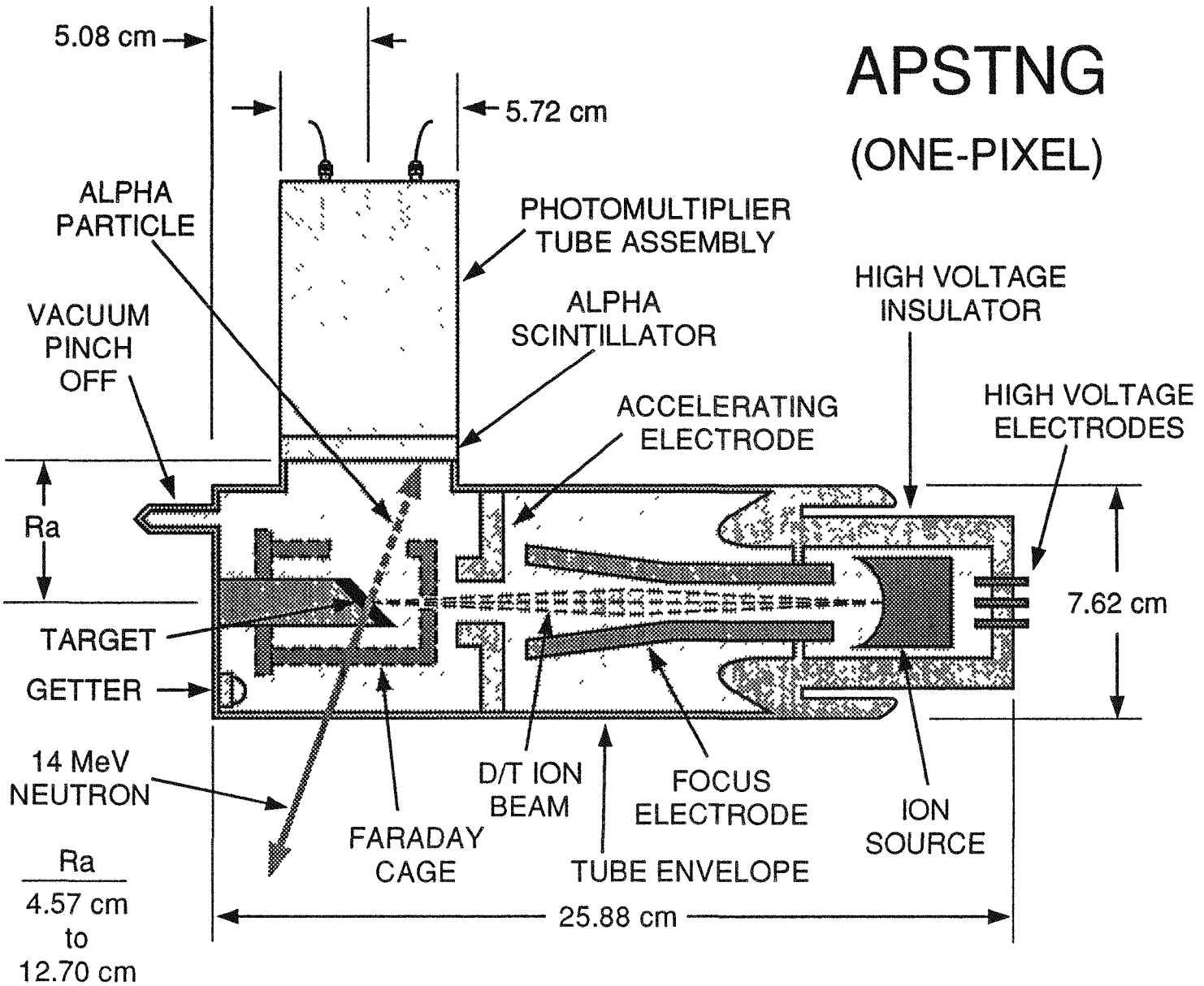

Figure 2. Schematic view of cross-section of APSTNG sealed neutron tube

The PC controls the measurements, calculates positions, records data, and displays and analyzes data and images. The usable neutron source strength is limited by the gamma ray accidental coincidence rate, the APSTNG tube design, or the maximum allowable alpha count rate, whichever yields the lowest value. Once the neutron source strength is at its maximum, any further gains in signal rate can be made only by increasing the gamma ray detector volume or the number of detectors. (A fielded system for a time-critical application would likely have a 2-D alpha detector and an array of gamma ray detectors with a relatively large total detection volume, in order to maximize information obtained from each interacting neutron and sufficiently minimize measurement time.)

Fast-neutron reactions in the object (primarily inelastic scattering) provide prompt gamma-ray spectra that can identify many nuclides. Nearly all nuclides with atomic number above boron have distinctive gamma-ray spectra for the EGRIS mode, with reaction cross sections of approximately 0.5 barn or so for 14-MeV neutrons. The inelastic gamma rays for heavy nuclides tend to be too low in energy (much below 1 MeV) to be detected against background. However, fissionable materials also emit higher-energy prompt fission gamma rays, with a characteristic gamma-ray spectrum. Although the APSTNG system does not identify chemical compounds, ratios of elements can be measured, and used to indicate the presence and location of ratios equal to those of specific compounds.

Because the gamma rays are emitted nearly isotropically, the APSTNG neutron tube and gamma-ray detectors can be located on the same side of the interrogated volume, allowing measurements when access is possible only from one side. And, the high-energy neutrons and gamma rays are highly penetrating. Thus a rather wide variety of sealed containers could be inspected, as well as regions behind walls. Gamma-ray signals from wall materials can be sorted out from signals originating behind the walls by sorting spectra according to the time after alpha detection events. For gamma rays above 1 MeV or so, background is greatly reduced, since background counts can only be accumulated during the nanosecond-range correlation interval. A relatively high signal-to-background ratio is obtained, allowing the use of a relatively small neutron source and conventional electronics. No collimators or personnel radiation shielding are fundamentally required for the EGRIS mode (or for any of the other modes mentioned below), and a complete APSTNG inspection system could be transported in an automotive van.

2.2 Additional Detection Modes

The EGRIS mode is normally the fundamental detection mode but it can be augmented by or replaced by other detection modes for specific applications. A detection mode quite similar to EGRIS is the emission neutron imaging and spectroscopy (ENIS) mode, for which the gamma-ray detectors are replaced (or augmented) by fast-neutron detectors. This mode could be used for detecting prompt neutron emission stimulated from fissionable materials, but it requires performing coarse neutron energy discrimination measurements in conjunction with time-coincidence. An initial study reported that this mode could be used, but that it was difficult in practice for the apparatus to distinguish prompt fission neutrons from scattered APSTNG neutrons.[3]

Neutron reactions generated by APSTNG neutrons that have been thermalized occur after variable time delays, and thus are not time-correlated with the alpha pulses on a nanosecond

scale, but they can provide nonimaging gamma-ray spectra that can aid nuclide identification, if the neutron beam is sufficiently moderated to thermal energies. The use of uncorrelated gamma-ray spectra with the neutron generator on is termed the UGRS mode. Since the EGRIS mode separates the correlated and uncorrelated events, UGRS data can be collected simultaneously with EGRIS data on the PC by sending the uncorrelated events to a multichannel analyzer card on the PC ISA bus. The gamma-ray spectra are generally more complex than for EGRIS mode, and backgrounds are much more prominent because the spectra cannot be processed for time-correlation with the alpha signals. Thermal-neutron capture cross sections are large for some nuclides of interest. In particular, thermal-neutron fission cross sections are large for fissile nuclides, yielding a much amplified fission gamma-ray spectrum. Unless the interrogated target contains considerable neutron moderating material, external moderator will probably be required for UGRS.

The passive gamma-ray spectroscopy (PGRS) mode, is simply the one for which the neutron generator is turned off. This mode detects gamma-ray radioactivity in the interrogated object and in its vicinity, including any activity induced by the neutrons as well as uncorrelated background. This mode is used for static system energy calibration with gamma-ray calibration sources (dynamic energy calibration is performed in the EGRIS mode using known materials and their reaction gamma-ray spectra). Because cross sections for inducing activity with a finite half-life (several seconds or more) are usually small, the PGRS mode normally would be employed only in cases for which the inspected object is suspected or known to be a radioactive gamma-ray emitter (as for radioactive waste and nuclear weapons).

The APSTNG also can be used in the fast-neutron transmission imaging (FNTI) mode. A coarse two-dimensional image can be obtained by placing an array of neutron detectors in the neutron cone, behind the interrogated object and counting only neutron events in time coincidence with alpha events. Alternately, if the APSTNG has an x-y position-sensitive alpha detector, transmission images could be obtained with a single large-area neutron detector placed in the neutron cone, behind the interrogated object. By measuring at a sufficient number of angles, three-dimensional tomography would be possible, measurement times permitting. No spectral distinction between nuclides is provided, but fast-neutron attenuation is mapped throughout the interrogated object. Also, a single detector could be used in a single-pixel version of FNIT by scanning it across the area of interest. We used this version of the FNTI mode to map and position the neutron correlation cone of the present system, by scanning a small plastic scintillator detector. FNTI, either single-pixel or coarse x-y imaging, could be used during inspections to check for the presence of hidden shielding.

2.3 Comparison with Alternative Technologies

Alternative neutron diagnostic technologies include simple prompt-neutron activation analysis (PNAA), ie. the use of a gamma-ray detector, a multichannel analyzer and a radioisotope neutron source or small neutron generator. PNAA in practice requires shielding against radiation from the source or generator; and this shielding may have to be configured to shield the detector from activation product radiation originating outside the region being inspected. The PNAA technologies share, with the APSTNG method, low sensitivity compared to chemical sampling methods. Both PNAA and APSTNG are truly nondestructive, unlike chemical sampling methods. And, both PNAA and APSTNG use highly penetrating 14 MeV neutrons for interrogation and

identify compositions by spectral analysis of highly penetrating gamma radiation. However, PNAA spectra are more complex and have substantially higher backgrounds than APSTNG spectra. Another difference is that the APSTNG data are processed on-line to electronically reject radiation from objects outside the correlation cone. PNAA systems require collimation to select data from a specific inspection object or region in space.

In the standard PNAA technique, neutron pulses are at least several microseconds in duration, which allows time separation of fast and thermal neutron reaction gamma rays, but spectra must be collected during the neutron pulses, which raises the background substantially and requires relatively high-bandwidth electronics; and there is no depth discrimination capability. Nanosecond-pulse PNAA provides separation of fast and thermal neutron reaction gamma rays as well as depth discrimination. A significantly more complex accelerator is required for nanosecond-pulse PNAA, which implies higher cost and higher weight. Neither of these PNAA techniques can provide two- or three-dimensional imaging without using a collimator (either a multichannel one, or a single-channel one physically scanned across the field of view).

The highly portable PINS system developed at INEL is a PNAA system using a radioactive Cf-252 fission source and a liquid nitrogen (LN) cooled HPGe detector. For field applications where it is adequate, it would be the system of choice.

APSTNG technology yields a relatively high signal-to-background ratio and separate fast-neutron and thermal-neutron reaction gamma-ray spectra. This allows the use of a relatively small neutron source and low-bandwidth data acquisition electronics. The APSTNG also has inherent depth discrimination. A multi-pixel alpha detector gives the APSTNG a coarse three-dimensional imaging capability. No collimators or personnel radiation shielding are needed, and a complete APSTNG inspection system could be transported in an automotive van. Thus, the APSTNG technology can provide enhanced performance in a transportable nondestructive inspection system.

3.0 ANL APSTNG SYSTEM

3.1 Apparatus Laboratory Deployment

Figure 3 is a posed photo of the components of an earlier model APSTNG system developed by C. W. Peters. The ANL APSTNG system is similar. Top, right, is the cylindrical APSTNG sealed accelerator tube, in a vertical position. Extending out from this tube is the cylindrical alpha detector. A NaI scintillation gamma-ray detector is located behind the sealed tube, and to the left. Top, left, is a rack containing, from top to bottom, the accelerator control unit, the HV supply, and flight-time electronic modules. In the foreground are the data acquisition electronics and PC with printer, above which is a suitcase to provide a sense of scale.

The ANL APSTNG system was assembled at ANL June 23, 1992 and made operational the same day. For convenience in laboratory operations, the APSTNG components were not used in a compact configuration. Figure 4 is a photo of the APSTNG control area as set up in the laboratory, showing left to right, the PC printer, PC, and data acquisition electronics modules. In Fig. 5, approximately 6 m behind the control area, connected by cables, is a rack with, from

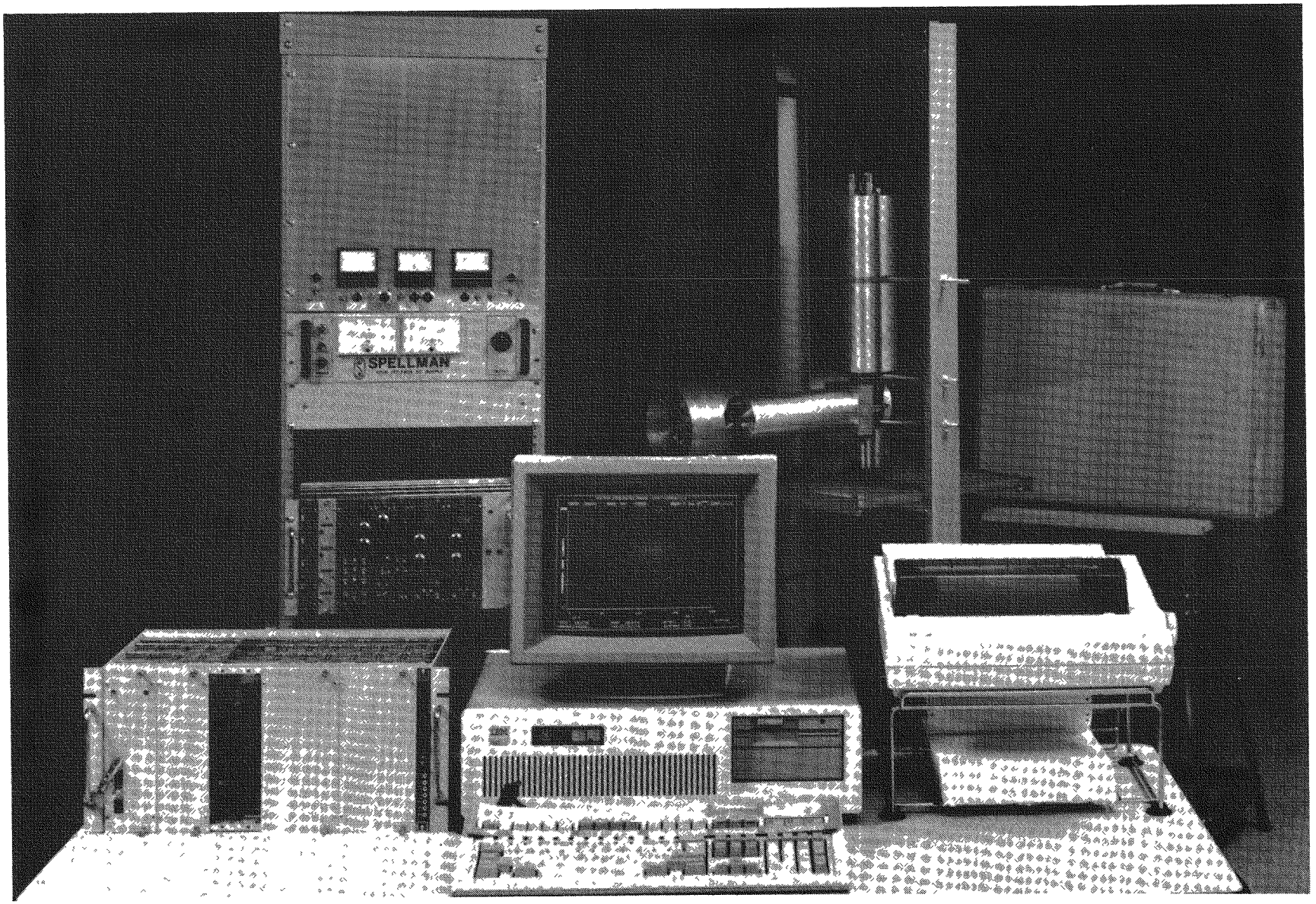

Figure 3. Posed photo of components of early model APSTNG system

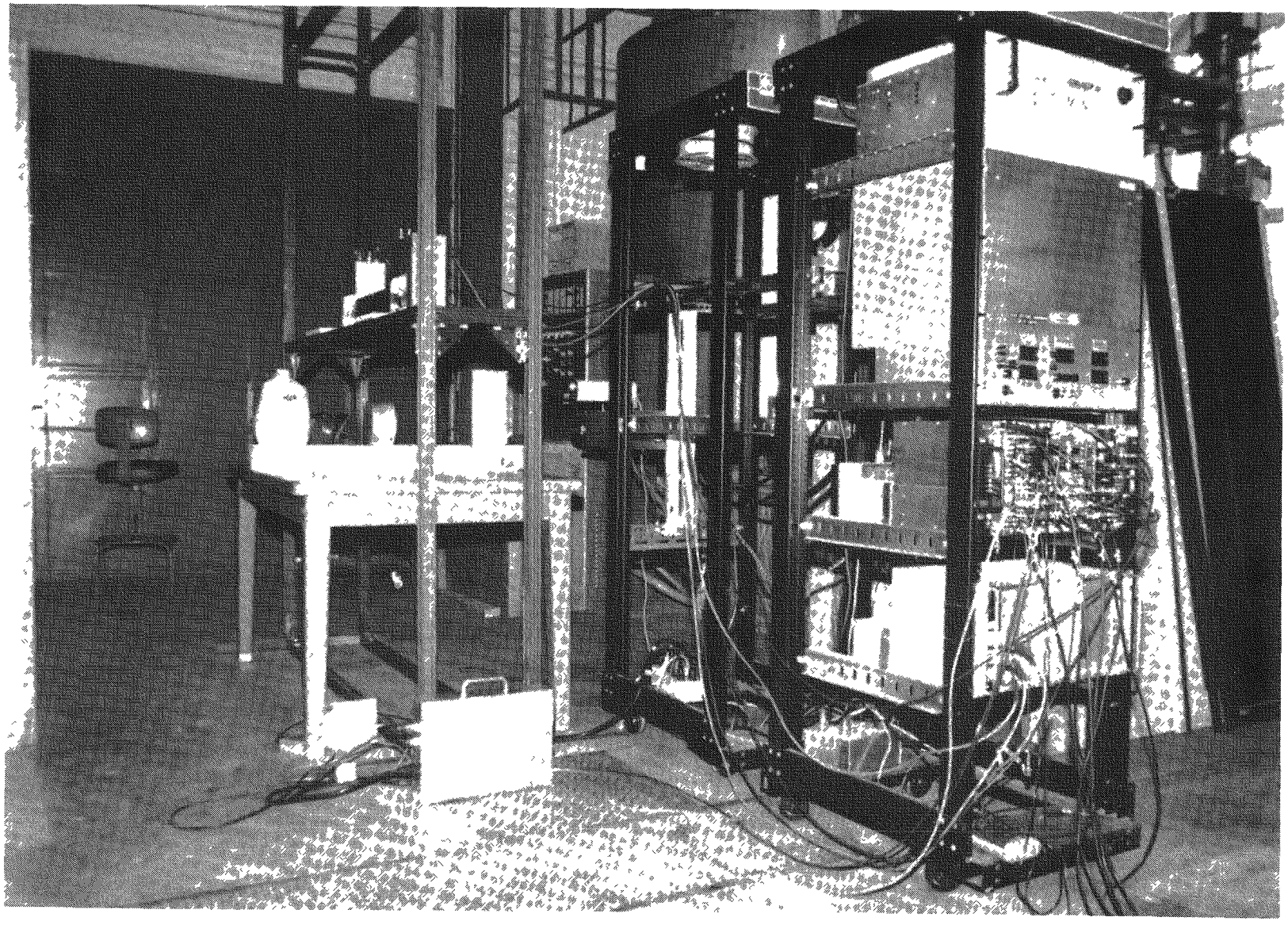

Figure 4. Photo of APSTNG control area in ANL laboratory (building 208 room B102)

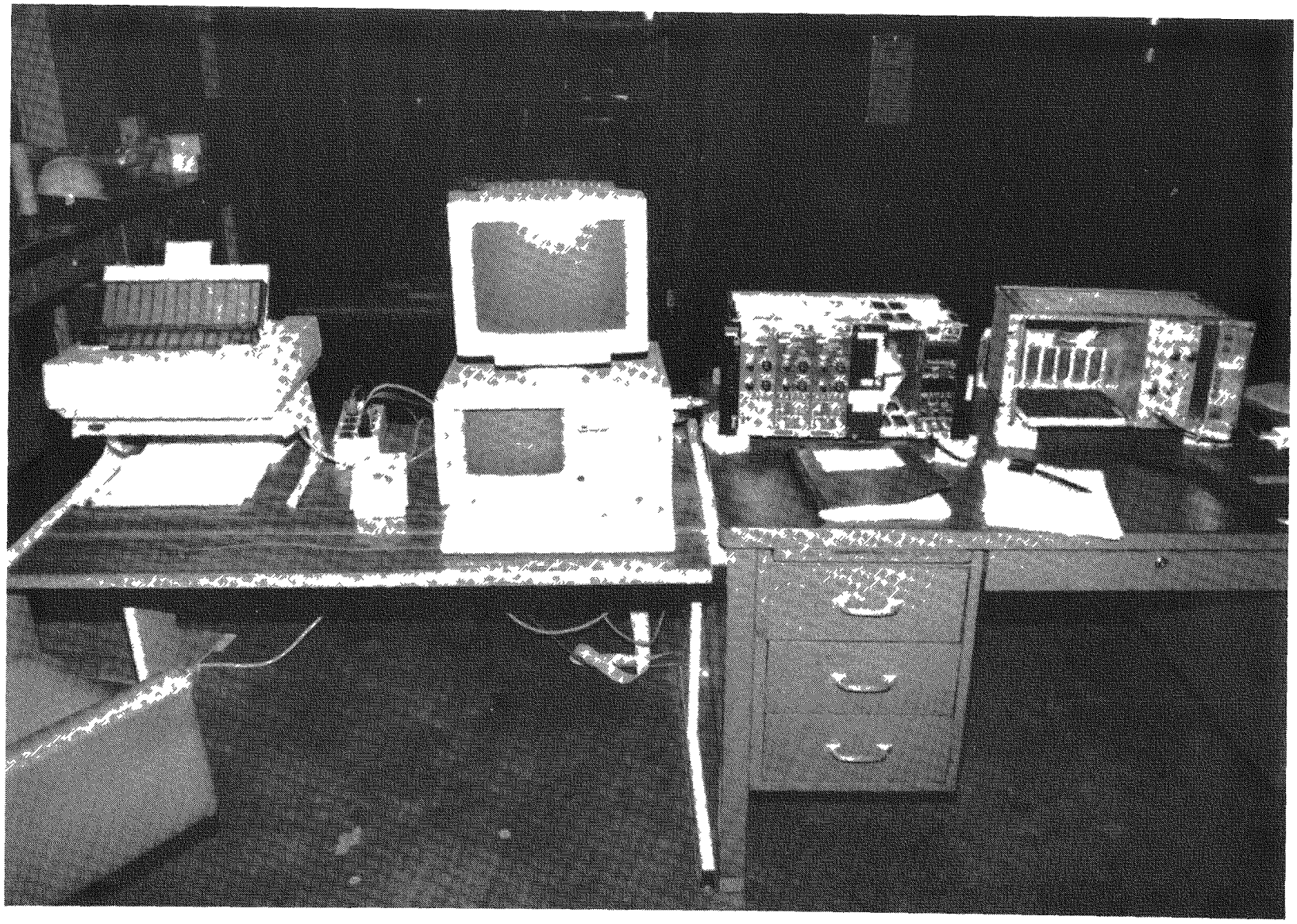

Figure 5. Photo of ANL APSTNG equipment rack, neutron generator tube, gamma-ray detector, and inspection table in laboratory

top to bottom, the neutron generator HV supply, its control unit, and the flight-time electronic modules. Behind this rack is an empty rack to which the neutron generator tube is mounted on an outrigger extending out behind, and to the left of the tube are three objects for inspection on a table. Above the table is a double-ended gamma-ray detector on a stand. Figure 6 is a rear view of this configuration, showing the alpha detector, laser pointer, and three test objects: C, Al, and water.

With regard to personnel safety and radiation dose rates, there is no detectable X-ray dose near the tube, because the ion source is enclosed within a 1.6-mm-thick lead shield. Operating at a total neutron source rate of about 2 x 10^7 neutrons/second (n/s), the measured dose rate 30 cm from the source is ~ 15 mRem/hr. The measured dose rate at the normal operator position is ~ 10 microRem/hr. No personnel shielding is required to meet DOE As Low As Reasonable Achievable (ALARA) radiation exposure guidelines. Neutrons are generated only when both the HV and the ion source are on. A keylock system with keys limited to qualified operators is used to limit access to controls for the HV supply. When the keylock is turned, a steady red light is activated. Turning on the ion source activates flashing red lights to indicate neutron production.

3.2 Apparatus Design and Procurement

The double-ended gamma-ray detector shown in Figs. 5 and 6 was designed to ANL specifications, to provide a relative large detector with good time and energy resolution. The detector was procured from Solon Technologies, and consists of a hermetically sealed block of relatively rugged Polyscin NaI 10.16 cm square by 40.64 cm long coupled to two fast Hammamatsu 4143 photomultiplier tubes of 6.5-cm active diameter, one on each end, inside a light-tight housing. NDS added electronic circuits in custom housings attached to each end of the detector, including: photomultiplier base resistor bias strings tuned for fast timing, Bertan PMT30CP-1 HV supplies with pots (potentiometers) and test points, Phillips 6950 anode preamps, and Ortec 113 dynode preamps. Each gamma-ray event gives rise to two output voltage pulses, one from each photomultiplier tube. These are summed to obtain a single pulse for pulse height analysis. The differences in timing between the two pulses are used to correct the flight time.

The alpha-particle detector assembly was designed by NDS to ANL specifications and includes a fast Hammamatsu 580-15 photomultiplier of 3.4-cm active diameter, base resistor bias string tuned for fast timing, Ultravolt 2A12-14-M HV supply with filter, pot, test points, and Phillips 6950 anode preamp, all enclosed in a housing that attaches securely to the APSTNG tube. Coil springs press the photomultiplier face onto the alpha window (silicon grease provides optical coupling). A rear plate can be removed to troubleshoot circuits. The APSTNG neutron correlation cone defined by the alpha detector solid angle can be changed by placing an aperture between the photomultiplier and alpha window; this may be accomplished either by removing the inner photomultiplier subassembly or by removing the entire assembly from the APSTNG tube. O-ring seals provide a light-tight housing. A shimmable mount is provided for a Metrologic ML800 0.5-mW helium-neon laser used as a pointer for the neutron cone.

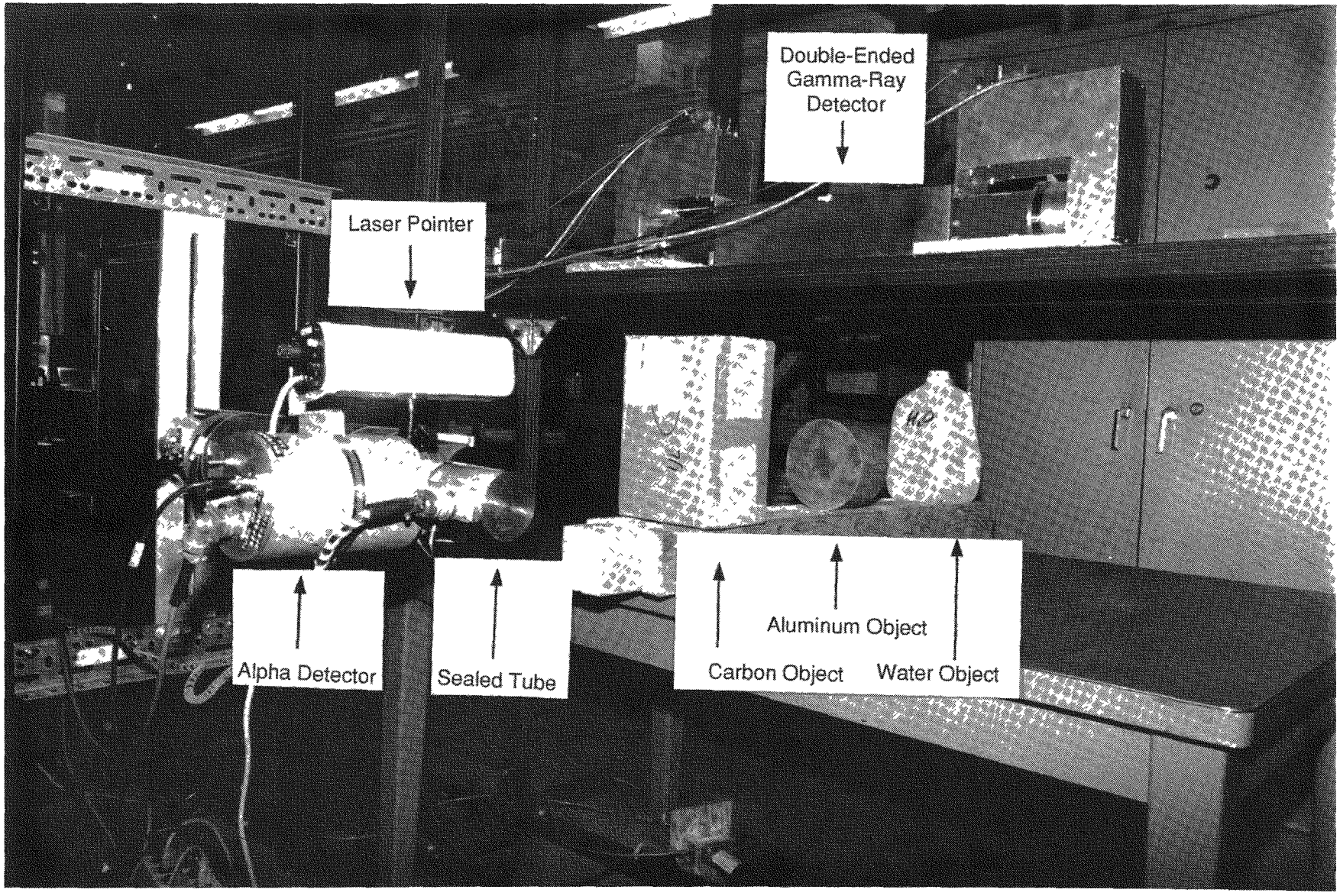

Figure 6. Photo of neutron generator tube in ANL laboratory, showing alpha-particle and gamma-ray detectors and three test objects

An electronic schematic layout of the ANL APSTNG system is shown in Fig. 7. The photomultiplier dynode output signals from each end of the gamma-ray detector are summed by an Ortec 533 Dual Sum and Invert unit, amplified by an Ortec 673 Linear Spectroscopy Amplifier, and delayed and gated to match up with the anode timing signals by an Ortec 542 Linear Gate and Stretcher, for the EGRIS mode. Time stability and lower thresholds for all detector anode signals are provided by an Ortec 935 Quad CFD. The coincidence unit shown in Fig. 7 is a Phillips Quad Four-fold Logic unit used in majority logic mode to ensure that the Ortec 567 TACs are not overloaded by the many uncorrelated pulses (start pulses that don't lead to valid stop pulses).

The TAC flight-time signals from the two ends of the gamma-ray detector and the gamma-ray energy signal are digitized by Ortec 800 ADCs at 256 channels each and read into a first-in first-out (FIFO) buffer of NDS design, as shown in Fig. 7. Every time the FIFO buffer accumulates 50 events, the data are transferred to the PC memory through a Keithley-Metrabyte PDMA-16 DMA interface card on the PC ISA bus. A separate counter/timer circuit sends alpha-particle detector pulses through the FIFO buffer unit to a Keithley-Metrabyte CTM-05 counter/timer ISA-bus card, which transfers the summed alpha counts to the EGRIS software data acquisition program, IGRIS. IGRIS is a C program written by NDS that runs under the MS-DOS operating system. Another C program that runs under DOS, IGNEWX, analyzes the EGRIS data after the experiment run is completed; it was also written by NDS but was modified by ANL during the course of the study.

The PC used for data acquisition and analysis has a standard full-size AT desktop case, is based on a Intel 386DX-33 microprocessor, has 4 MB memory, and includes a Bernoulli removable 150-MB disk unit. The aluminum APSTNG tube mount in Fig. 6 (which can orient the tube at any orientation and can be adjusted vertically) and control unit in Fig. 5 were custom-designed and built by NDS. All the APSTNG system components were integrated and tested at NDS and then were delivered to ANL for final acceptance testing.

3.3 APSTNG Sealed-Tube Neutron Generators

The APSTNG sealed tube is a relatively small sealed module that is readily replaced without support from the manufacturer. The sealed-tube design prevents tritium contamination. A schematic cross section of the NDS APSTNG tube initially procured by ANL, serial no. C-10, is shown in Fig. 2. The single-pixel alpha detector consists of a 4.30-cm diameter ZnS coating deposited inside the sealed tube, on a window that is optically coupled to an external photomultiplier. The alpha scintillator is limited to materials that can withstand the tube bake-out temperatures during manufacture. The distance from the center of the ion beam target spot to the inside surface of the sealed-tube window is 4.60 cm, yielding a maximum cone apex angle of 50.1° for the detection of alpha particles. Currently the maximum cone angle is limited by the 3.4-cm diameter active face of the photomultiplier tube on the outer surface of the window to 40.6°. The solid angle of this cone can be reduced (e.g., for scanning an object, or optimizing signal-to-background ratios) by placing an aperture between the window and the photomultiplier. After tube C-10 failed (see Section 3.4), it was replaced by the only APSTNG tube available, serial no. C-11. C-10 and C-11 have the same design, except that the inner surface of the C-11 alpha window is 12.7 cm from the beam spot. This results in a maximum C-11 cone apex angle of 19.2°, 15.2° with the 3.4-cm diameter photomultiplier.

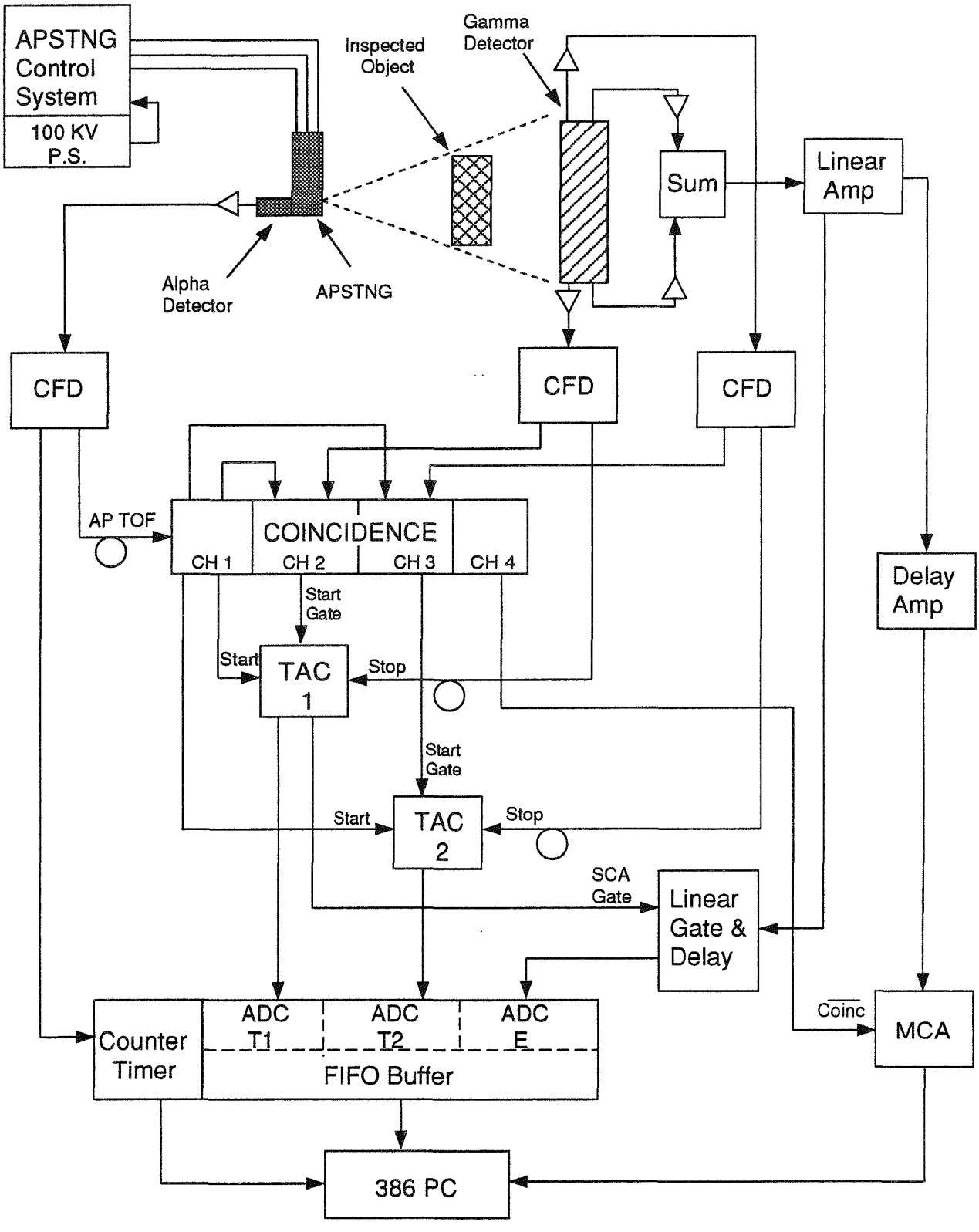

Figure 7. Electronic schematic layout of ANL APSTNG system

As shown in Fig. 2, a Penning ion source inside the APSTNG emits a continuous mixed beam of deuterium and tritium ions that is accelerated and focused on a small spot (about 1 mm diameter) on the target, tritiating the target and producing neutrons and alpha particles. (Focussing the beam to a small spot is necessary to obtain good spatial resolution.) The Faraday cage around the target drives secondary electrons from the target back into the target, helping reduce background from the alpha scintillator and providing accurate target current readings. The cage has a hole allowing passage of the alpha particles. A getter of sintered zirconium powder controls the pressure of the gaseous mixture of deuterium and tritium. The ions are accelerated by a high voltage of 95 kV and focused by a variable extraction voltage, nominally 15 kV. The ion beam current (about 1 μA to get 10^6 n/s) is controlled by varying the getter heating current. Internal pressure is the order of 10^{-9} Torr without getter heating and the order of 10^{-5} Torr under normal operating conditions. The welded metal-ceramic tube contains 0.4 Ci tritium at low pressure compared to the atmosphere, and the tritium is contained in the getter when the tube is not operating. If the tube has not been used for several weeks, a number of getter and ion source start-stop cycles are required to reach full neutron output.

Not shown in Fig. 2 is the HV coupling for the neutron tube. An aluminum can 12.7 cm in diameter and 30.5 cm long is fitted to the tube with a large O-ring seal, located along the tube between the alpha window and the electrodes. An O-ring sealed lid on the back of the can provides O-ring sealed connectors for the HV cables and access to fiberglass guide tubes to the tube electrodes. Before operation of the neutron tube, the HV cables are inserted through the can guide tubes into the tube electrodes, and the can is placed in an upright position and filled with Fluorinert insulating fluid, through a hole in the lid. The Fluorinert also serves as a coolant for the ion source.

Shown in Fig. 5, a Spellman UHR100P10 HV supply with a slow ramp-up feeds up to 100 kV to the NDS custom-built SC-5 APSTNG control unit, which furnishes and monitors neutron tube operating voltages and currents. The SC-5 front panel provides pots to adjust the getter current up to 4 mA and the focus voltage up to 20 kV, as well as LCD meters for getter current, focus voltage, ion source current, target current, and Faraday current. It provides HV cables to the neutron tube anode, cathode, and focus electrodes through the HV coupling and a control cable to the other end of the neutron tube with leads for the getter, target, and Faraday cage. The ion source has an RF power supply isolated on top of the Spellman HV and the focus supply. Ion source current is sent by an isolated optical link to the front panel meter and to the getter power circuit to provide feedback to control tube gas pressure. The focus power supply is similar to the ion source supply.

The operating history of each APSTNG neutron tube made by NDS was monitored and documented by NDS. Initial maximum output of a typical APSTNG is around 3×10^7 n/s, but the maximum output soon falls to about the level of 10^7 n/s, as the cathode target is sputtered away, and slowly decreases thereafter. An output of ~ 10^6 n/s typically can be maintained for ~ 2000 hours by increasing the ion current to compensate for target loss by sputtering. Eighteen production model ceramic tubes have been made, fourteen of which passed quality control tests (a 78% yield). Eleven of these tubes were put in operation. Two tubes failed after continuous operation at voltages well in excess of NDS specification. The average lifetime output for the nine tubes that were operated within specifications is 7.35×10^{12} neutrons, if end of life is defined as being reached when either the tube fails or the maximum output becomes less than 10^6 n/s.

The design of the APSTNG differs substantially from the current well-logging neutron generator tubes, which cannot be used for associated-particle operation. Well-logging tubes are usually pulsed, have no capability to focus the ion beam on a small spot on the target, and have no provisions to detect alpha particles.

3.4 System Operational Experience

3.4.1 Overall Experience

The APSTNG system experience was good, except for sealed tube damage caused by breakdowns in the HV control unit. A more reliable HV control unit with current-limiting circuits would prevent loss of sealed tubes due to HV breakdown. No tritium contamination occurred with either the original tube or the replacement tube.

The APSTNG system was operated from completion of installation on June 23, 1992 until July 12, 1994, when a HV control unit breakdown occurred. As of July, 12, 1994, C-10 had achieved total neutron output of 75% of the expected life of 7.35×10^{12} neutrons. During its operating life, C-10 operated stably at higher neutron output rates than typically employed by NDS. Figure 8 is a graph of the neutron output operating history of the tube. It had been run at output levels up to 2×10^{7} n/s in experiment runs earlier in July, 1994. The HV control unit suddenly exhibited repetitive high-voltage breakdown and arcing. The HV was turned off as soon as possible after arcing was observed. However, the getter circuit was found to have very high post-breakdown resistance, indicating a burned-out getter. After the control unit was repaired, it was found that tube C-10 could not generate neutrons: it could not be brought up to full voltage without drawing excessive current, and the ion source also drew excessive current. Visual inspection found evidence of damage to the Fluorinert insulating fluid (charred appearance) and identification of an overheated spot on a welded joint, that apparently caused an air leak. No tritium contamination occurred.

The HV control unit was repaired, and the only neutron tube available for purchase, serial number C-11, was procured. At the time C-10 failed, NDS no longer supplied neutron generators. Another company, Multipixel Systems, had acquired NDS neutron tubes but had no tube manufacturing capability. Multipixel Systems supplied the tube and modified our alpha detector assembly to fit on it. C-11 was put into operation September 7, 1994 and performed properly until September 15, when high voltage breakdown and arcing occurred again. The HV supply was shut down promptly by the operator. Visual inspection showed no evidence of damage to tube or Fluorinert. There was just time to ship the HV control circuit to Multipixel Systems to be repaired again, with shipment of the repaired unit to INEL, with final checkout of the HV control circuit with the C-11 tube to take place at RWMC. This re-assembly and checkout was performed in consultation with a representative of Multipixel Systems who traveled to the ANL-INEL site for systems support. However, the C-11 tube would not generate neutrons when the HV control unit was re-installed. No tritium contamination occurred.

The relatively large double-ended NaI detector has performed well. This detector is suitable as a prototype for future NaI systems, including larger arrays for applications for which high count rates are important. If improved energy resolution is important, additional high-resolution detectors could be employed.

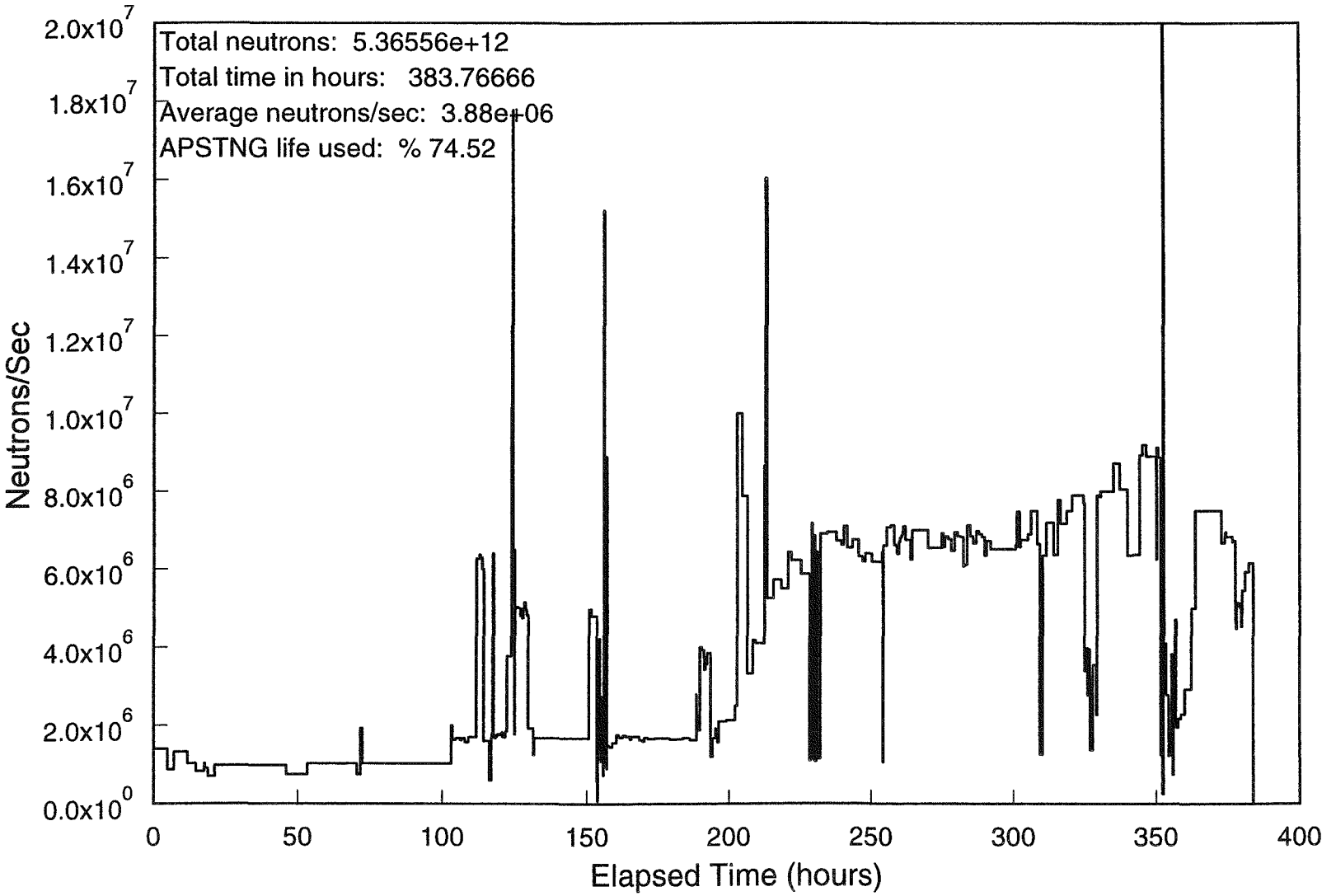

Figure 8. APSTNG tube C-10 neutron output rate operating history

3.4.2 Maintenance Experience

The alpha detector assembly internal HV supply was repaired once and replaced once. Trouble-shooting the alpha electronics was difficult because the photomultiplier is exposed to light and can't be operated when the alpha detector internal electronic modules are accessed. One photomultiplier was damaged when the HV backplate switch was inadvertently switched on during trouble-shooting. Another photomultiplier was damaged by a light leak caused when the O-ring seal around the alpha window was not properly reseated during assembly (visual inspection of this seal is difficult). The PDMA-16 DMA card was repaired once. Also, one Ortec 800 ADC was replaced.

In Section 5 we list the relatively straightforward recommendations for assuring dependable operation.

4.0 EXPERIMENTAL RESULTS

This Section summarizes representative measurements performed by ANL to characterize APSTNG capabilities, presented in approximately chronological order. Measurements done to understand detailed instrument performance and normalize data (such as beam mapping, detector response, and energy and time calibrations) are not described in this report.

4.1 EGRIS Characterization by Spectrum Signature and Flight Time

As examples of characteristic spectra, Figs. 9 and 10 show reference EGRIS gamma-ray spectra for carbon and aluminum, respectively. (The gamma channel discriminators were set at relatively high thresholds, excluding energies below 1 MeV.) Carbon exhibits a strong peak at 4.43 MeV, as shown in Fig. 9. This carbon gamma-ray energy is high enough that electron-positron pair production in the scintillation detector is a significant component of the total events in the detector, and there are secondary carbon peaks at 3.92 and 3.41 MeV, arising from single-escape and double-escape pair production events, respectively, from the 4.43 MeV gamma ray. Single escape peaks are designated as (E) and double-escape peaks as (DE). Prominent peaks in the aluminum spectrum seen in Fig. 10 arise from gamma rays of 1.81, 2.21, and 2.99 MeV. (The 1.81-MeV line overlaps a 1.72-MeV line of lesser intensity.)

The APSTNG system is designed to have the basic EGRIS mode capabilities of distinguishing objects on the basis of different element compositions and also on the basis of distance from the neutron source. As a demonstration of object discrimination by distance from the source, Fig. 11 shows the EGRIS counts, by flight time, for two aluminum plates, 0.95 cm thick (along the cone axis), 40.6 cm wide and 35.6 cm high, located perpendicular to the APSTNG cone axis, with the plate front faces 44.4 cm and 67.3 cm from the neutron source, respectively. The front face of the gamma-ray detector was located 61 cm from the centerline of the APSTNG interrogation cone. Data were collected for 60 minutes at a neutron source strength of 7×10^6 n/s. The interrogation cone was defined by an alpha scintillator window aperture 9.9 mm x 19.5 mm. The two aluminum plates are thin, in the context of the APSTNG

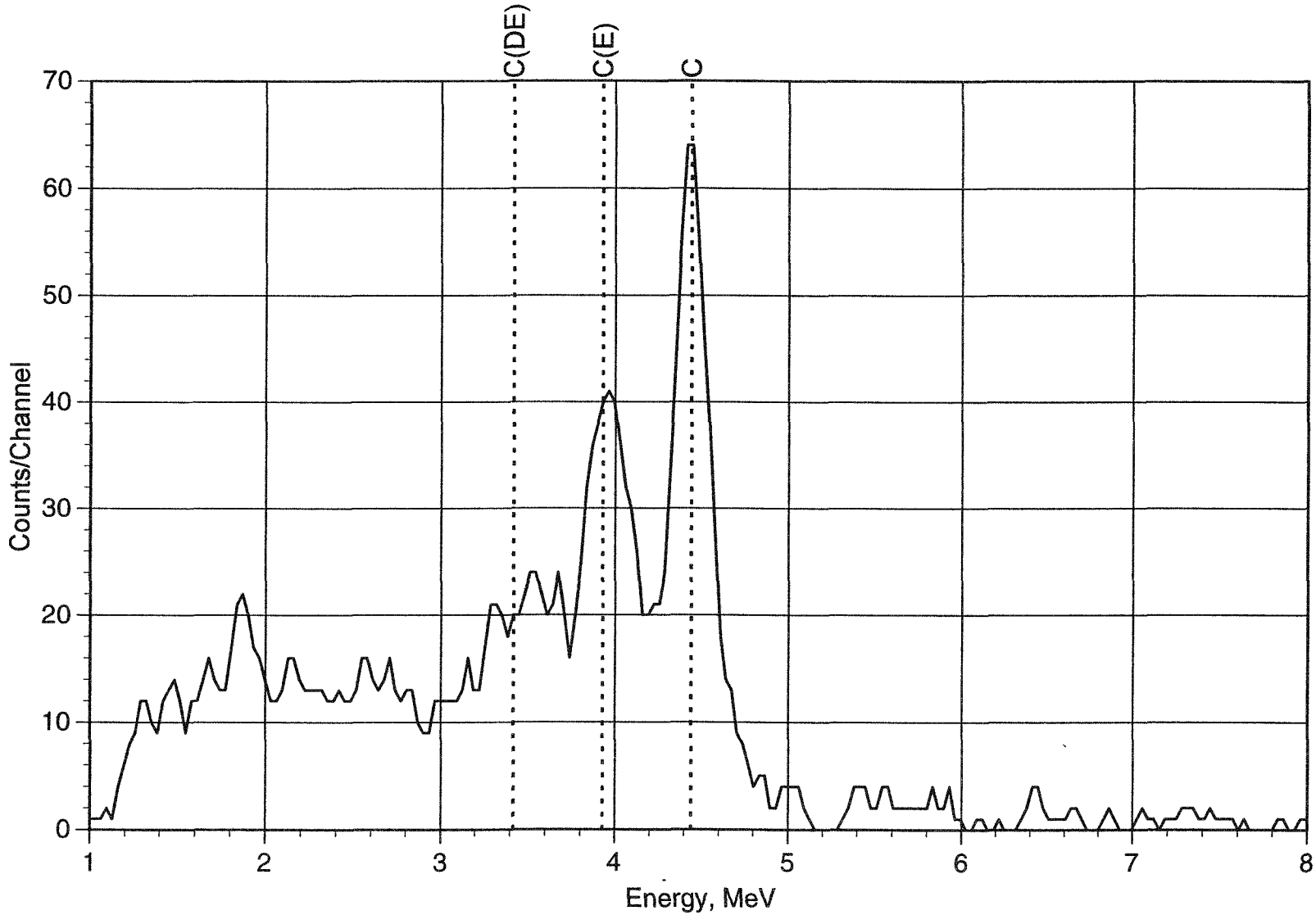

Figure 9. Reference EGRIS energy spectrum measured for carbon

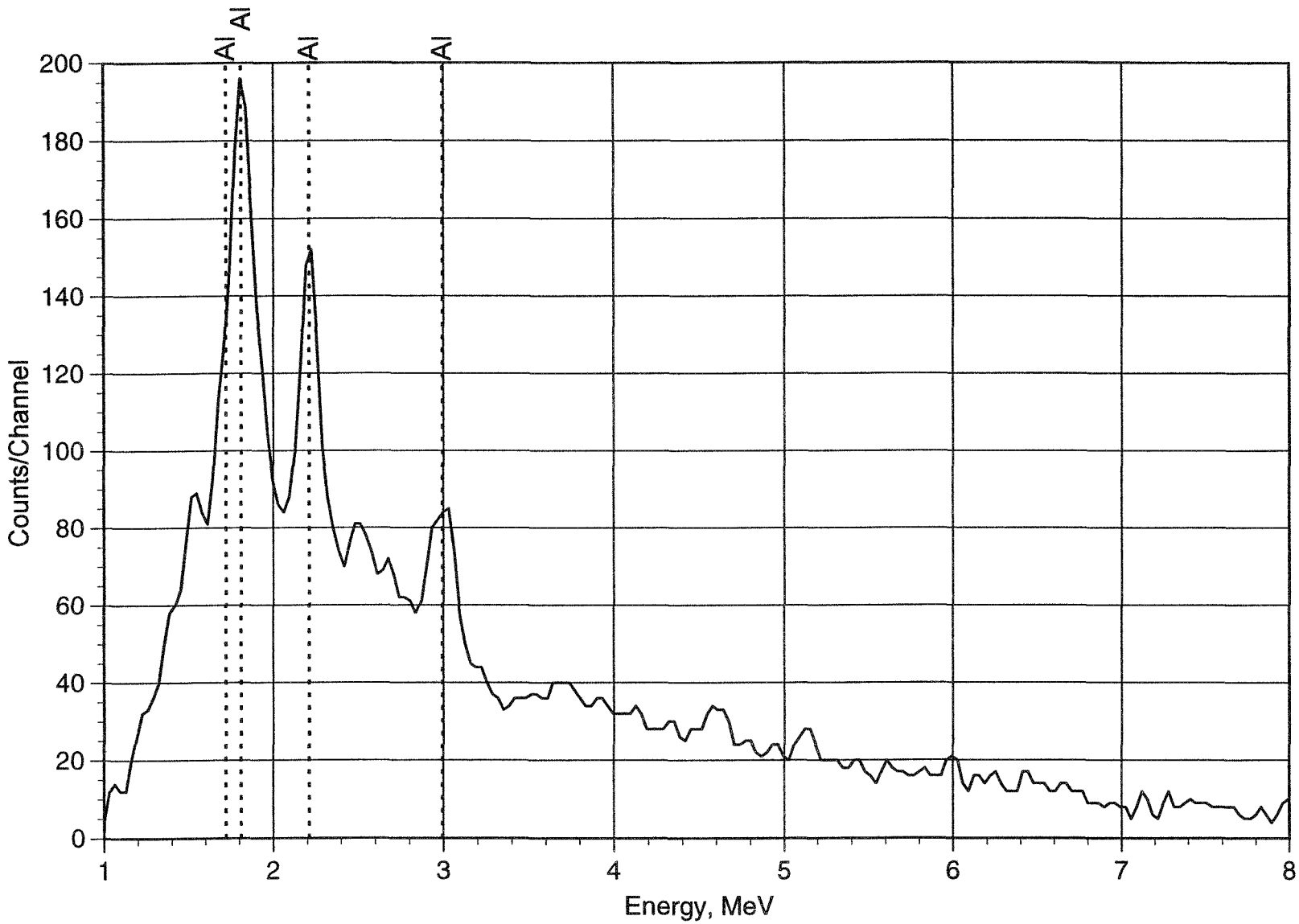

Figure 10. Reference EGRIS energy spectrum measured for aluminum

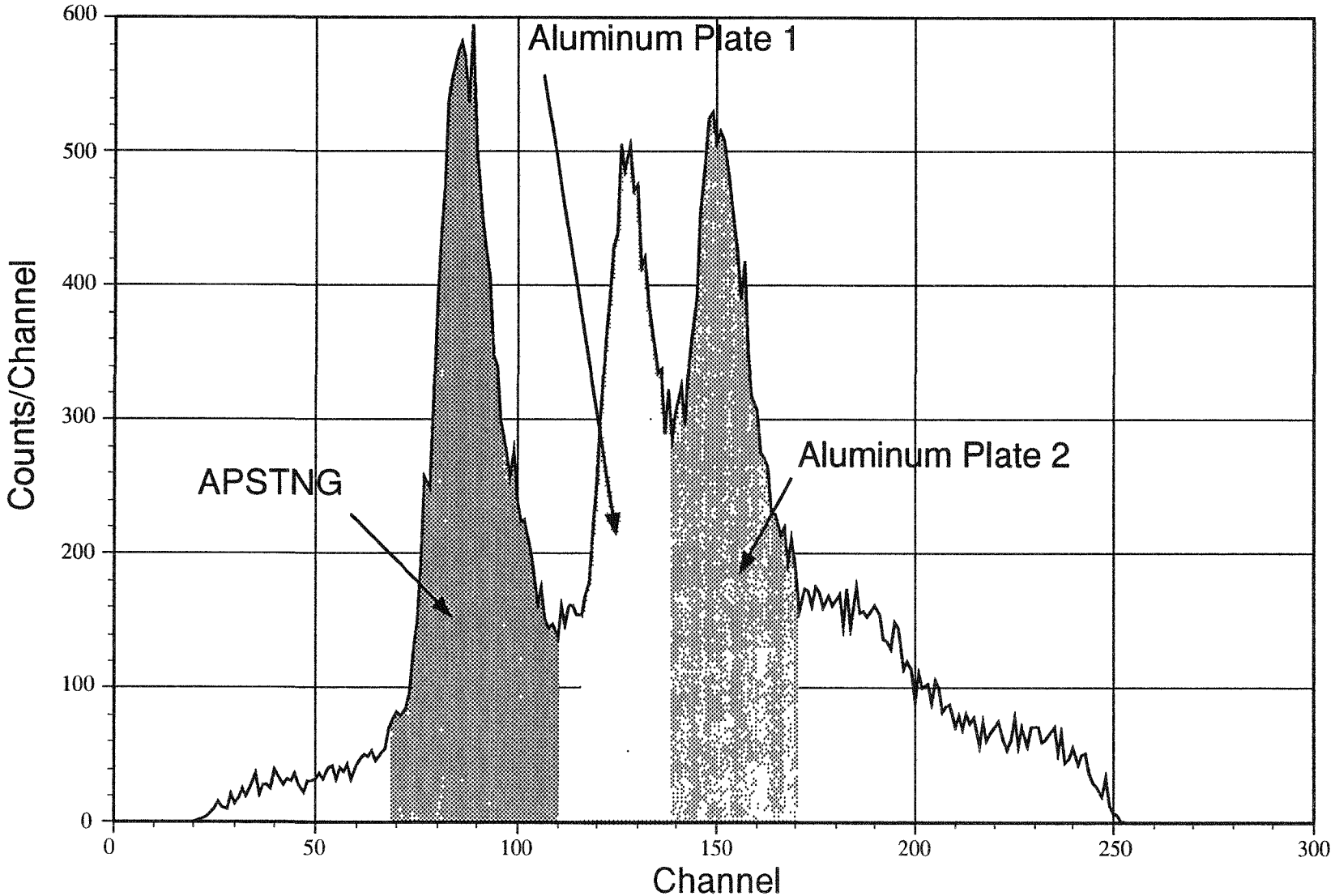

Figure11. EGRIS counts per flight-time channel for two aluminum plates

system time-of-flight spatial resolution. Three time channel peaks are seen in Fig. 11, the "early" APSTNG peak arising from radiation emitted from the region of the neutron tube itself, and peaks for the two plates, well resolved at this separation of 22.9 cm.

Figure 12 shows the combined energy spectrum from a measurement performed with two objects: a carbon-filled box, 133.4 mm deep x 171.5 mm wide x 127 mm high, and an aluminum cylinder, 76.2 mm radius x 79.1 mm deep (along the cone axis). The centers of the carbon and aluminum objects were located along the axis of the APSTNG interrogation cone, at distances from the neutron source of 47.3 cm and 81.8 cm, respectively. The double-ended gamma-ray detector was located with its long axis parallel to and 29.8 cm from the line joining the centers of the two objects. This spectrum was recorded in 20 minutes, at an APSTNG emission of 5×10^6 n/s. The prominent peaks in the carbon and aluminum spectrum signatures of Figs. 9 and 10 are seen clearly in Fig. 12.

Figure 13 shows the distribution of total EGRIS counts from the carbon and aluminum objects, as a function of time channels, equivalent to sorting out the two objects by distance from the neutron source. Only two time peaks are clearly seen in the figure: the "early" peak from interactions in the sealed tube region is subdued. The carbon peak corresponds to the location of the carbon object, and the aluminum peak corresponds to the location of the aluminum object.

At this point in analysis of the EGRIS data, the APSTNG data analysis program may be used in either of two basic modes:

1. ROIs (regions of interest) may be defined in the time channels domain, corresponding to object distances from the neutron source. This mode generates spectra characteristic of elemental compositions in selected object spatial regions. Figures 14 and 15 display EGRIS spectra sorted out by this spatial separation mode, yielding separate gamma-ray spectra signatures for carbon and aluminum, respectively. These gamma-ray signatures match the reference signatures for these elements shown earlier in Figs. 9 and 10.

2. ROIs may be defined in the gamma-ray spectrum, corresponding to selected element signatures. This mode generates distributions of elements as a function of distance from the neutron source.

4.2 Fission Signature

The 14-MeV APSTNG neutrons stimulate emission of both prompt fission neutrons and prompt fission gamma rays from fissionable materials. Either induced radiation can potentially be used for identification by employing the EGRIS and/or ENIS modes. Because these spectra are nearly identical for all the isotopes of uranium and plutonium, these modes cannot, however, by themselves distinguish between isotopes (but this distinction may not be necessary, depending on the role and scenario). Actinide inelastic scattering gamma rays are of too low energy to be detected reliably against background in the EGRIS mode. The ENIS mode would appear to have

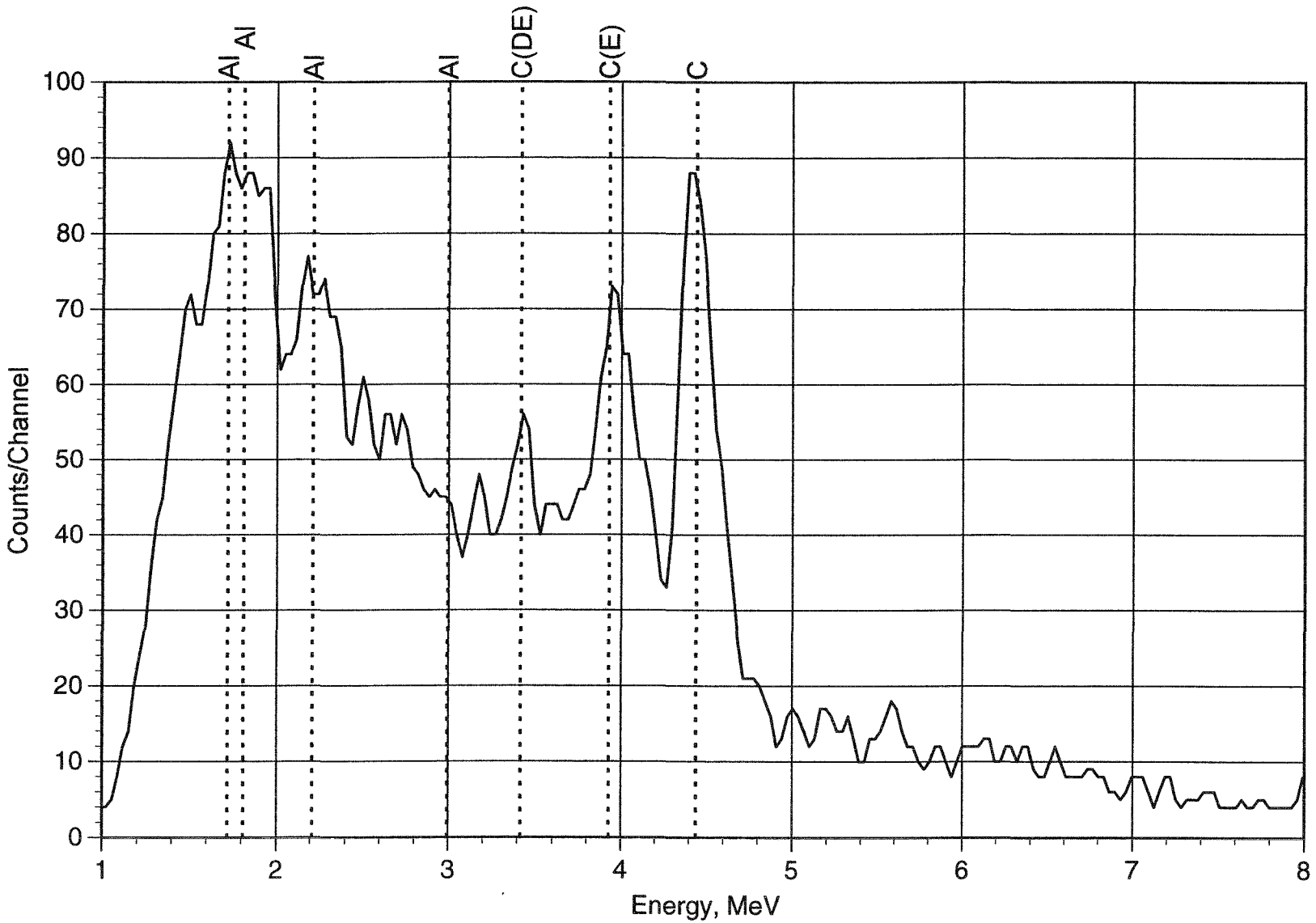

Figure 12. EGRIS energy spectrum for carbon and aluminum objects

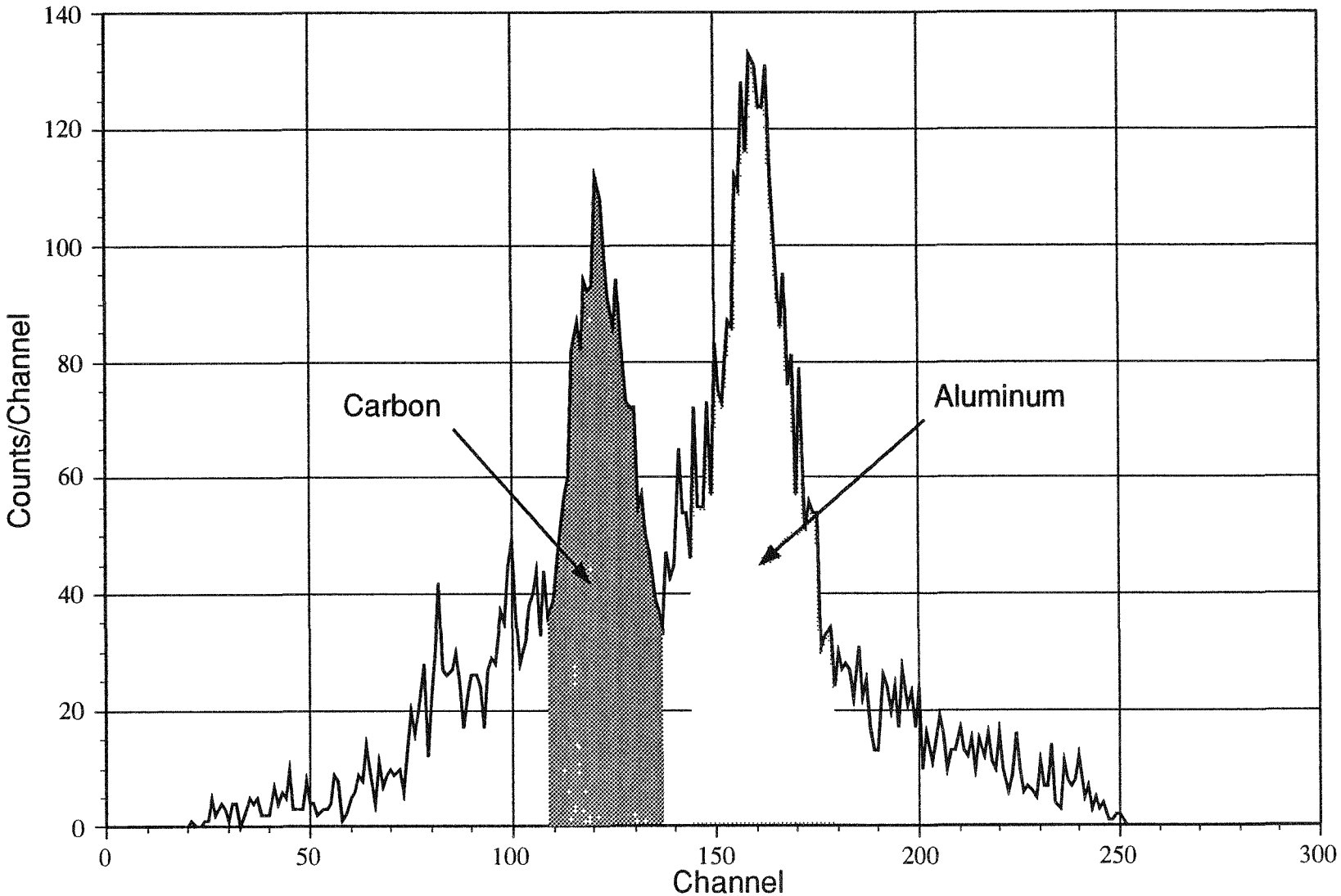

Figure 13. EGRIS counts per flight-time channel for carbon and aluminum objects

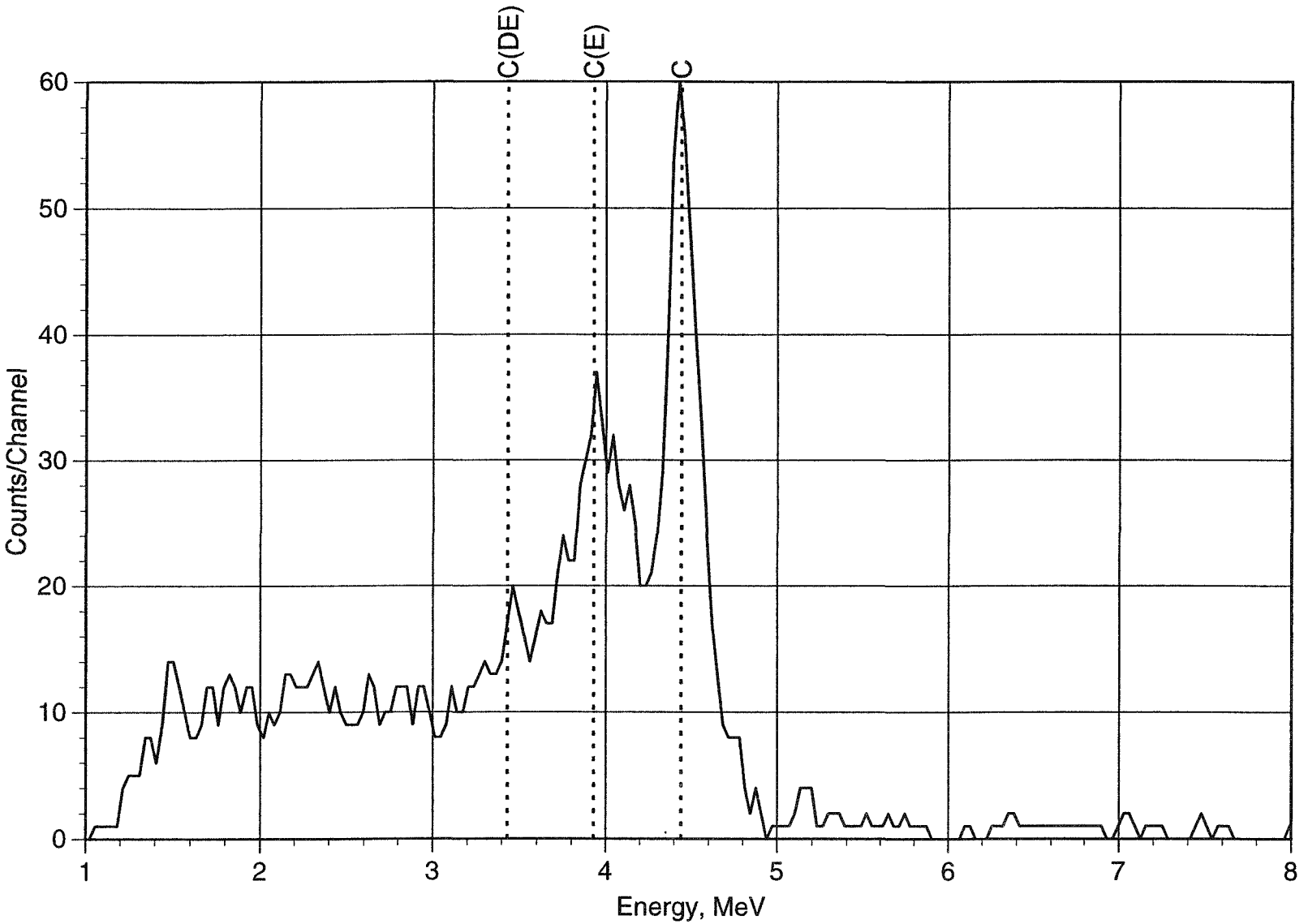

Figure 14. EGRIS energy spectrum time selected from location of carbon object

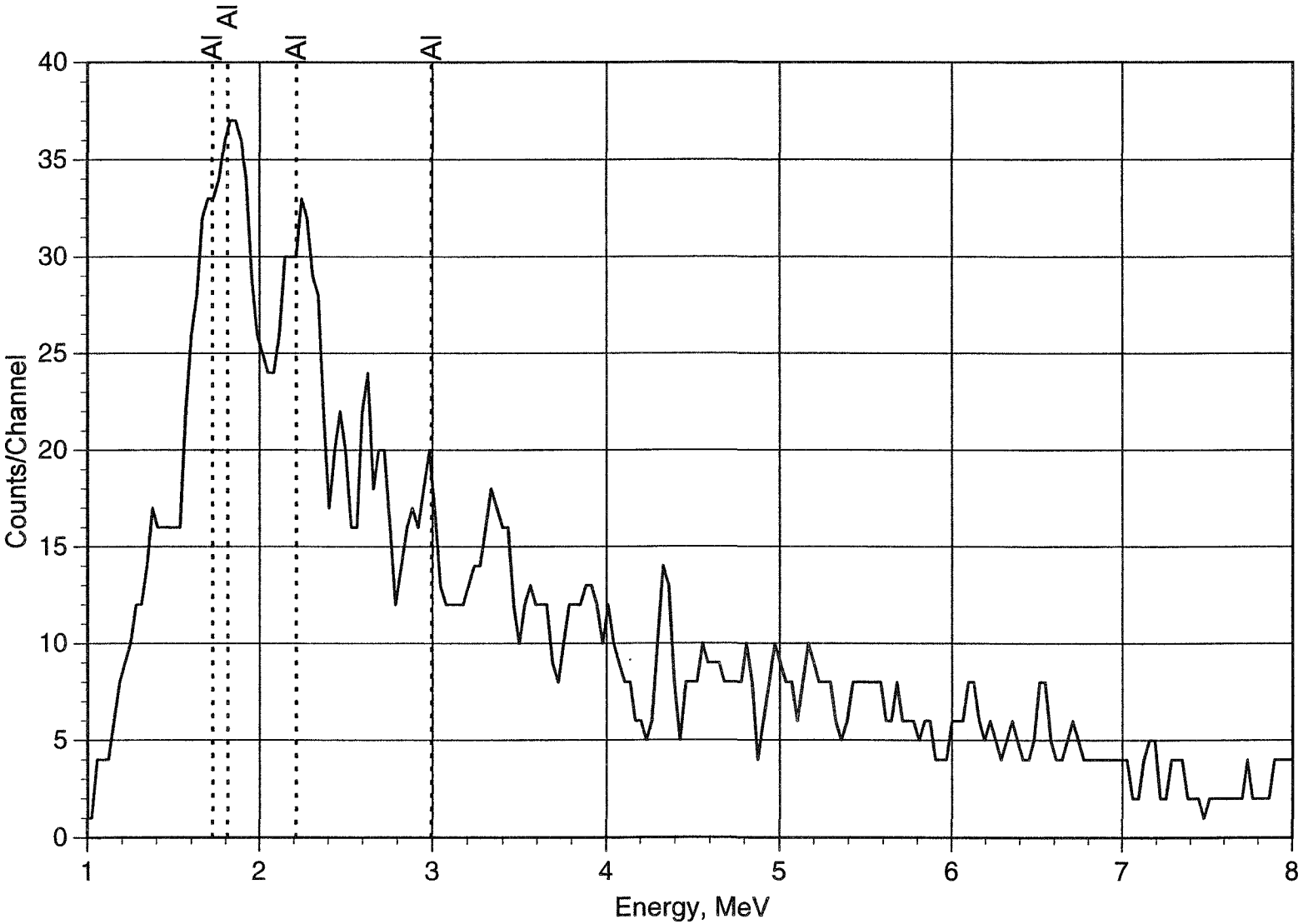

Figure 15. EGRIS energy spectrum time-selected from location of aluminum object

an advantage over the EGRIS mode, since the fission neutrons, unlike the fission gamma rays, do not have to be distinguished from spectra caused by other reactions. However the fission neutrons have a wide range of velocities and do not lose much energy in scattering, which cause substantial degradation in spatial resolution and difficulty in distinguishing the fission neutrons from incident APSTNG neutrons; these effects are exacerbated by the low energy resolution and high gamma-ray sensitivity of typical fast-neutron detectors. Experiments performed by NDS during the initial advanced concepts stage with plastic neutron detectors and no spectrum unfolding and no collimators indicated that the EGRIS mode with fission gamma-ray detection was more promising.[3]

Approximately 7 prompt gamma rays, with a total energy of about 7 MeV, are emitted, on average, per U-235 fission. The prompt fission gamma-ray spectrum peaks below 1 MeV, and then decreases approximately exponentially with increasing energy, up to about 7 MeV. This characteristic shape applies approximately to 14-MeV-neutron-induced fission of U-235, U-238, Pu-239, Pu-240, Pu-241, and Pu-242. The lowest-energy gammas in this spectrum are undetectable against background and the higher-energy gammas are too few to detect; thus, we focus on the 1-3 MeV region as the range of interest. In the 1-3 MeV range, about 2.4 gamma rays are emitted per fission. The U-238 cross section for fission by neutrons in the 14 MeV region is about 1 barn, about one-half the value for U-235.

Figure 16 shows the measured EGRIS prompt gamma-ray spectrum from APSTNG-induced fission in U-238. The dashed line shows the characteristic prompt fission gamma signature obtained from these data. The U-238 object was a rectangular parallelopiped, 12.7 cm deep, 7.6 cm wide and 7.6 cm high. The front face of the uranium block was located 69.2 cm from the neutron source, and the front face of the double-ended gamma-ray detector was 35.6 cm from the axis of the APSTNG interrogation cone, formed by a 3.2-mm diameter aperture over the alpha window. These data were collected for 60 minutes at a neutron source strength of 6×10^6 n/s.

EGRIS spectra measured for enriched U are similar to Fig. 16, but without the two superimposed peaks. These two small peaks result from the U-238 daughter Pa-234m decay lines at 0.766 and 1.001 MeV manifested as background accidental coincidences because of the substantial amount of U-238 present, yielding a (nonimaging) signature for U-238.

The first application considered for EGRIS fission gammas was counting warheads on missiles. Proof-of-principle warhead detection gave favorable results, as described in Appendix A. When it became evident that active neutron interrogation of nuclear warheads would not likely be an allowed treaty verification procedure, interest turned to possible dismantlement and nonproliferation applications. ANL built a generic one-dimensional proof-of-principle mockup including plates of depleted U (as a stand-in for all fissionable materials), ammonium bicarbonate (to simulate high explosives), high-density plastic foam, and Li-6 fluoride powder.

Scans over this mockup have been performed in the EGRIS mode using a very small alpha aperture to enhance spatial resolution. It was possible to coarsely identify boundaries of the 5-cm wide strips of fissionable materials and to detect (but not image) boundaries of the non-fissionable materials (explosives and plastics).

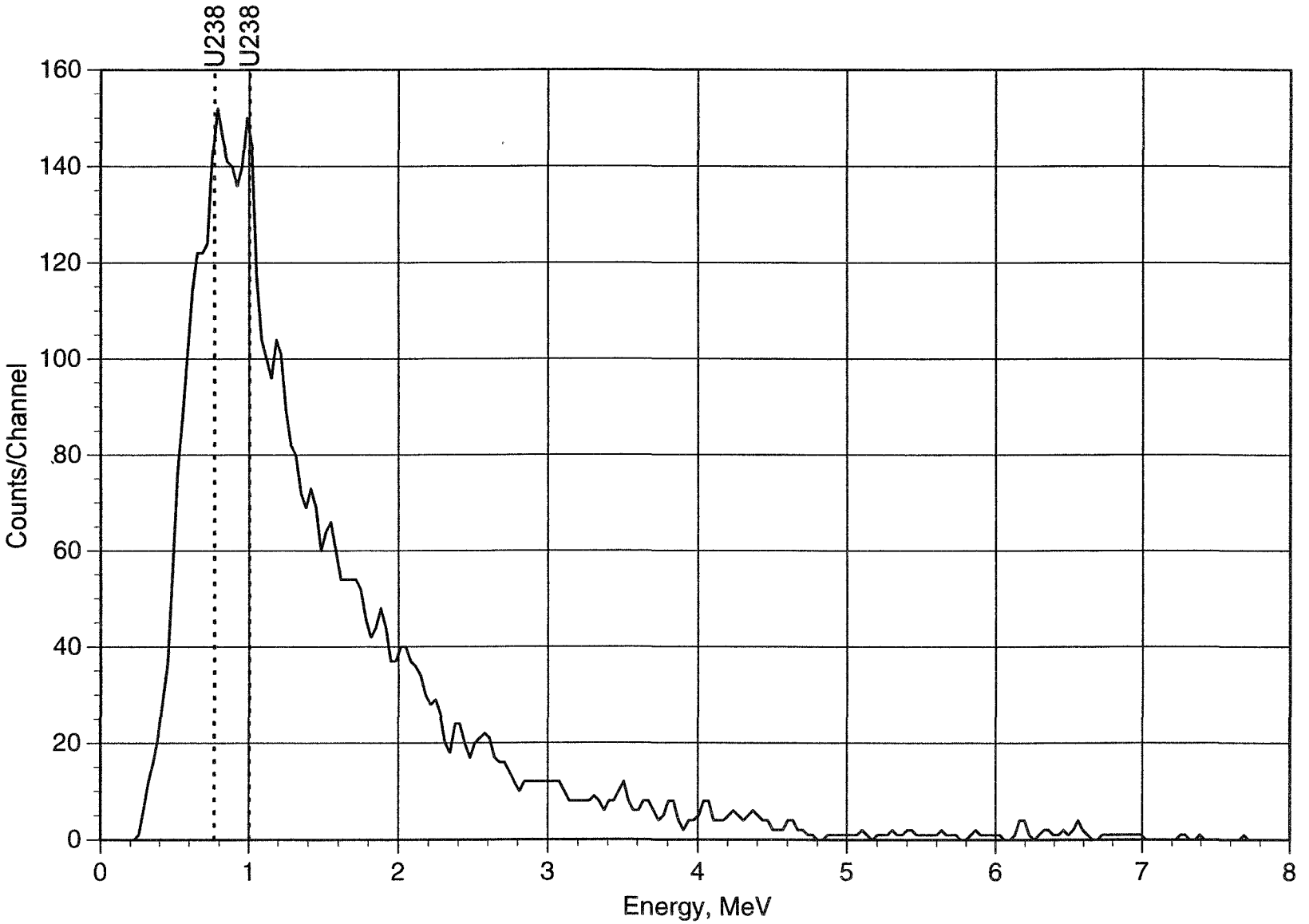

Figure 16. EGRIS energy spectrum measuered for U-238 fission

4.3 CW Munitions Identification Demonstration

This demonstration was performed prior to redirection of DOE funding to exclude chemical warfare (CW)-related activities. ANL prepared surrogates for CW agents HD (mustard gas), GB (volatile nerve gas), and VX (persistent nerve gas) according to simulation formulas made available by another national laboratory, constructed mockups of munitions containing these agents and containing high explosives (HE), measured the simulated munitions using the APSTNG, and attempted to identify each one from the data alone. First, however, we measured APSTNG spectra for the elements of munitions interest: chlorine, phosphorus, sulfur, fluorine, and iron. These reference EGRIS spectra are shown in Figs. 17-21. The spectra for Cl, F, and Fe were obtained from the materials LiCl, ^{6}LiF, and steel, respectively. The spectral peak at 0.85 MeV is due to iron accidental counts from steel in the neutron tube. (Data were not time-sorted to discriminate against this source of iron gammas.)

The surrogate mix formulas for HD, VX, and GB used various combinations of the liquid chemicals dimethyl sulfide, dichloroethane, perfluoro-methylcyclohexane, heptane, triethyl phosphite, dimethyl sulfide, and propylamine. MSDS's for these chemicals were obtained and handling requirements were determined in meetings with ANL ESH representatives and the RE Experiment Safety Review Committee. Since these chemicals are somewhat volatile, computations were made of airborne concentrations in case of spillage and of container cover gas pressures. An experiment safety plan was written that contained operational procedures, checksheets for chemical transfers, and emergency procedures. After facility tours, procurement of protective aprons, gloves, and goggles for experiment personnel, and installation of an eyewash station in the laboratory in addition to an existing emergency shower, the plan was approved.

The surrogate chemicals were mixed in an ANL chemistry laboratory and placed in sealed 2.3-l glass safety bottles with Teflon-lined caps for use. The liquid level in each bottle was specified to leave sufficient head space to avoid significant overpressure. APSTNG EGRIS measurements were made of the individual bottles with and without a steel collar 34.5 cm long by 17.8 cm outer diam, with 1.9 cm wall (to simulate the steel wall thickness of a 155-mm howitzer shell), using our double-ended NaI detector. A new alpha window aperture 19.4 mm in height and 9.9 mm wide that provided coverage of the oblong munition shape was made specifically for the CW munition detection demonstration. Data were taken with the surrogate centered on the correlation cone axis 61.5 cm from the neutron tube target, the gamma detector was aligned along the cone axis a distance of 52 cm from the surrogate, the neutron output rate was ~ 3×10^{6} n/s, and the measurement time was 1 hour.

Shown in Figs. 22-24 are the resulting spectra for the HD, GB, and VX surrogates, respectively, without a steel collar. In Fig. 25 is the spectrum for ammonium bicarbonate, used here as a surrogate for high explosives (HE). Ammonium bicarbonate has element ratios typical of common explosives, but has about half the density. There are a relatively large number of gamma peaks that tend to overlap at the energy resolution of our NaI detector. For this reason, basic minimum-variance spectral matching tests were performed on the data sets. Using these simple tests, the three CW surrogates could be reliably distinguished from the HE surrogate, the HD surrogate could be reliably distinguished from the surrogates of VX and GB, but the VX and GB surrogates could not be reliably distinguished from each other.

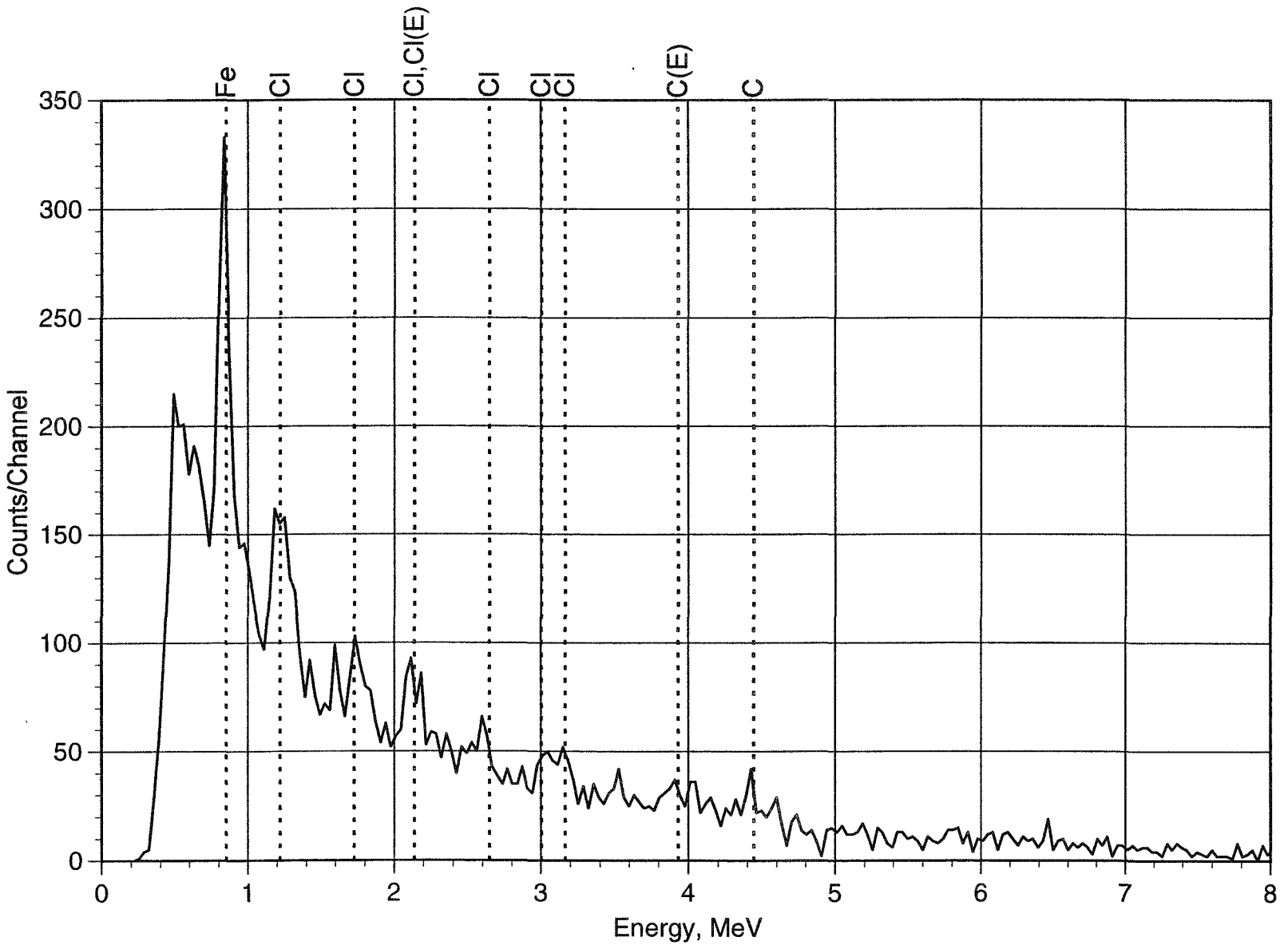

Figure 17. Reference EGRIS energy spectrum for chlorine (LiCl)

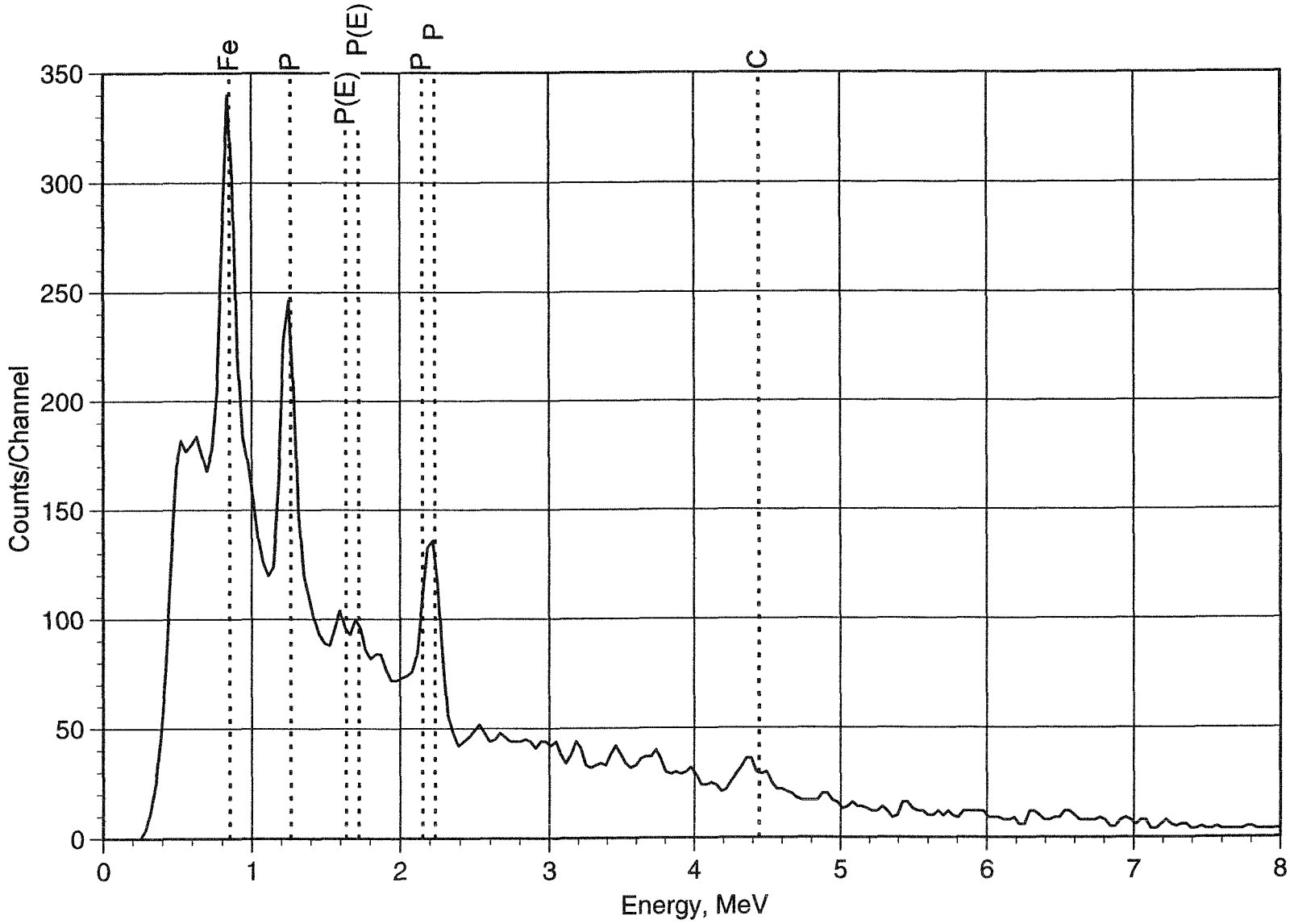

Figure 18. Reference EGRIS energy spectrum for phosphorous

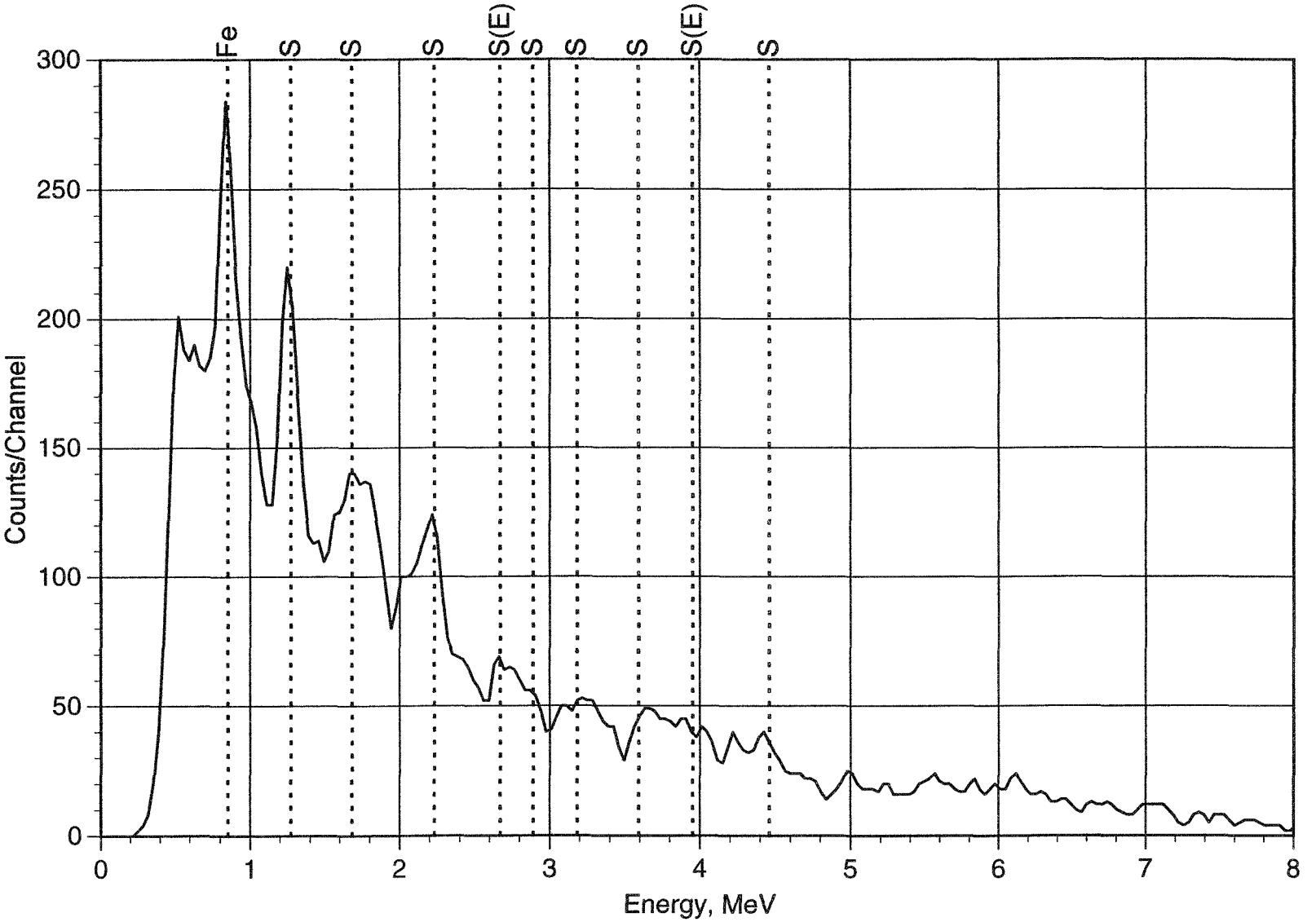

Figure 19. Reference EGRIS energy spectrum for sulphur

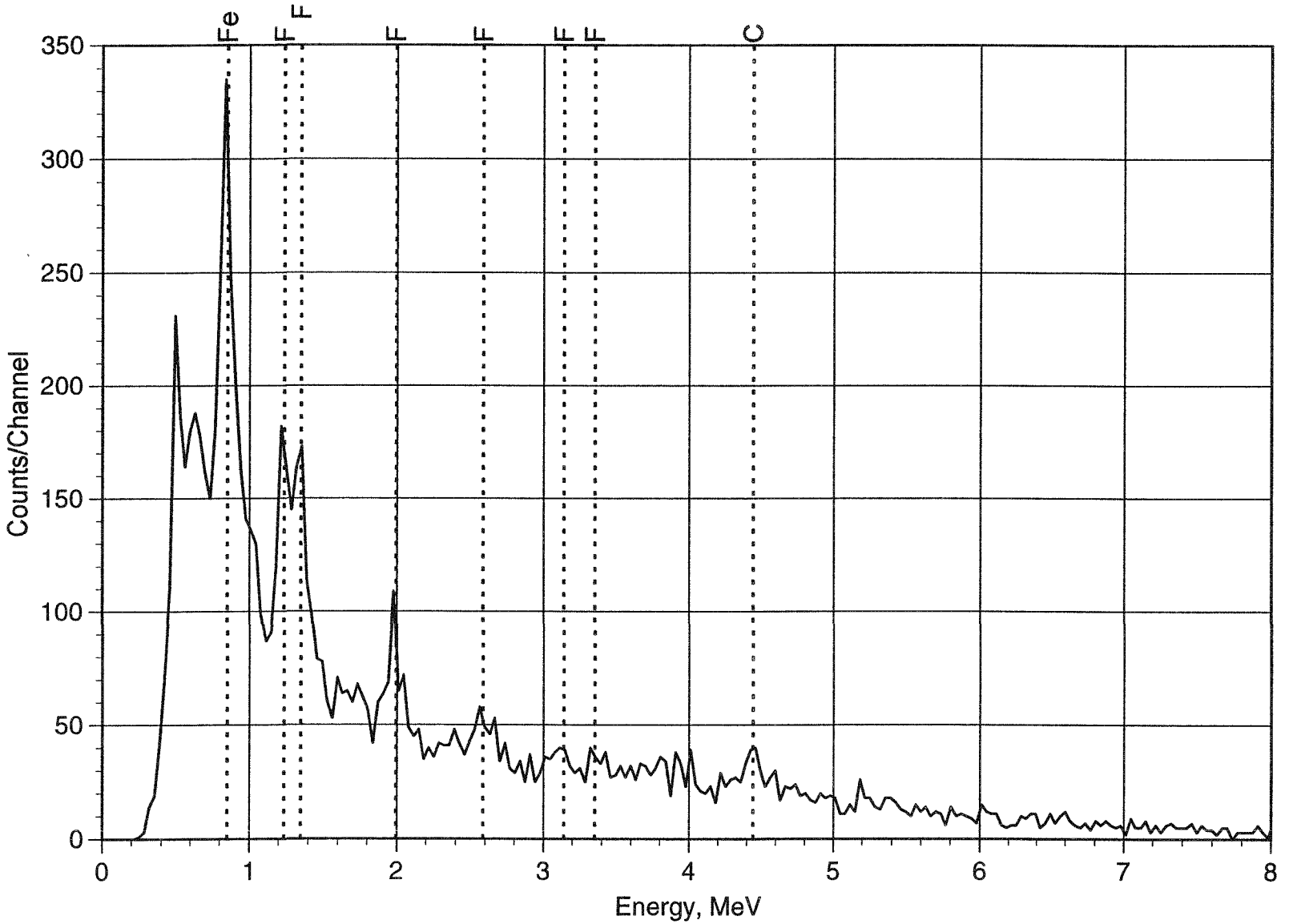

Figure 20. Reference EGRIS energy spectrum for fluorine (^{6}LiF)

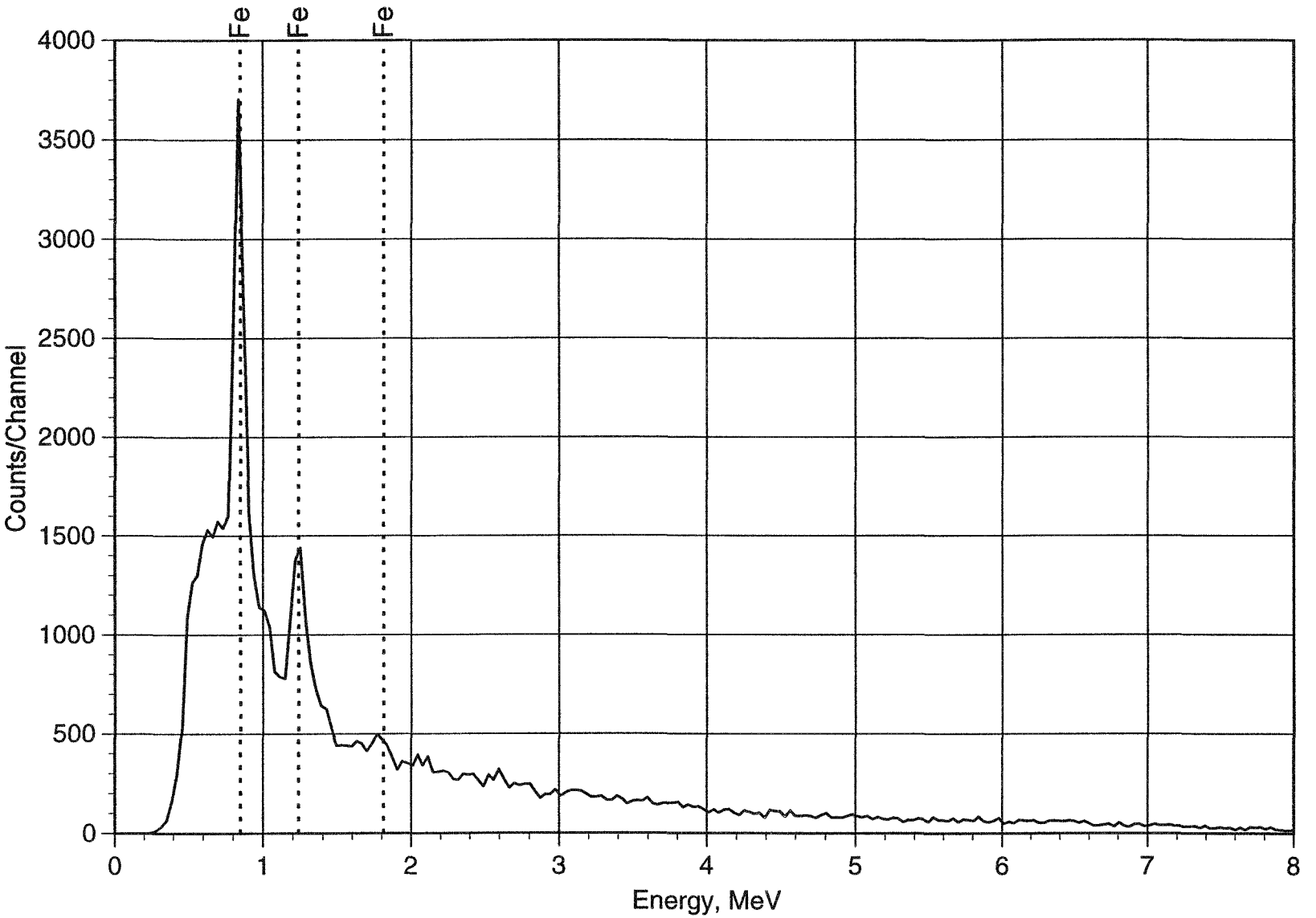

Figure 21. Reference EGRIS energy spectrum for iron (steel)

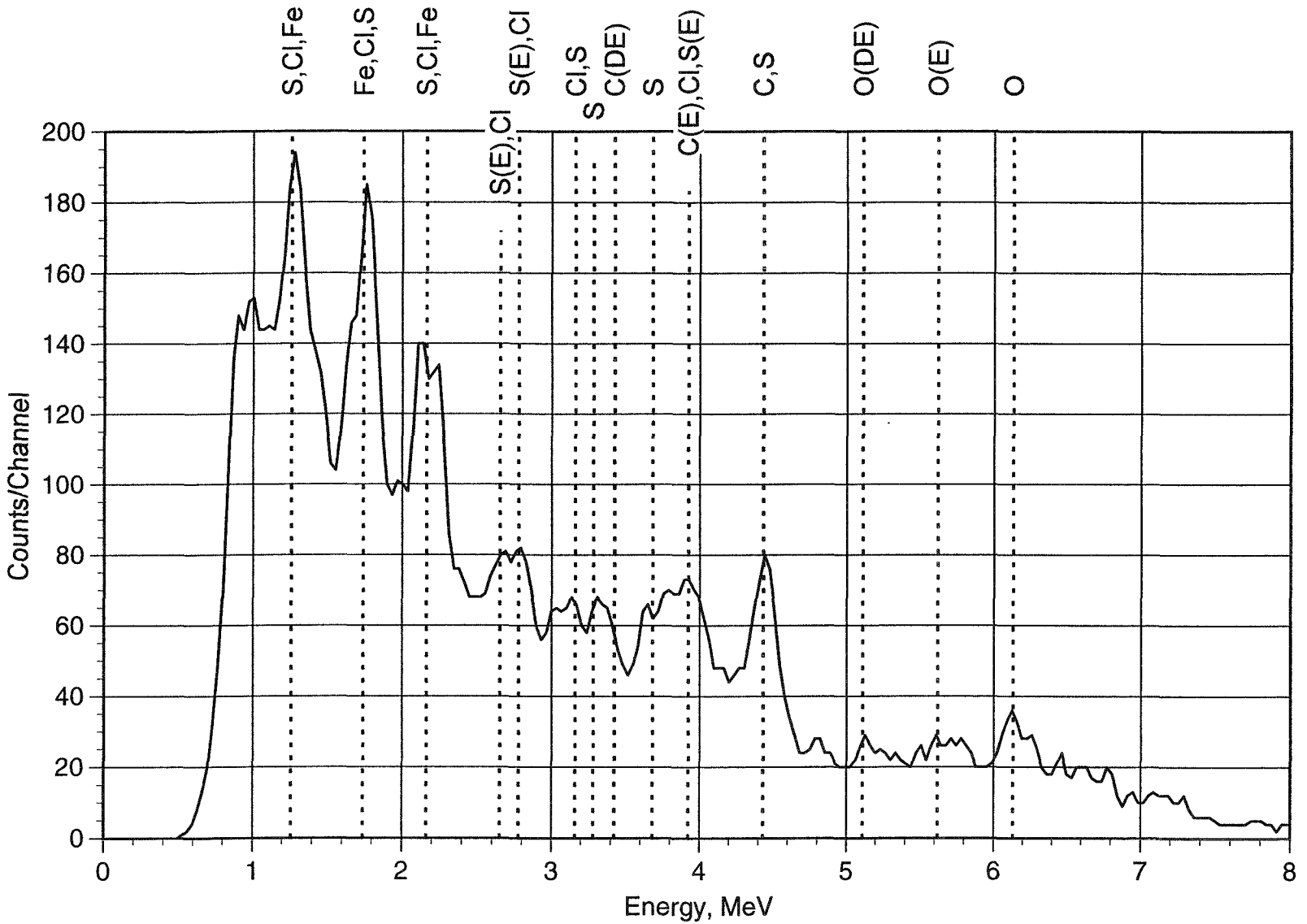

Figure 22. EGRIS energy spectrum for HD surrogate

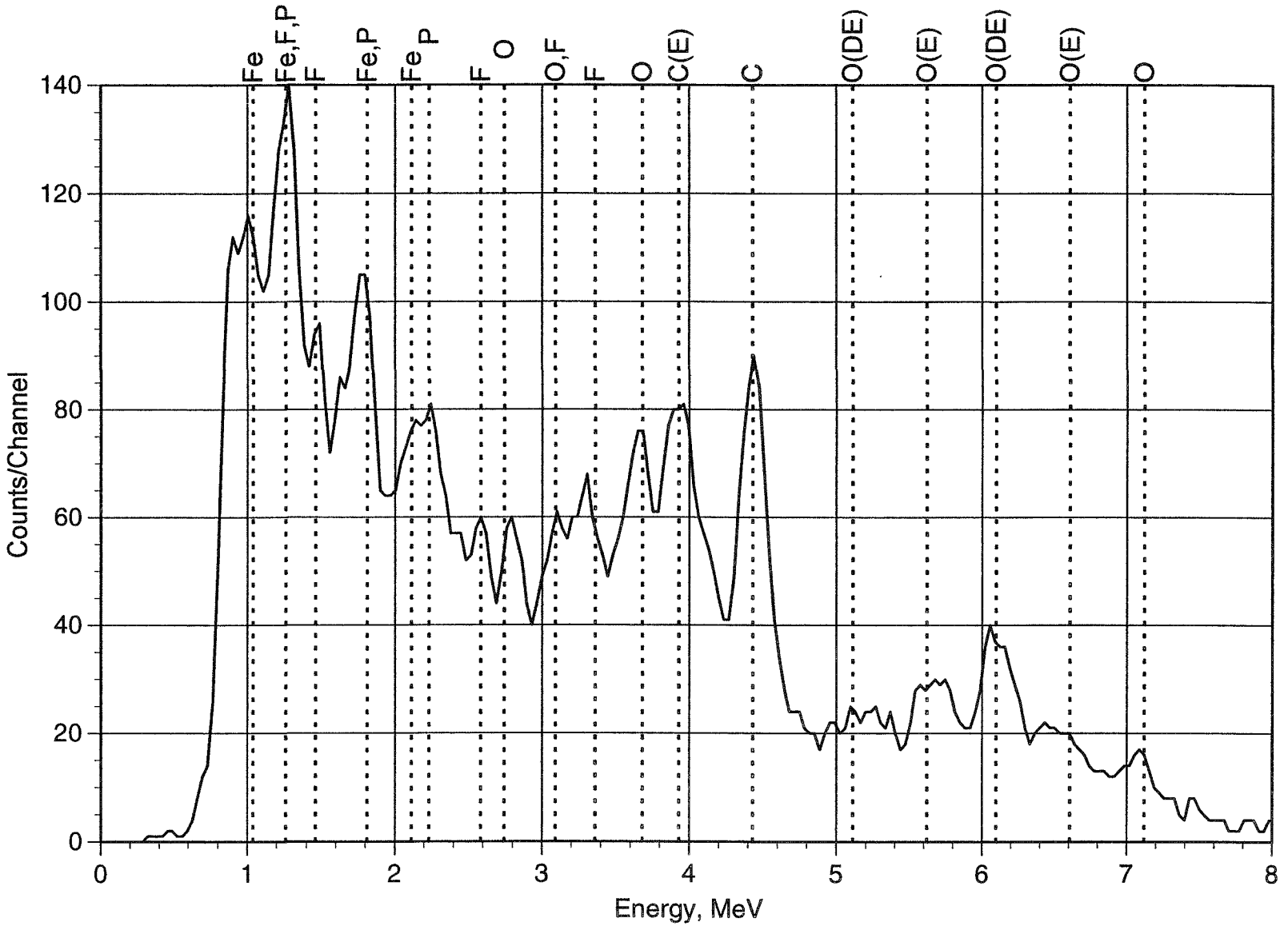

Figure 23. EGRIS energy sectrum for GB surrogate

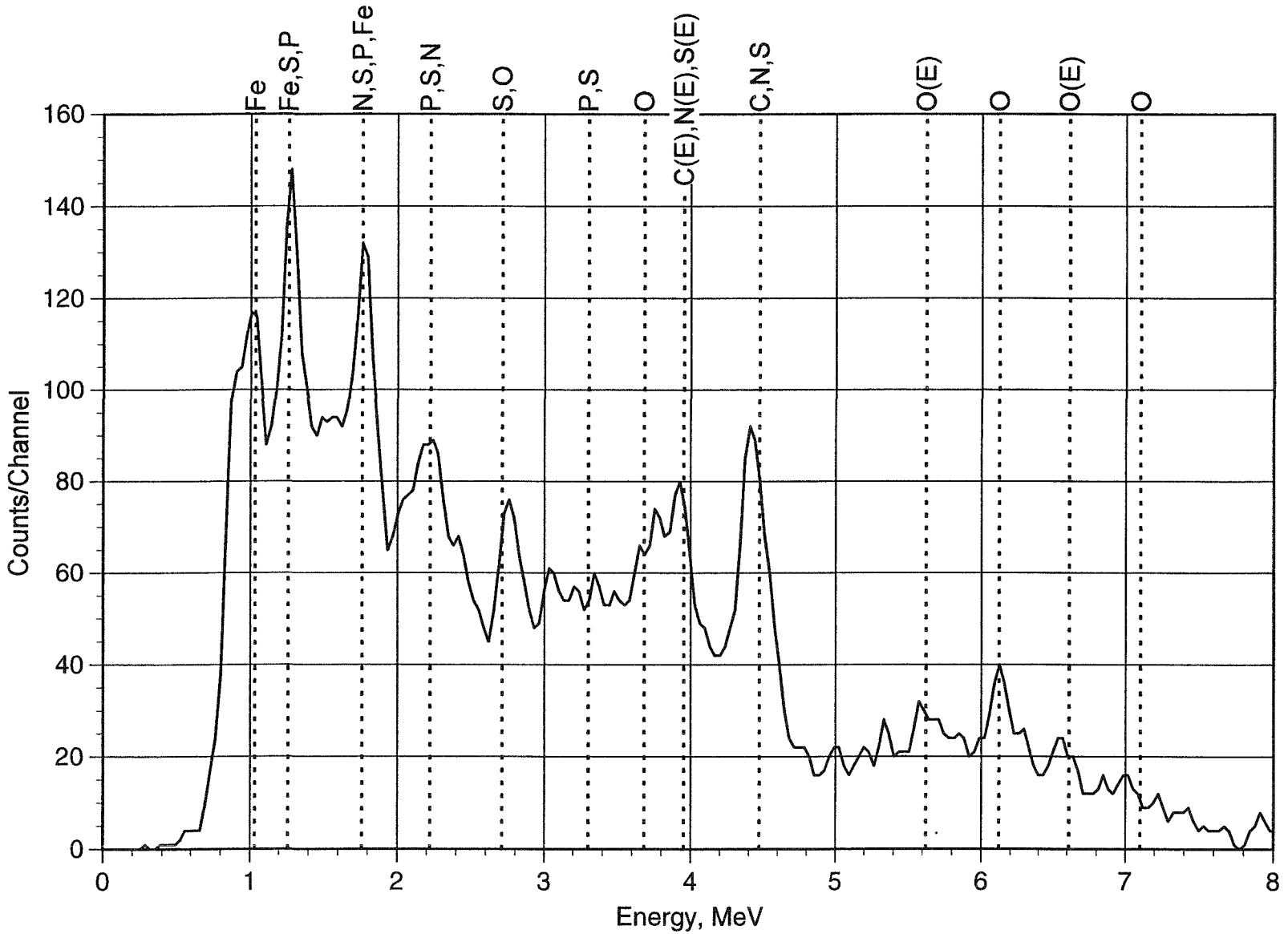

Figure 24. EGRIS energy spectrum for VX surrogate

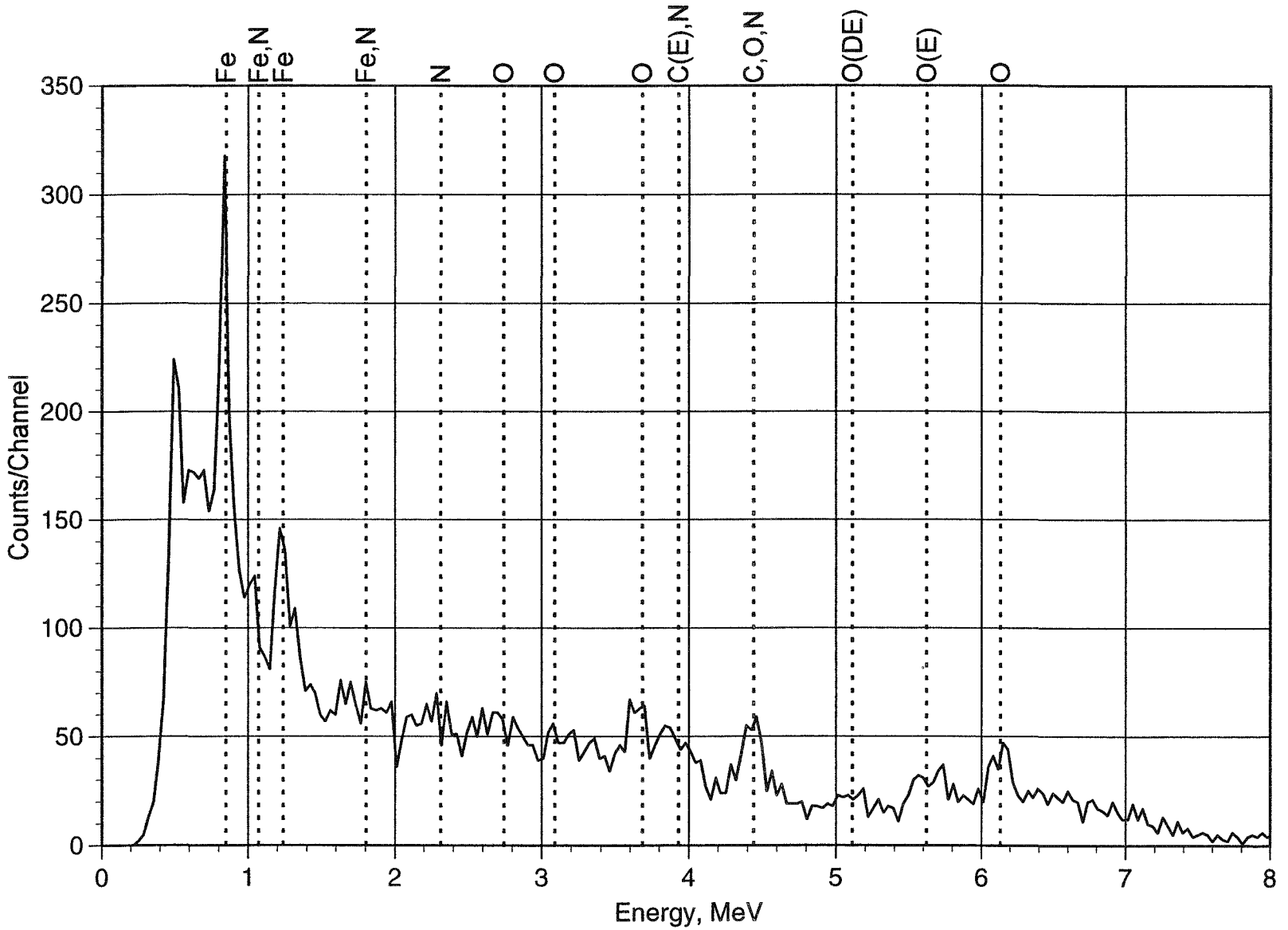

Figure 25. EGRIS energy spectrum for HE surrogate (NH_4HCO_3)

These measurements were repeated with the steel collar around each bottle. Gamma-ray Compton scattering in the steel collar decreased the separation and relative heights of the spectrum peaks. For these data, the HD, VX, and GB surrogates could be reliably distinguished from the high-explosives simulant, but could not be reliably distinguished among themselves. Fig. 26 shows the spectrum from the HD surrogate with steel collar and Fig. 27 shows the spectrum from the HE surrogate.

After analysis of the data had been completed, the detailed mix formulas were checked against the elemental ratios of the actual agents. It was found that the atom ratios of key identifying elements were not accurately simulated in the surrogate mixes. Table I lists the elemental compositions of the CW surrogate mixes used and the actual agents. There are clear discrepancies between surrogates and agents in the atom ratios of: Cl/C (HD), F/C and P/C (GB), and N/C, P/C and S/C (VX). In fact, the VX value of the P/C ratio is much better matched by the P/C ratio of the GB simulant than the P/C ratio of the VX simulant.

Table I. CW Surrogate Mixes Used

Component	Formula	Density (g/cm^3)*	Moles	Molar Frac.	Mass (g)	Mass Frac.	Vol (cm^3)	Vol Frac.
HD Simulant								
Dimethyl Sulfide	C_2H_6S	0.8465	12.0768	0.6140	750.4	0.4997	886.5	0.5975
Dichloroethane	$C_2H_4Cl_2$	1.2584	7.5930	0.3860	751.4	0.5003	597.1	0.4025
Total Mix	$C_4H_{10.5}Cl_{1.5}S_{1.2}$	1.0123	19.6698	1.0000	1501.8	1.0000	1483.6	1.0000
HD Agent	$C_4H_8Cl_2S$	1.2741						
GB Simulant								
Perfluoro Methylcyclohexane	C_7F_{14}	1.7977	0.3122	0.0316	109.3	0.0728	60.8	0.0374
Heptane	$CH_3(CH_2)_5CH_3$	0.6845	2.9859	0.3025	299.2	0.1994	437.1	0.2689
Triethyl Phosphite	$C_6H_{15}O_3P$	0.9688	6.5733	0.6659	1092.2	0.7278	1127.4	0.6937
Total Mix	$C_{9.5}H_{22.67}F_{0.66}O_3P$	0.9233	9.8714	1.0000	1500.7	1.0000	1625.3	1.0000
GB Agent	$C_4H_{10}FO_2P$	1.0887						
VX Simulant								
Triethyl Phosphite	$C_6H_{15}O_3P$	0.9694	3.0098	0.1541	500.1	0.3332	515.9	0.2863
Dimethyl Sulfide	C_2H_6S	0.8467	8.0533	0.4123	500.4	0.3334	591.0	0.3279
Propylamine	C_3H_9N	0.7200	8.4688	0.4336	500.6	0.3335	695.3	0.3858
Total Mix	$C_{3.05}H_{56.38}N_{2.81}O_3PS_{2.68}$	0.8329	19.5319	1.0000	1501.1	1.0000	1802.2	1.0000
VX Agent	$C_{11}H_{26}NO_2PS$	1.008						

*Component densities calculated from measured masses and volumes.

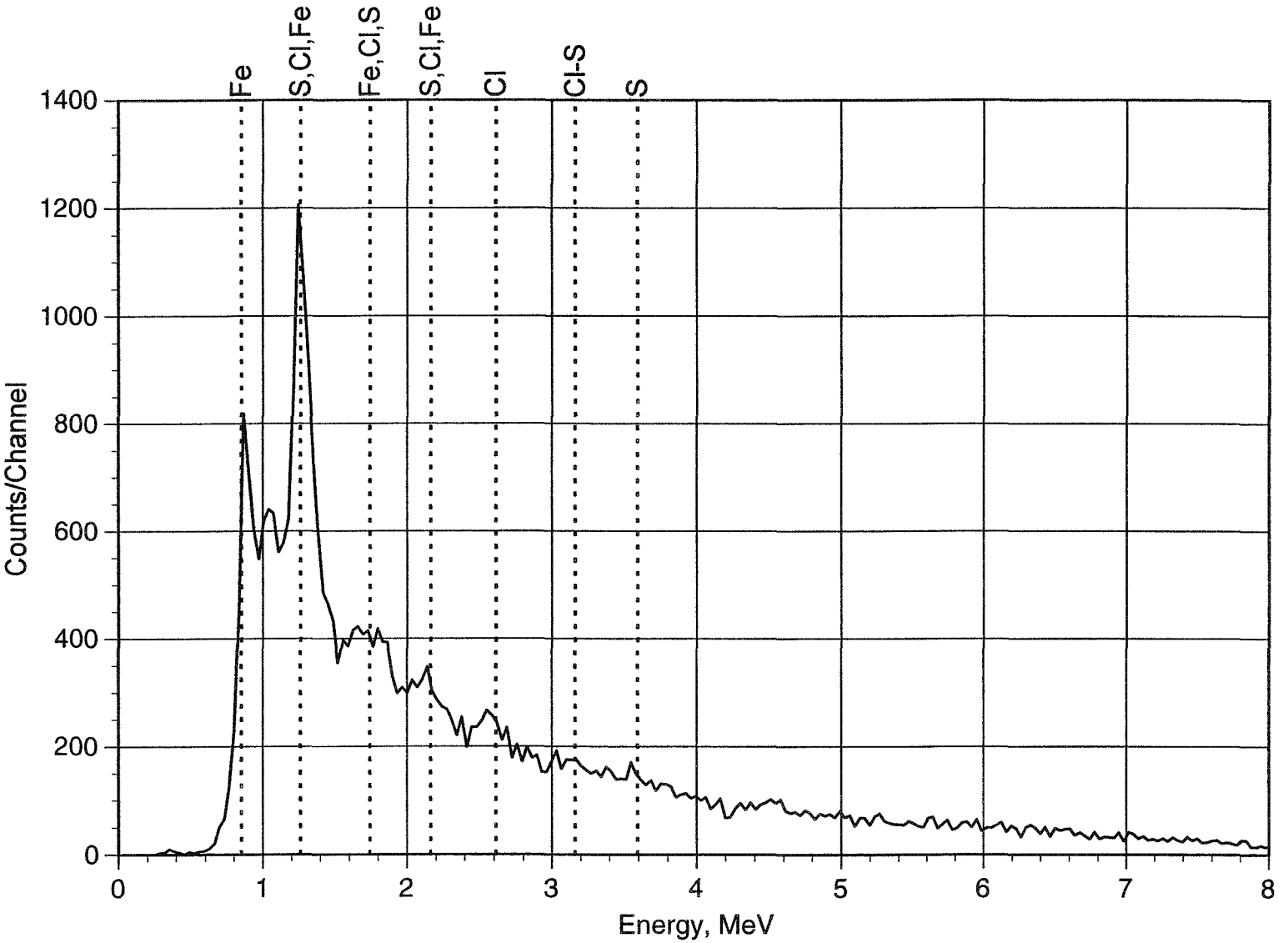

Figure 26. EGRIS energy spectrum for HD surrogate with steel collar

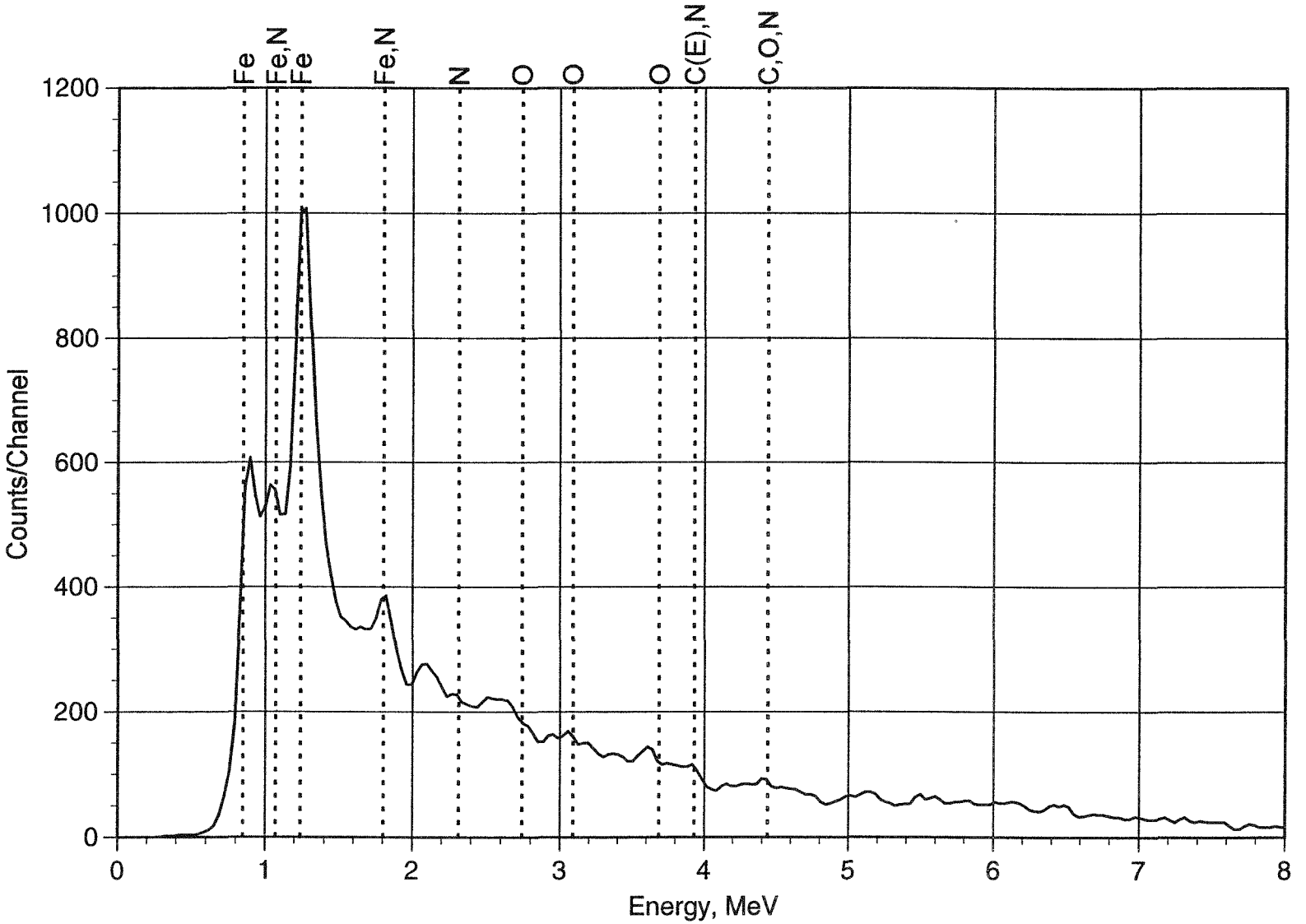

Figure 27. EGRIS energy spectrum for HE surrogate with steel collar

A new set of mixes, of proposed surrogates, was computed that accurately simulated the elemental composition of the agents. The proposed surrogate mixes used the same simulant chemicals, plus dimethyl phosphite in place of trimethyl phosphite as a component for the new GB surrogate.

Table II presents the compositions of the suggested new CW surrogate mixes. A comparison of the formulas for total mix and agent in Table II indicates much more accuracy for the suggested new surrogates than Table I. The only significant discrepancies between simulants and agents for the items in Table II are that the GB and VX surrogates contain 50% more oxygen than the agents. The Table I mix *mass* fractions for HD and VX simulants are the same as the Table II *molar* fractions, indicating that a miscommunication probably occurred in conveying the mix instructions.

Table II. Suggested New CW Surrogate Mixes

Component	Formula	Density (g/cm^3)	Moles	Molar Frac.	Mass (g)	Mass Frac.	Vol (cm^3)	Vol Frac.
HD Simulant								
Dimethyl Sulfide	C_2H_6S	0.8460	9.8532	0.5000	612.2	0.3857	723.7	0.4825
Dichloroethane	$C_2H_4Cl_2$	1.2560	9.8532	0.5000	975.1	0.6143	776.3	0.5175
Total Mix	$C_4H_{10}Cl_2S$	1.0582	19.7063	1.0000	1587.3	1.0000	1500.0	1.0000
HD Agent	$C_4H_8Cl_2S$	1.2741						
GB Simulant								
Perfluoro Methylcyclohexane	C_7F_{14}	1.7870	0.7817	0.0556	273.6	0.1597	153.1	0.1021
Dimethyl Phosphite	$C_2H_7O_3P$	1.2004	10.9440	0.7778	1204.4	0.7031	1003.3	0.6689
Heptane	$CH_3(CH_2)_5CH_3$	0.6840	2.3451	0.1667	235.0	0.1372	343.6	0.2290
Total Mix	$C_4H_{10.43}FO_3P$	1.1420	14.0708	1.0000	1713.0	1.0000	1500.0	1.0000
GB Agent	$C_4H_{10}FO_2P$	1.0887						
VX Simulant								
Triethyl Phosphite	$C_6H_{15}O_3P$	0.9690	4.5853	0.3333	761.9	0.5781	786.3	0.5242
Dimethyl Sulfide	C_2H_6S	0.8460	4.5853	0.3333	284.9	0.2162	336.8	0.2245
Propylamine	C_3H_9N	0.7190	4.5853	0.3333	271.0	0.2057	377.0	0.2513
Total Mix	$C_{11}H_{30}NO_3PS$	0.8786	13.7559	1.0000	1317.8	1.0000	1500.0	1.0000
VX Agent	$C_{11}H_{26}NO_2PS$	1.008						

The element densities of the CW agents, surrogates used, and suggested surrogates are given in Table III. The densities of the key identifying elements fluorine, phosphorus, and chlorine are seen to be much smaller in the surrogates used than in the actual agents.

Because of the redirection of DOE from work on CW, none of the suggested mixtures has been prepared.

Table III. Element Densities of CW Agents and Surrogates

	Atomic Density (g/cm^3)							
Element:	H	C	N	O	F	P	S	Cl
True Agents								
HD	0.06458	0.3848	0	0	0	0	0.2568	0.5679
GB	0.07833	0.3734	0	0.2487	0.1476	0.2407	0	0
VX	0.09880	0.4981	0.05281	0.1206	0	0.1168	0.1209	0
Surrogates Used								
HD	0.06980	0.3181	0	0	0	0	0.2609	0.3622
GB	0.09077	0.4619	0	0.1942	0.05079	0.1253	0	0
VX	0.09481	0.3967	0.06573	0.08013	0	0.05171	0.1432	0
Suggested Surrogates								
HD	0.06621	0.3156	0	0	0	0	0.2106	0.4658
GB	0.07669	0.3505	0	0.3502	0.1386	0.2260	0	0
VX	0.09243	0.4039	0.04281	0.1467	0	0.09468	0.09802	0

4.4 Cocaine Detection Demonstration

One of the series of APSTNG measurements made to study the capability of the system to detect chemicals inside closed containers without sampling, was a demonstration of cocaine detection. The application is the detection of cocaine hidden inside large liquid propane tanks, falsely declared by the shipper to be either "empty" or "full of propane". Detection of cocaine inside a tank declared to be empty is straightforward, because a tank that is really empty would exhibit only the signature of the tank wall composition: the observation of any gamma-ray lines from carbon, nitrogen and oxygen in cocaine hydrochloride would be an automatic detection. (The steel tank signature would partly interfere with detection of chlorine, as described below.)

Because discriminating between cocaine and propane is somewhat more complicated, a direct demonstration of discrimination between cocaine and propane was performed. The scientific basis for this demonstration is as follows: Cocaine hydrochloride ($C_{17}H_{22}Cl\ N\ O_4$) is the form most likely to be smuggled, rather than free-base cocaine ($C_{17}H_{21}\ N\ O_4$). The elemental composition of propane is C_3H_8. Thus, cocaine detection may be focussed on detecting the presence of one or more of the following elements: chlorine, nitrogen, and oxygen. Chlorine has major gamma-ray peaks at 1.22, 1.76, and 2.15 MeV, and a number of smaller peaks between 0.79 and 3.16 MeV (see Fig. 17). Nitrogen has a number of gamma rays, including major peaks at 1.63, 2.31, 4.46, 5.10, and 7.03 MeV. Oxygen has gamma rays from 2.74 to 7.12 MeV, with a major peak at 6.13 MeV (giving rise to single-escape and double-escape pair production peaks at 5.62 and 5.11 MeV). (The nitrogen and oxygen lines are shown in Fig. 25.) Hydrogen has no inelastic scattering. The carbon signature is the 4.43 MeV gamma-ray peak plus single-escape and double-escape pair production peaks at 3.92 and 3.41 MeV (see Fig. 9). The major signature of iron in the steel container is a pair of gamma-ray peaks, located at 0.85 and 1.24 MeV (see Fig. 21).

Polyethylene (C_2H_4) was selected as the simulant for liquid propane, in the form of beads of density 0.576 g/cm^3, yielding a carbon density of 0.492 g/cm^3. This compares favorably with propane, which has a density of 0.501 g/cm^3 and a carbon density of 0.410 g/cm^3. Table IV describes candidate surrogates for cocaine and cocaine hydrochloride made from commercially available plastic feedstocks and carbon (C), including polyacrylonitrile (PAN), poly(1,4 butylene terephthalate) (PBT), polymethyl methacrylate (PMMA), polyethylene (PE) and polyvinyl chloride (PVC). The presence of black carbon granules in two of the candidates in Table IV has the potential of being used for visual estimates of the mix uniformity, but only the candidate labeled "Cocaine HCl (used)" was made.

The materials were separately ground to a small grain size in a blender with dry ice. The polyethylene was tough enough to require further milling to get a relatively small grain size. As shown in Table IV, the materials were then combined in ratios such that the final mixed product duplicated the relative elemental densities of cocaine hydrochloride. In order to ascertain the actual composition and composition variation of the surrogate, chemical analyses of samples from the top, middle, and bottom of the container were performed. The results, shown in Table V, indicate the surrogate mix is uniformly distributed and is an excellent "nuclear" simulant of cocaine HCl.

Table IV. Candidate Surrogate Mixtures of Cocaine [$C_{17}H_{21}NO_4$] and Cocaine Hydrochloride [$C_{17}H_{22}ClNO_4$]

Drug Simulated	Component	Relative No. Moles	Per Cent by Weight	Atoms Contributed				
				C	H	Cl	N	O
Cocaine	PMMA	2	66.0	10	16	---	---	4
(suggested)	PAN	1	17.5	3	3	---	1	---
	PE	0.5	4.6	1	2	---	---	---
	C	3	11.9	3	---	---	---	---
	Total Mix		100.0	17	21	---	1	4
Cocaine	PAN	1	15.6	3	3	---	1	---
HCl	PVC	1	18.4	2	3	1	---	---
(used)	PMMA	1	29.5	5	8	---	---	2
	PBT	0.5	32.4	6	6	---	---	2
	PE	0.5	4.1	1	2	---	---	---
	Total Mix		100.0	17	22	1	1	4
Cocaine	PMMA	2	58.9	10	16	---	---	4
HCl	PAN	1	15.6	3	3	---	1	---
(suggested)	PVC	1	18.4	2	3	1	---	---
	C	2	7.1	2	---	---	---	---
	Total Mix		100.0	17	22	1	1	4

Table V. Sample Analysis of Cocaine Hydrochloride Surrogate

Sample Position	Element Wt. %					Stoichiometry[d]
	C[a]	H[a]	N[a]	Cl[b]	O[c]	
A, Top	59.2	6.45	4.55	10.3	19.5	$C_{17}H_{22.0}N_{1.1}O_{4.2}Cl_{1.0}$
	±1.7	±0.20	±0.13	±0.5	±1.8	
B, Middle	56.4	6.39	3.94	12.4	20.9	$C_{17}H_{23.0}N_{1.0}O_{4.7}Cl_{1.3}$
	±1.7	±0.20	±0.12	±0.6	±1.8	
C, Bottom	60.5	6.44	5.36	12.6	15.6	$C_{17}H_{21.8}N_{1.1}O_{3.3}Cl_{1.2}$
	60.7	6.52	4.14	±0.6	±1.8	
	60.6	6.48	4.75			
	±1.8	±0.20	±0.12			
Bulk Average[e]	58.7	6.44	4.41	11.8	18.6	$C_{17}H_{22.3}N_{1.1}O_{4.0}Cl_{1.2}$
	±5.3	±0.12	±1.07	±3.2	±6.3	±2.1 ±0.3 ±1.4 ±0.3
Target Values[f]	60.1	6.53	4.12	10.4	18.8	$C_{17}H_{22}N_{1.0}O_{4.0}Cl_{1.0}$

[a] Measured with LECO Model 900 CHN Analyzer.

[b] Measured by Ion Chromatography after Oxygen Bomb Combustion.

[c] Calculated by difference.

[d] Elemental composition normalized to C_{17} basis.

[e] Composition calculated from average results from samples A, B, and C.

[f] Composition corresponding to cocaine hydrochloride stoichiometry.

The cocaine HCl surrogate in its cylindrical bottle has a net density of 0.709 g/cm^3, with a carbon density of 0.426 g/cm^3 (similar to propane, so the carbon signals will approximately cancel), an oxygen density of 0.133 g/cm^3, a chlorine density of 0.074 g/cm^3, and a nitrogen density of 0.029g/cm^3. Thus, we would expect the oxygen to be easiest to detect, the chlorine to be harder to detect, and the nitrogen to be hardest to detect (everything else being equal). Measurements were made with small samples compared to those expected in the actual application. The interrogated masses were 718 g for the cocaine hydrochloride simulant and 671 g for the liquid propane simulant.

The alpha scintillator window aperture was 9.9 mm wide and 19.4 mm high. Each sample was enclosed in a 30.5 cm high steel cylinder, 20.3 cm o.d., with 0.64 cm wall to include the effects of tank material. Because of uncertainty in actual geometry, the sample was enclosed by steel, rather than being placed behind a steel plate. This "steel enclosure" geometry, which prevented time-rejection of the steel signature, thus provided a conservative demonstration arrangement. If the actual application were to involve inspection of material behind a large diameter tank wall, the gamma-ray signature from the material to be evaluated could be time-discriminated from the tank wall signature, and this rejection of steel background would facilitate discrimination between cocaine and propane.

Measurement geometry was identical for the two cases: Source to center-of-object distance was 30.5 cm, and distance from the detector front face to center of the object was also 30.5 cm. The neutron source rate was ~ 4×10^6 n/s for the propane simulant in steel, and somewhat less for the cocaine hydrochloride simulant in steel. Counting time for each of these two relatively small samples was 60 minutes. For analysis, the two sets of numerical spectrum data were normalized to equal alpha counts (this is equivalent to normalizing to equal time-integrated neutron fluxes). Figure 28 shows the result of subtracting the normalized energy spectrum of simulated propane from the energy spectrum of simulated cocaine hydrochloride. Note that this subtraction results in approximately zero net counts in the ROI of the carbon peak, providing an independent check that the normalization was carried out properly. The net spectrum from this subtraction results from the presence of chlorine, nitrogen and oxygen in the cocaine hydrochloride simulant, and shows up clearly in Fig. 28.

The relevant spectrum peaks are marked in Fig. 28. Although the large iron peak located at 1.24 MeV is subtracted out by the spectrum comparison, it introduces some statistical uncertainty in the significance in the main chlorine ROI just above 1 MeV, but the chlorine identification is conclusive, and is confirmed by higher energy chlorine signature peaks. Nitrogen also is present. The large high-energy oxygen ROI is quite prominent. The difference in counts in the oxygen ROI from measurements with these two simulants is statistically very significant: The ratio of counts in the higher-energy portion of the oxygen ROI (defined as a window from 5.44 to 6.40 MeV) to the counts in a carbon ROI (3.76 to 4.66 MeV) is 0.9497 ± 0.014 for the cocaine hydrochloride simulant case, but only 0.5657 ± 0.017 for the propane simulant case. (Uncertainties given are for count statistics alone.)

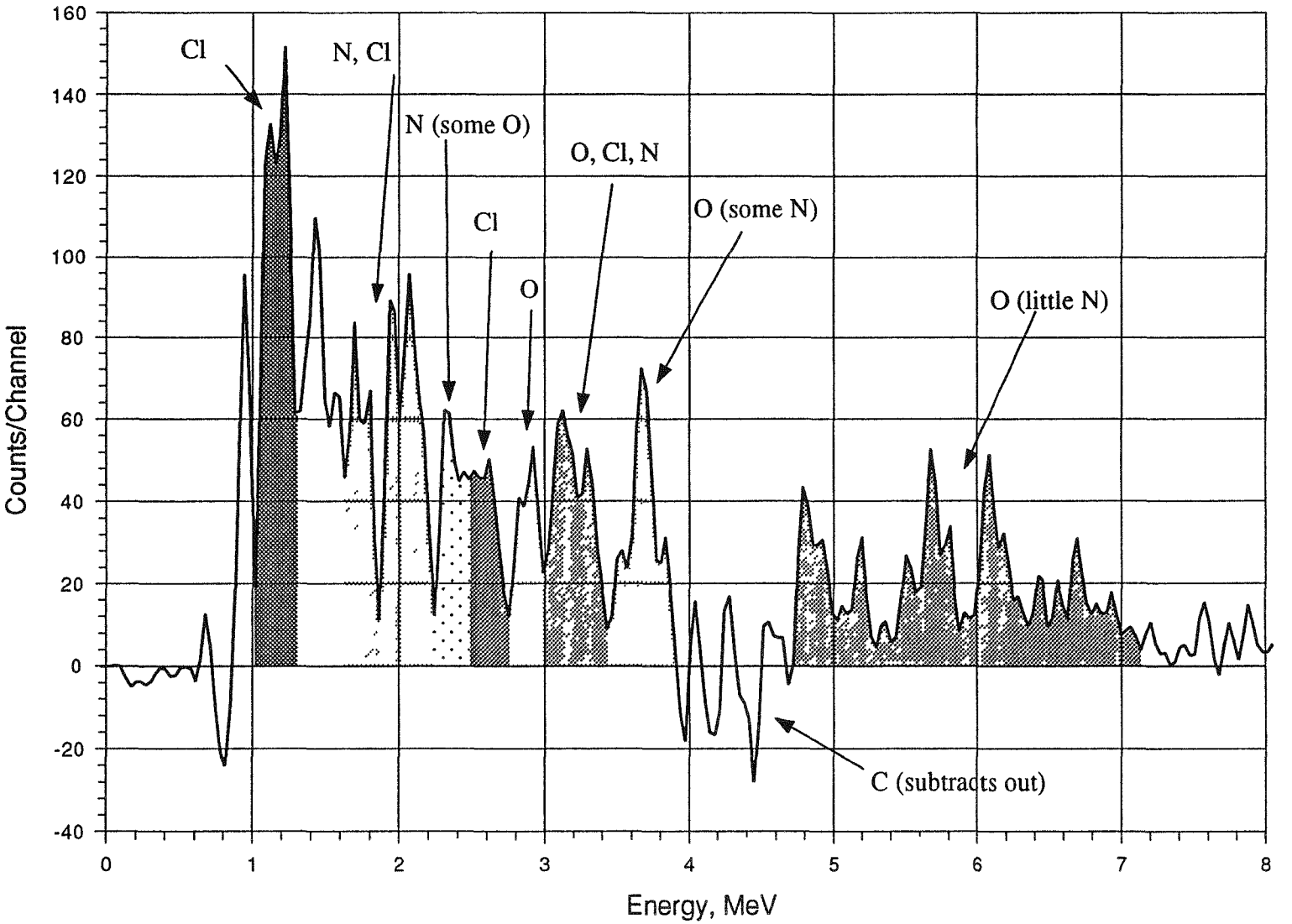

Figure 28. Detection of cocaine hydrochloride in propane by spectrum subtraction

4.5 Radwaste Benchmark Experiments at RWMC

One of the applications under consideration for APSTNG technology is the measurement of radioactive waste. The APSTNG capability to coarsely determine locations and shapes of fissionable materials and toxic chemicals by EGRIS measurements of fission and inelastic gamma rays could be useful in characterizing radioactive waste in assay of soils and drums. Current radwaste assay methods focus on high-energy x-radiography and passive measurements of radiation, rather than material-specific location or identification of non-radioactive elements or chemicals. An APSTNG system could supplement other technologies in characterization of waste containers. If attenuation by materials in the container is small, passive radiation detection will be substantially more sensitive than active neutron interrogation. If attenuation is large, the opposite will be true; for example, the 186-keV U-235 gamma ray and the 414-keV Pu-239 gamma ray are much easier to attenuate than the prompt fission gamma rays resulting from APSTNG interrogation. The use of active neutron interrogation for identification of toxic chemicals, such as chlorinated compounds, will help classify the radwaste as to mixed waste content, and the ability to detect local regions of water will address criticality issues.

D. Akers of INEL was contacted concerning possible radwaste benchmark experiments using our APSTNG system at the INEL Radioactive Waste Management Center (RWMC). A preliminary RWMC site visit in December, 1993 determined that the best option was to measure radwaste and calibration drums from the Stored Waste Examination Pilot Plant (SWEPP), locating the APSTNG system in the nearby TRUPACT building. The APSTNG visit had to be scheduled in accord with the requirements of the RWMC as an operating facility, and the visit was conducted the last week of September, 1994.

4.5.1 Preparatory Measurements at ANL

ANL selected the SWEPP heterogeneous mixed metals calibration drum configuration for preparatory laboratory measurements at ANL. This configuration consists of a 55-gallon steel drum containing column structures of plates and pipes of steel, lead, copper, and aluminum of various sizes. Three aluminum tubes of 40-mm i. d. positioned at different radii run the length of the drum and allow samples to be inserted inside the drum. A tube insert is provided that can carry a number of nominally 1-g high-purity Pu-239 Nuclear Accident Dosimeter (NAD) sources. Because of SWEPP operational needs for calibration drums, we designed and fabricated a calibration drum of our own, and used it in laboratory experiments at ANL in preparation for the INEL visit. The design of the ANL calibration drum is fashioned after the SWEPP heterogeneous mixed metals drum; however, the ANL drum has 84-mm i.d. sample tubes, to accommodate a wider range of sample items. The ANL drum is described in Appendix B. The top third of this drum is a projection of the cross-sections of the SWEPP drum, from top to bottom, i.e., all of the column structures at various heights in the SWEPP drum are represented as shortened columns filling the top third of the ANL drum. The central third of the ANL drum is left void, to provide space for future configurations. The bottom third of the drum is filled with concrete mortar, similar to a SWEPP concrete sludge calibration drum.

An alpha window aperture 12.7 mm wide and 25.4 mm high was made for the radwaste experiments, to allow some coarse scanning but still provide significant count rates, for the new C-11 neutron tube with 127 mm distance from the target to the window. For the laboratory

preparatory experiments, a LiCl sample of ~ 400 g in a ~ 102 mm high bottle of ~ 76 mm diameter and a depleted U sample 25.4 mm square and 127 mm high were placed inside tubes of the ANL radwaste calibration drum that were aligned along the neutron correlation cone axis. The 55-gallon drum, of diameter ~ 58 cm, was located 38 cm from the neutron tube. The APSTNG neutron rate was kept near 6×10^6 n/s and the runs were 1 hour long.

To avoid background from scattered neutrons in the energy spectrum for the EGRIS time ROIs caused by neutron response of the gamma detector, the gamma detector should be located far enough away from the interrogated object that any scattered neutrons arrive after the gamma rays. The larger the object, the greater this separation distance becomes. For this particular measurement geometry, this criterion gives a separation of 76 cm between the 55-gallon drum and the gamma detector. However this separation would substantially decrease gamma-ray count rate. Thus, for this experiment it was decided to move the gamma detector much closer to increase its count rate and accept some background from scattered neutrons, which provide a continuous contribution to the energy spectrum. The axis of the gamma-ray detector was parallel to the cone axis, and the side of the scintillator was 14 cm from the nearest drum edge, or 43 cm from the drum center. The scattered neutrons were found to distort the flight-time spectra enough that it was necessary to subtract a background flight-time spectrum (measured in a run in which the samples were absent), in order to easily identify the time ROIs.

In one measurement the samples were vertically centered in the top third of the drum, the heterogeneous mixed metals section, with the LiCl sample located in the tube nearest the drum edge, 46 cm from the neutron tube, and the depleted U sample in the tube farthest from the LiCl, 81 cm from the neutron tube. Figures 29 and 30 present the results from this run. In both figures, the prompt fission gamma signature from Fig. 16 is shown as a dashed line, normalized to the 1,001 keV U-238 peak. In Fig. 29, the EGRIS energy spectrum for flight-time channels 62-93, corresponding to the position of the LiCl sample, is seen to exhibit the identifying gamma-ray peaks for chlorine. Fig. 30 is the energy spectrum for flight-time channels 124-139, corresponding to the position of the depleted U sample, showing the enhanced fission gamma-ray signature, along with gamma-ray peaks from chlorine background.

In another measurement the samples were vertically centered in the bottom third of the drum, the concrete sludge section, with samples positioned horizontally as in the previous measurement, except the depleted U sample was in the center tube, 67 cm from the neutron tube. Figs. 31 and 32 show the EGRIS energy spectrum for flight-time channels 60-93, corresponding to the position of the LiCl sample, and that for flight-time channels 93-119, corresponding to the position of the depleted U sample. In both figures, the prompt fission gamma signature from Fig. 16 is shown as a dashed line, normalized to the 1,001 keV U-238 peak. Both figures show the gamma-ray peaks for chlorine, and oxygen gamma-ray peaks from SiO_2 (sand) and residual water in the surrounding concrete mortar. The chlorine peaks are more prominent above the fission gamma signature in Fig. 31 than in Fig. 32. Figs. 30 and 32 illustrate an issue that arises in identifying fissionable materials by the fission gamma-ray spectrum when there are other materials present. Gamma-ray peaks from the other materials must be stripped off if the fission signature is to be normalized in order to make an estimate of the amount of fissionable material present. Also, the accidental count spectrum, and in this case the background spectrum from neutron scattering, must be subtracted.

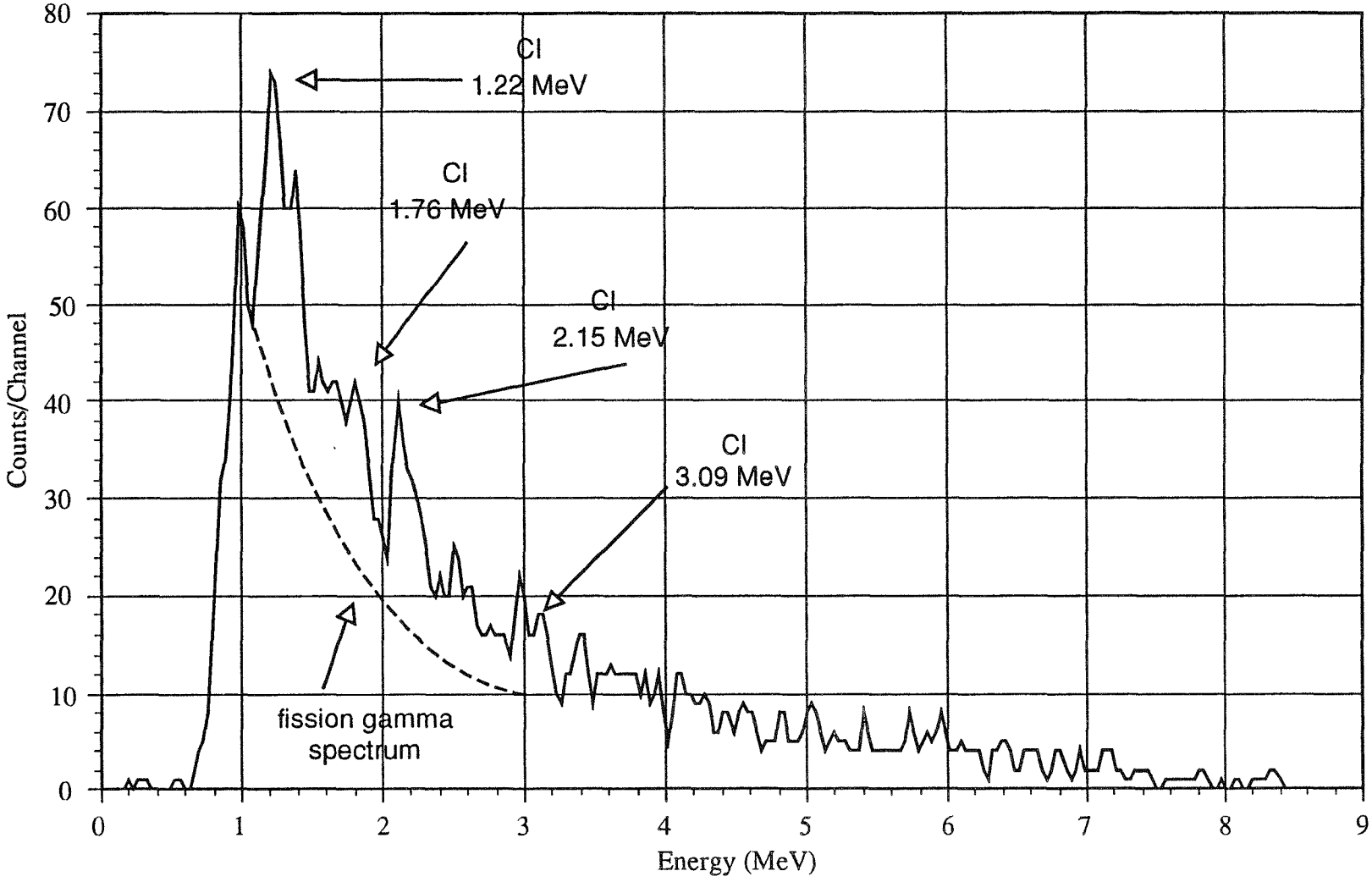

Figure 29. Chlorine and depleted uranium in heterogenous metals section of ANL radwaste calibration drum.
EGRIS energy spectrum for flight-time channels 62-93

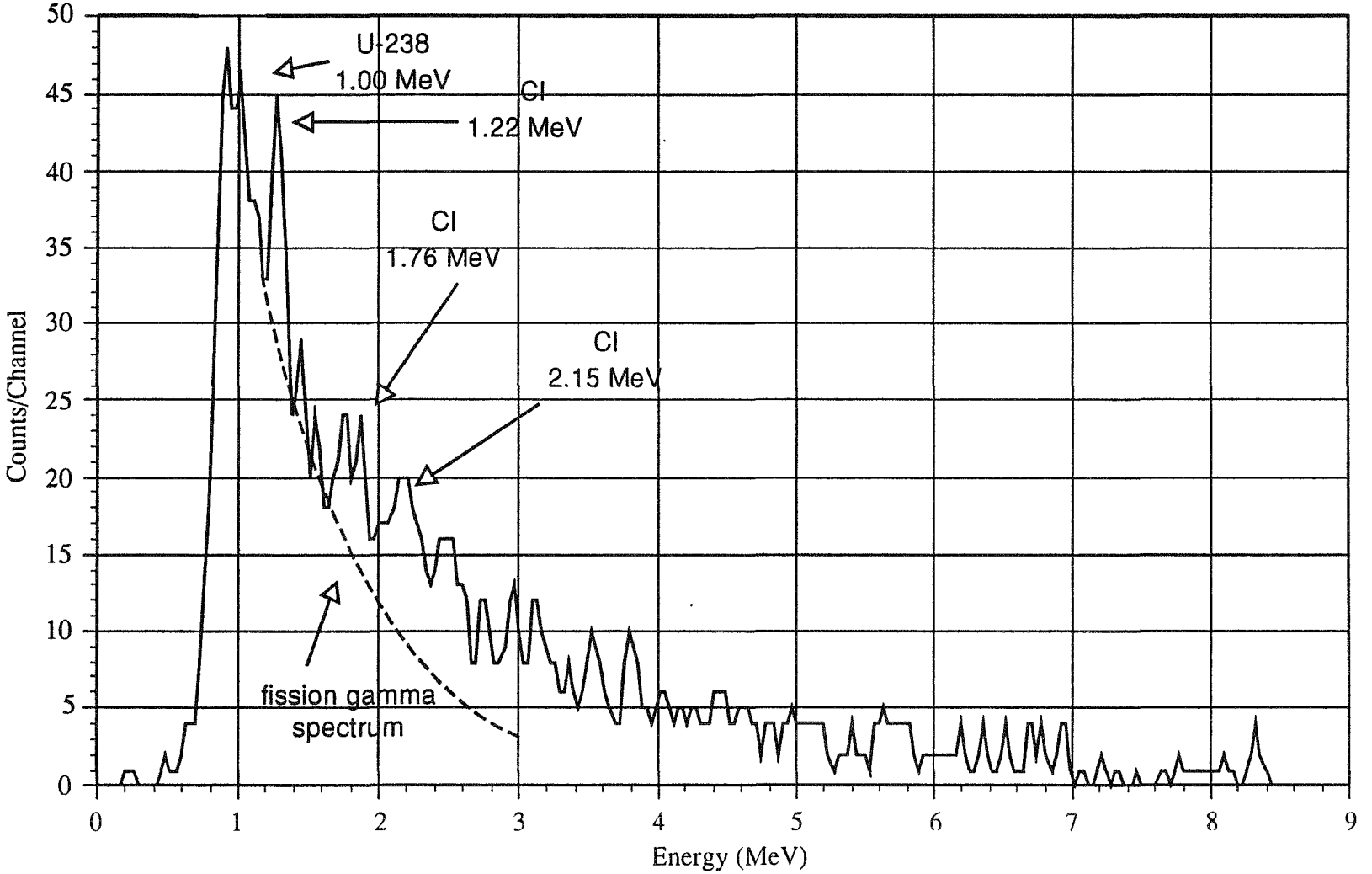

Figure 30. Chlorine and depleted uranium in heterogenous metals section of ANL radwaste calibration drum. EGRIS energy spectrum for flight-time channels 124-139

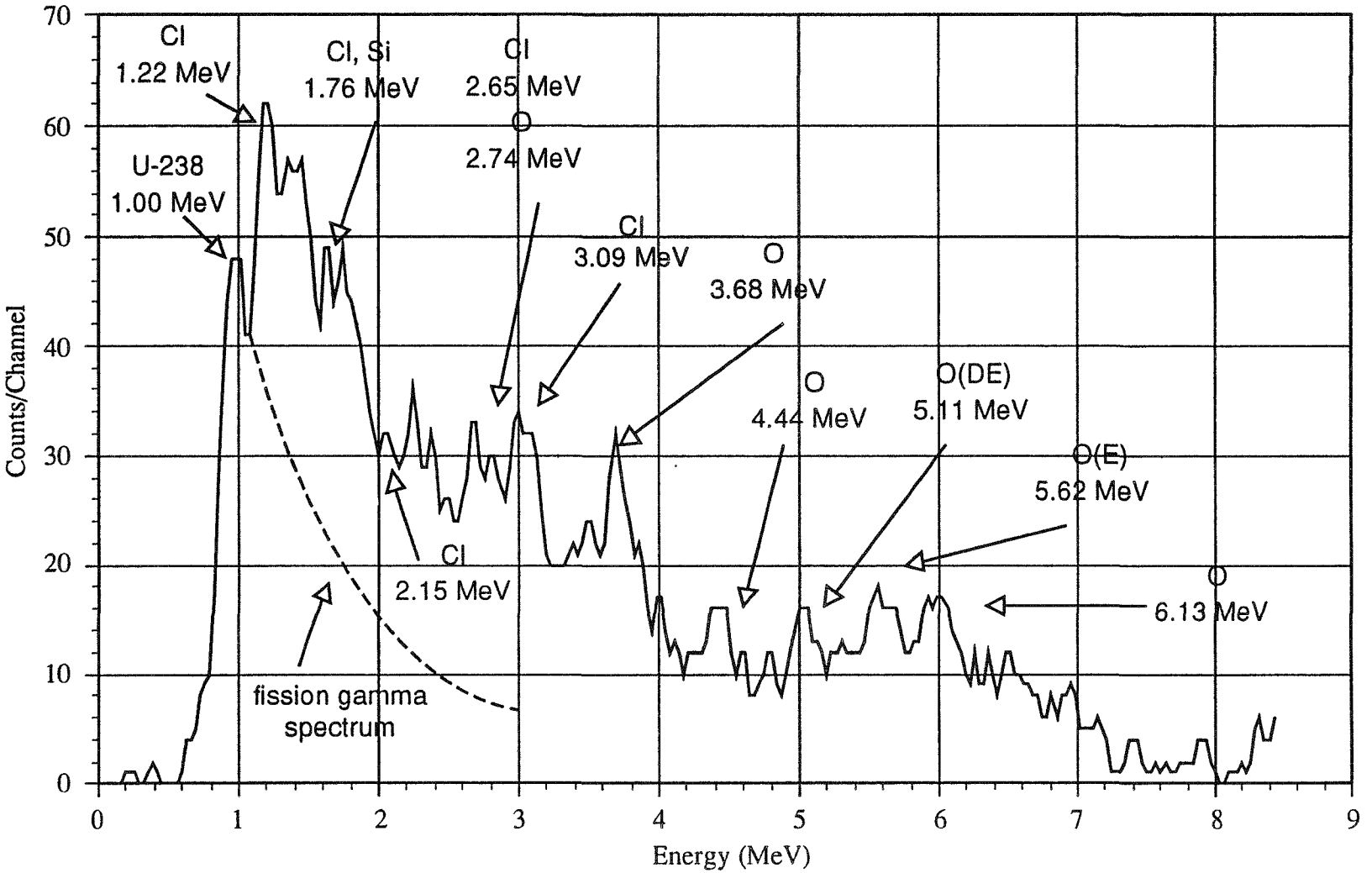

Figure 31. Chlorine and depleted uranium in concrete sludge section of ANL radwaste calibration drum.
EGRIS energy spectrum for flight-time channels 60-93

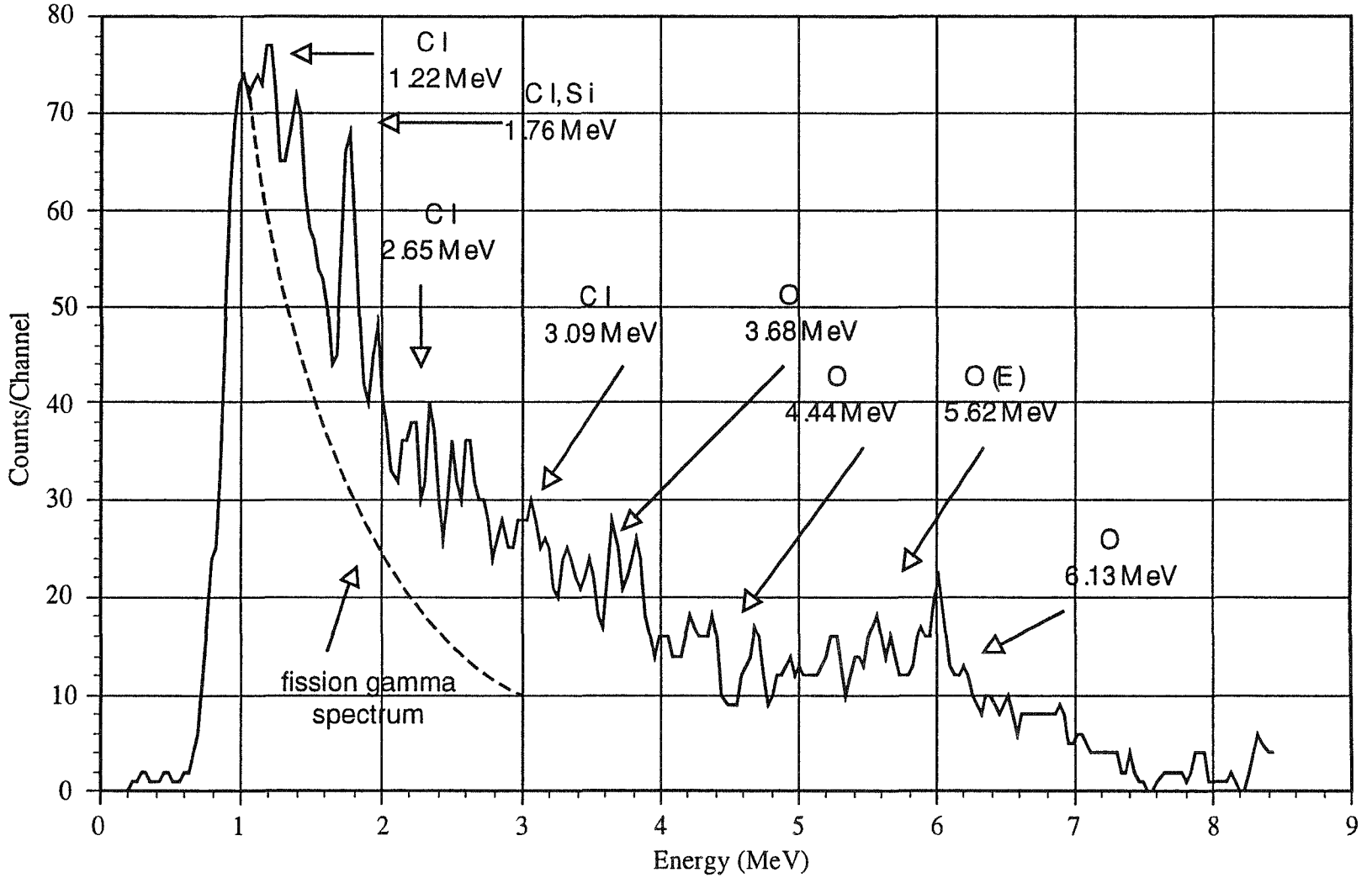

Figure 32. Chlorine and depleted uranium in concrete sludge section of ANL radwaste calibration drum. EGRIS energy spectrum for flight-time channels 93-119

4.5.2 Passive Gamma-ray Measurements at INEL

As noted above, the preparatory laboratory experiments were performed at ANL using the C-11 replacement APSTNG neutron tube and the repaired HV control circuit. This control circuit malfunctioned again just before the scheduled shipment to INEL. There was just time for the HV control circuit to be repaired again and shipped directly to RWMC. After re-assembly of the system at RWMC, the C-11 was found to be inoperative. However, the passive gamma-ray measurements of actual radwaste drums in the work schedule were performed, as planned, in the TRUPACT building at RWMC. Data were collected in the PGRS mode from the large double-ended NaI detector using the Aptec MCA card in the PC. Results of these spectral measurements are shown in Figs. 33-37, where signal runs are designated in black and background runs are designated in gray. All runs were 10 minutes long, except that the background run taken in the absence of radwaste sludge drums was only 100 s long.

Shown in Fig. 33 is the spectrum obtained from a single 1-g Pu-239 NAD source 30 cm in front of the center of the detector. The Pu-239 is easily identified by the 333-451 keV group of peaks, which overlap due to the NaI energy resolution. There are strong background components from Am-241 and K-40. Two measurements were performed with Pu-239 NAD sources inserted in the center of a source holder that was placed inside the center tube in sludge calibration drum #1 (content code 1). The front face of the detector was horizontal and 25 cm from the drum outer surface, centered vertically on the drum. Figure 34 shows the spectrum from 1 g of Pu-239 (a single NAD source) after subtraction of background. A sufficient Pu-239 signature is observed to show that 1 g of Pu-239 is detectable in the middle of the concrete sludge drum. Fig. 35 presents the spectrum measurement from 5 g of Pu-239 (5 NAD sources), in the middle of the concrete sludge drum. Background is included in Fig. 35 for comparison.

Four 55-gallon radioactive waste drums of the concrete sludge category were measured in the PGRS mode. We did not have available results of detailed RWMC measurements, and did not know which of these drums, if any, contained plutonium. Three drums were found to contain Pu-239 and one drum was found to contain U-238, the latter isotope identified by the gamma-ray lines from daughter products. None of the drums measured was found to contain both Pu-239 and U-238. The gamma-ray spectra for the drums containing Pu-239 differed significantly only in the intensity of the Pu-239 peaks.

Shown in Fig. 36 is the spectrum obtained for sludge drum #RF074404275 (content code 4, 293 kg). The Pu-239 peak group is quite evident, as are background peaks from Am-241, K-40, and either U-232 or Th-232. (The 2614 keV gamma ray comes primarily from Tl-208, which can be a daughter of either U-232 or Th-232. In this context, the parent isotope almost certainly is Th-232.) The dose rate for this drum was 1.1 mr/hr on contact, and the drum had to be set at 50 cm from the detector to avoid excessive detector deadtime counting losses. Otherwise the detector-drum geometry was the same as for the concrete sludge calibration drum #1 (content code 1) mentioned above. Shown in Fig. 37 is the PGRS spectrum obtained for sludge drum #RF74703133 (content code 7, 200 kg). The dose rate was 0.2 mr/hr on contact, and the drum was positioned 14.6 cm from the detector face. Clearly evident are the 766 and 1001 keV peaks from the Pa-234m daughter of U-238, as again are background peaks from Am-241, K-40, and Tl-208.

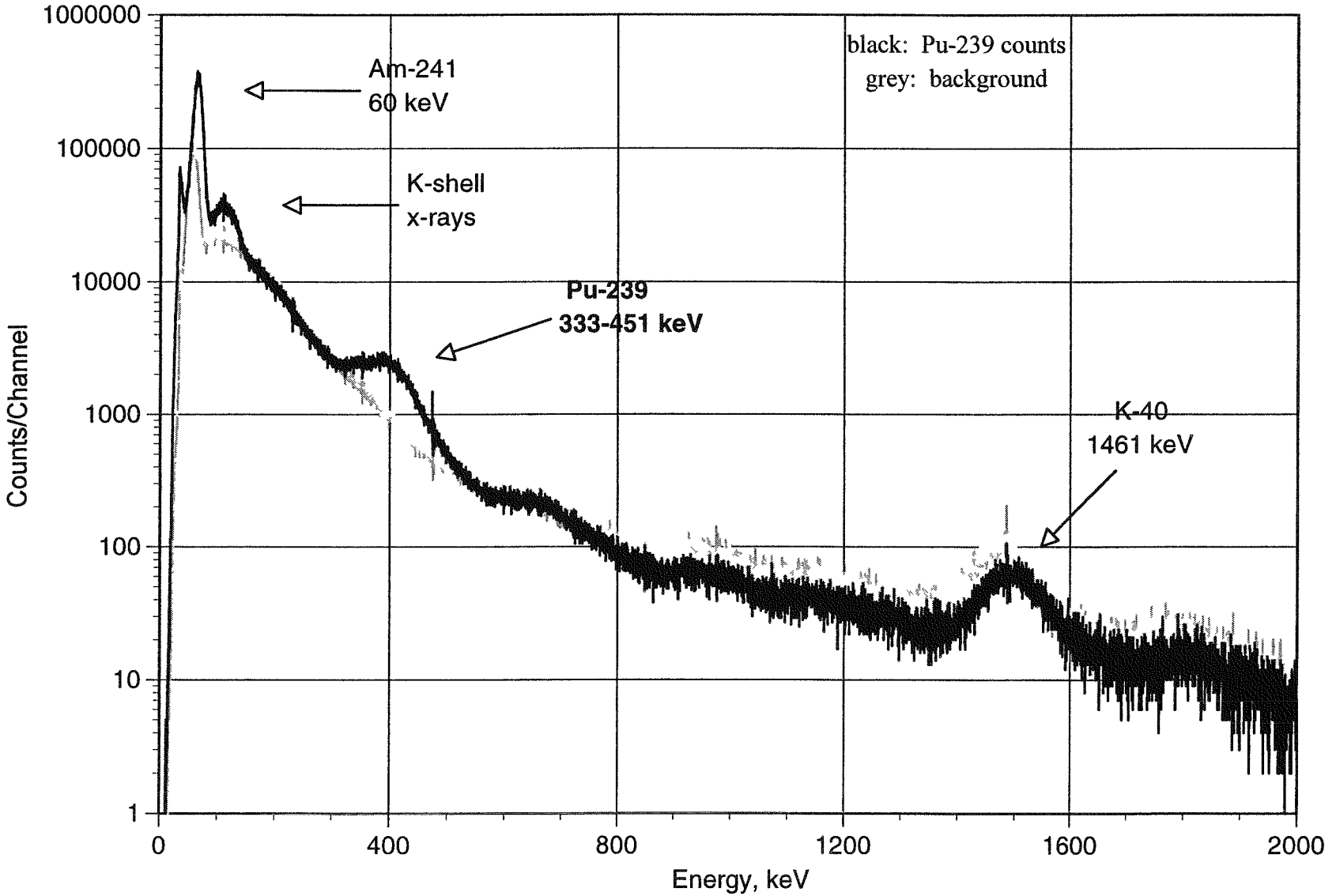

Figure 33 Passive gamma-ray spectrum for 1-g Pu-239 source

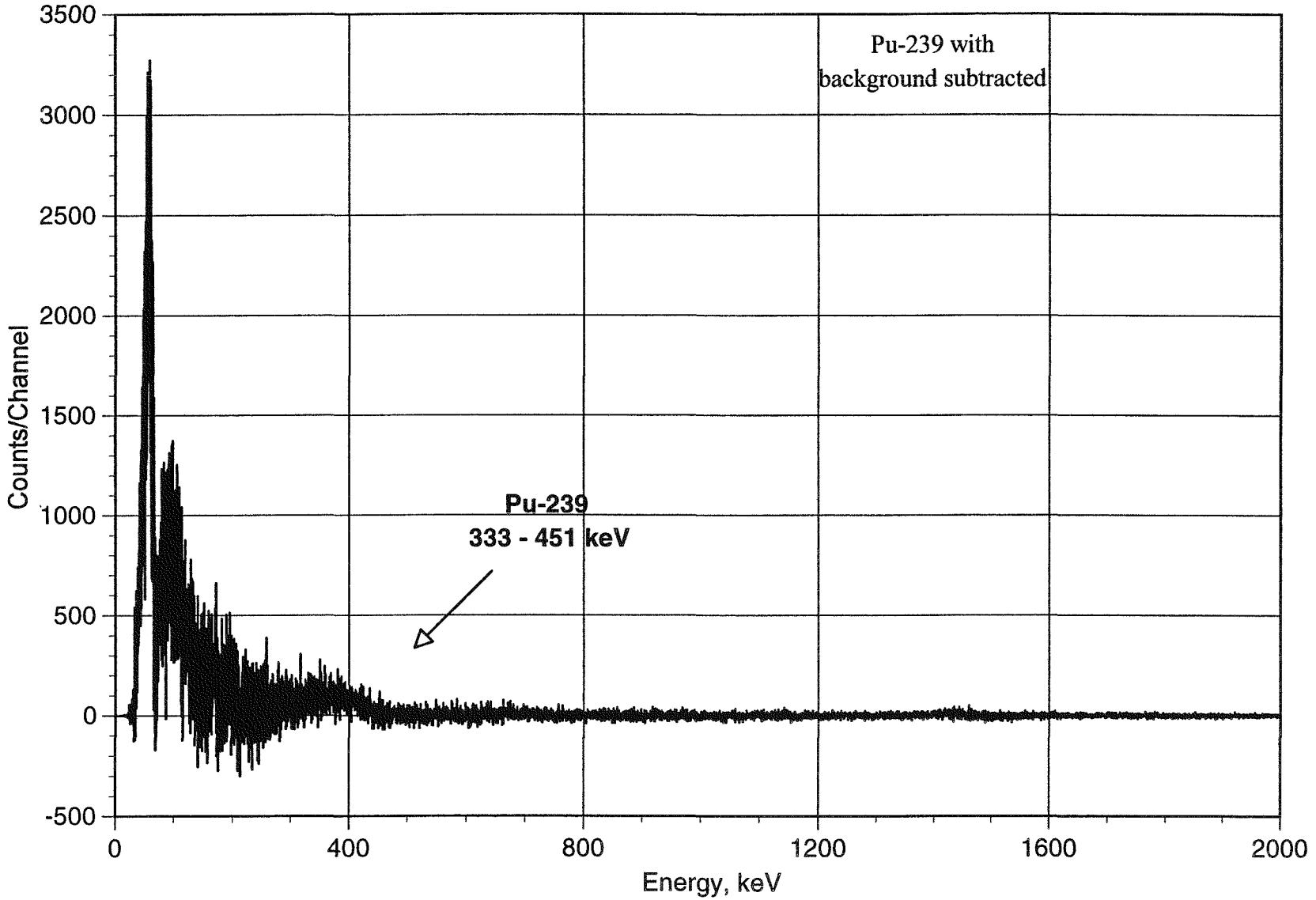

Figure 34. 1-g Pu-239 source inside RWMC sludge radwaste calibration drum

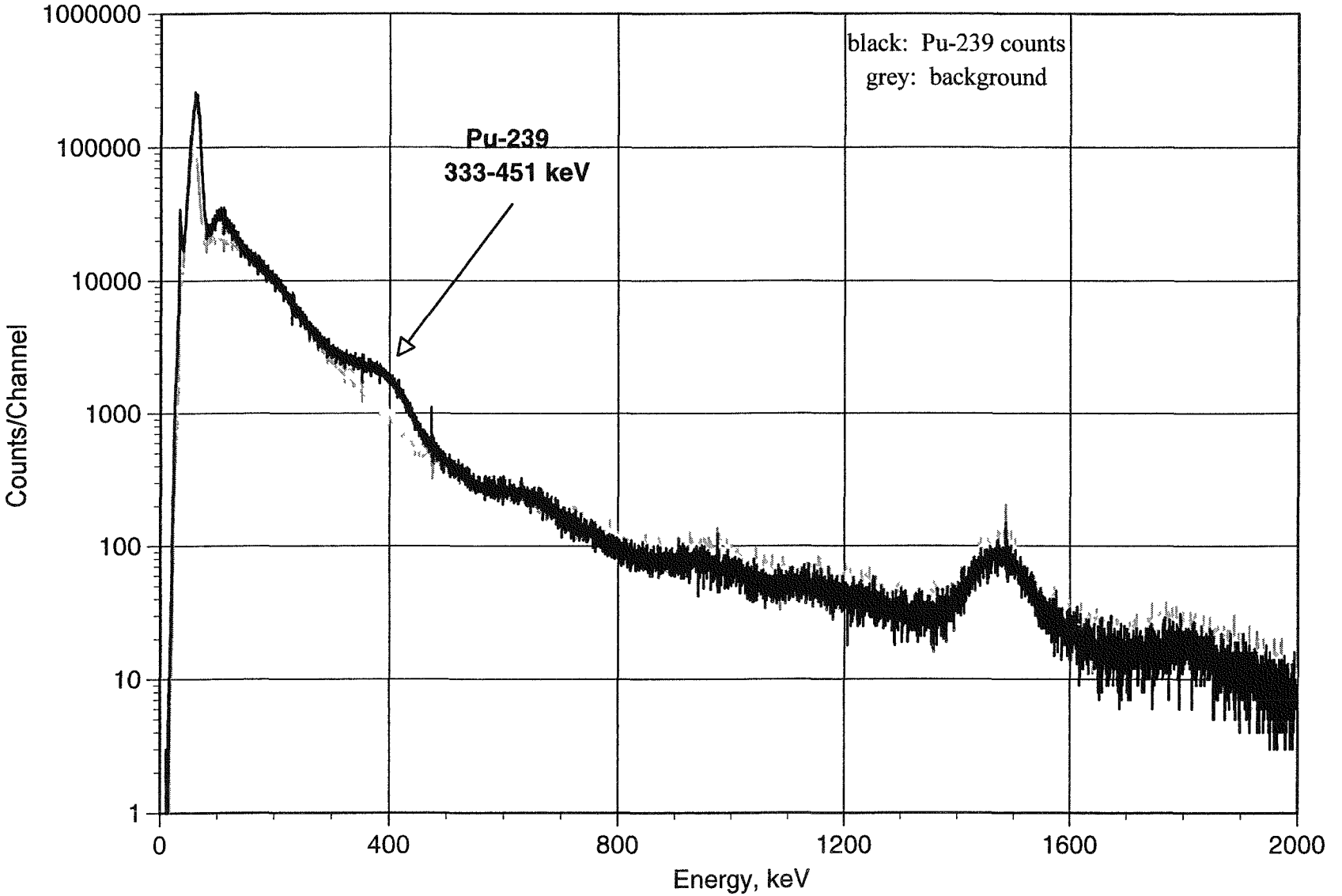

Figure 35. 5-g Pu-239 source inside RWMC sludge radwaste calibration drum

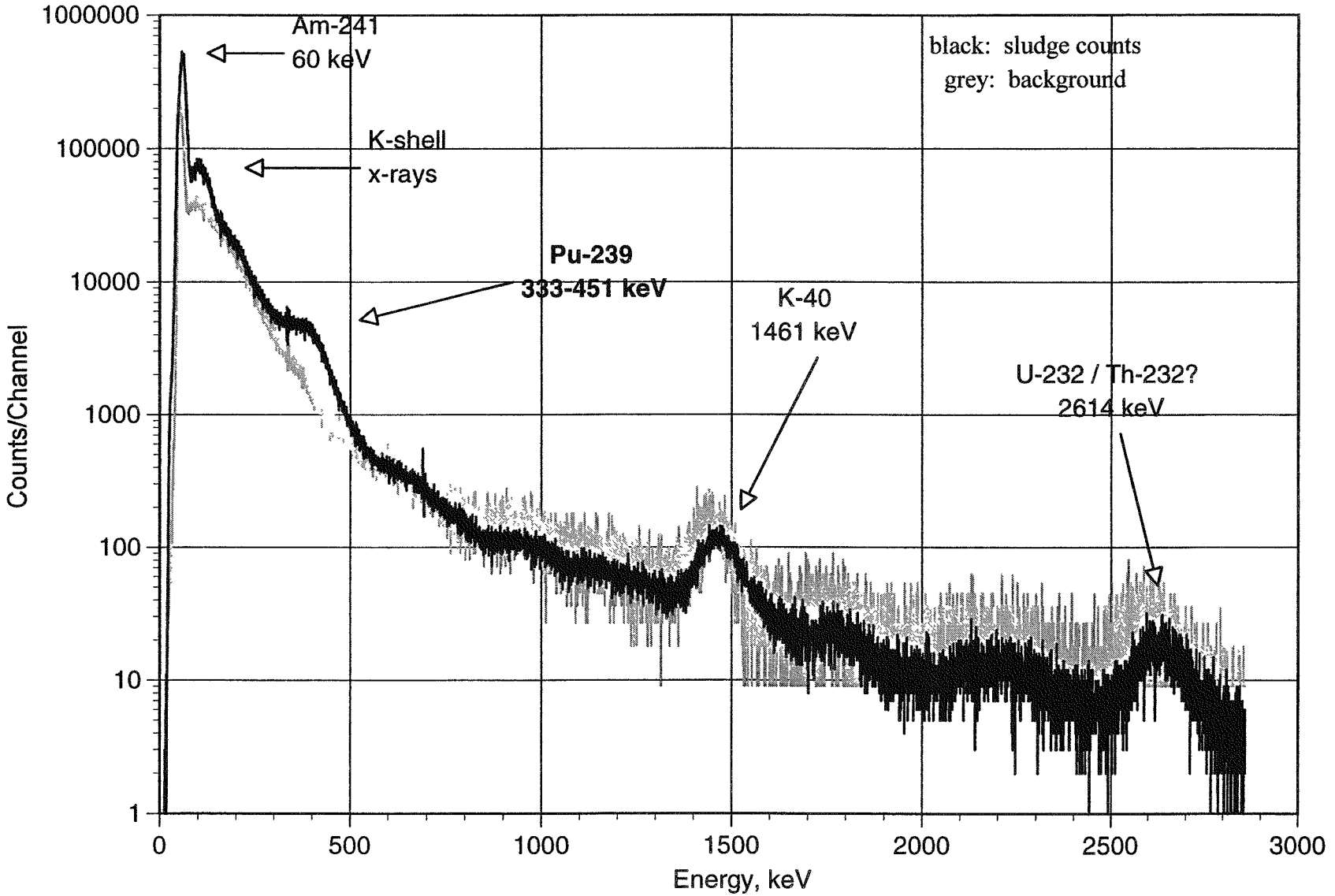

Figure 36. Passive gamma-ray spectrum of RWMC radwaste sludge drum RF074404275

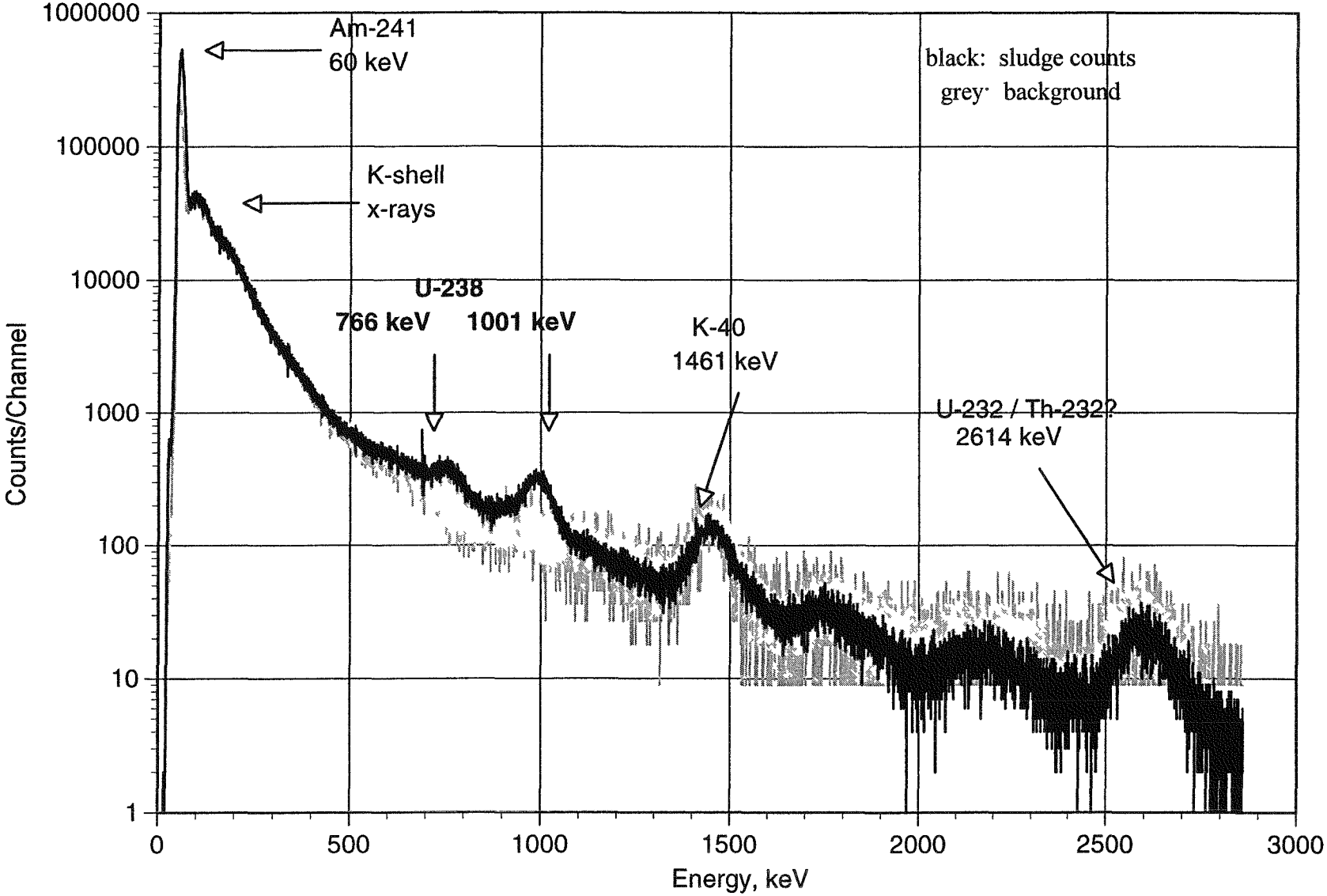

Figure 37 Passive gamma-ray spectrum of RWMC radwaste sludge drum RF74703133

No evidence of the prominent 186-keV gamma ray from U-235 decay was found in the spectrum for any of the drums measured. A very small U-235 peak, presumably from residual U-235 contained in the depleted uranium, has been seen in SWEPP radwaste drum spectra obtained with high-resolution HPGe detectors.[4]

5.0 DISCUSSION OF RESULTS AND APPLICATIONS

5.1 Operational Performance of APSTNG System

System reliability and neutron generator tube lifetime were identified initially as two key issues for this technology. The C-10 APSTNG tube performed in a reliable and stable fashion up to approximately 75% of its expected lifetime, and there is no reason to believe that it would not have continued to operate to its lifetime, if it had not been damaged by failure of the HV control system. Until the HV control system failed, this tube performed in a reliable and stable manner at output levels up to 2×10^7 n/s. Thus, we consider the basic technical feasibility of the APSTNG to have been confirmed. Our experience leads us to identify specific actions that should be taken to provide adequate HV control system reliability and protect the sealed tube against HV control system faults.

5.2 Design Recommendations

In addition to changes needed in the design of the HV control unit, there are design changes in other components that we feel will enhance the APSTNG capabilities:

1. The HV power supplies should be equipped with safety circuits to limit over-voltage and short-circuit current output. A remote cutoff switch is recommended. Also, we recommend that the ion source meter be made direct reading, and the potentiometer in the getter control circuit be more closely matched to the circuit, for better current control.

2. Because of concern over possible leaks of Fluorinert insulating fluid during transportation, the present tube assembly is disassembled and drained before shipping; and then it is reassembled, refilled and realigned before being used again. Although these steps are routine, they can increase both pre-shipment and post-shipment operations by up to an hour. More important, we would prefer to reduce the need to perform disassembly/reassembly operations. Thus, we recommend that the HV coupling components be redesigned so that disassembly, reassembly and realignment are not needed when the tube is transported. Also, we recommend design changes to aleviate concerns over the possibility of leakage of the Fluorinert.

3. We recommend changes in the alpha detector assembly, so that the electronics can be accessed without exposing the alpha scintillator to ambient light, and we recommend that the light seal design be modified to facilitate light-tight assembly. We also recommend a modification to allow easier changing of alpha window apertures, as needed for scanning and correlation cone mapping.

4. We recommend a more robust getter design, and provision of two getters inside each tube.

5. We recommend serious consideration of modifying the sealed tube design to provide higher output: it would be desirable to run at up to 10^7 n/s in many applications, so that a substantially longer lifetime than ~ 200 hours at 10^7 n/s is desirable.

6. We recommend serious consideration of incorporating a multipixel alpha detector (such as a microchannel plate) that provides two-dimensional position location data in the plane transverse to the correlation cone axis. This would greatly facilitate beam mapping, and would permit consideration of applications involving coarse three-dimensional imaging. Although not discussed in this report, a multipixel capability can increase the signal-to-background ratio for radiation from localized sources, in analogy with the use of time-of-flight sorting to exclude gamma-ray background from container walls.

With the above recommendations implemented, there is good reason to expect that the reliability and performance of APSTNG units in the field will be excellent.

5.3 Measurement Times

Another key issue identified at the beginning of this project was that of measurement times required to collect sufficient counts for detection and identification of objects. In general, the EGRIS signal count rate is proportional to: the number of neutrons per second emitted from the generator tube target, the target-to-object solid angle subtended by the object, the macroscopic neutron reaction cross-section of the object, the average number of gamma rays emitted in the reaction, object thickness along the correlation cone axis, inverse square of the object-to-detector distance, the total detector face area (over all gamma-ray detectors), and detector efficiency. Care must be exercised to assure that the operating conditions do not produce excessive accidental-coincidence background count rates. Although the source-to-object distance and object-to-detector distance depend on specific applications, the values for these distances used in our measurements are in a reasonable range. The source emission levels for the measurements shown herein were all well within the operational envelope of the APSTNG system.

Only one NaI scintillation detector was used in these measurements. It has a relatively large volume, and it exhibited satisfactory performance in the double-ended photomultiplier configuration. Measurement times for the data shown in this report ranged from 20 to 60 minutes. These measurement times could readily be cut, approximately inversely proportional to the number of additional detectors of this same type, to a few minutes.

5.4 Detection of Fissionable Materials

5.4.1 General Characteristics

The passive gamma-ray measurements reported in Section 4.5 indicate that Pu-239 and U-235 are easily identified by passive detection of gamma rays at 333-451 keV and 186 keV, respectively, in relatively unshielded applications. However, these gamma rays are much more highly attenuated by gamma-ray shielding than prompt fission gammas, of, say, 1 MeV and above: one cm of lead shielding would transmit unscattered approximately 46% of 1 MeV gamma rays, but would transmit only 10% of 400 keV gamma rays. Similarly, the 14-MeV

APSTNG probe neutrons penetrate borated plastic neutron shielding significantly more easily than the lower energy fission neutrons.

Based on the demonstrated APSTNG capability to distinguish fissionable materials by identifying the fission gamma-ray spectrum, ANL has considered a number of treaty verification and nonproliferation applications for an APSTNG system. Potential treaty verification roles include monitoring output streams of dismantlement facilities and inspecting cruise missiles declared to be conventionally armed for hidden nuclear warheads. Nonproliferation roles might include production facility monitoring for SNM control, IAEA monitoring of reactor facilities, fixed-portal SNM monitoring at ports of entry, and challenge inspections.

If the application requires discriminating between fissile SNM (such as Pu-239 or U-235) and U-238, a separate measurement can be performed in which moderating material is placed around the interrogated object and the APSTNG operated in the uncorrelated, UGRS mode. For detection of hidden neutron shielding that might be used for cloaking, it may be desirable to employ the APSTNG FNTI mode to determine when anomalously high attenuation of the neutron beam occurs.

Thus, the APSTNG technology should be given strong consideration in comparison with passive gamma detection, for applications in which the low-energy intrinsic gamma radiation from fissionable materials could be significantly attenuated. Further, the APSTNG's ability to detect a wide range of materials would be important for applications in which the possibility of hidden gamma-ray or neutron shielding could be an issue.

5.4.2 Illustrations of Application of the APSTNG Capabilities

We present brief descriptions of two potential applications of the APSTNG technology to illustrate its capabilities. We emphasize that the applicability of any specific technology to a specific inspection scenario depends strongly on the detailed inspection protocols, as well as the specific details of the inspection items, facility design, and facility layout.

5.4.2.1 Monitoring Warhead Dismantlement

We consider a generic operation in which a stream of nuclear weapons enters the dismantlement facility, and two streams exit: one of dismantled fissile components, and one of non-fissile items. The APSTNG would monitor (not assay) the input stream, and then inspect in the uncorrelated mode using inspector-provided moderator to enhance the response from U-235 and Pu-239, and discriminate against U-238. Concerns over hidden gamma-ray or neutron shielding would be addressed by analyzing the APSTNG gamma-ray data for presence of such materials. For example, a check for the presence of hydrogenous neutron shielding would be done by looking for correlated carbon inelastic scattering gamma-ray peaks plus uncorrelated hydrogen capture gammas. A more sensitive check for shielding materials is not necessary because of the relatively high transmission of the APSTNG neutrons and the gamma rays of interest. In fact, the protocol could specify checks for gamma rays from high explosive inside the weapon. The APSTNG could be equipped with coarse imaging capability, if specified under the protocol, to assure that the fissionable materials were, in fact, distributed in space in a declared-weapons-like geometry. Details of geometry would not be revealed, because of the

coarse three-dimensional resolution, and scattering of the source neutrons and reaction gamma rays.

The two streams of output items would be monitored by the APSTNG in similar fashion. Particular concerns for output streams include checking for hidden moderator around special nuclear material items in the fissile stream to enhance the response in order to hide the diversion of fissile material from this stream. This concern is coupled with checking the containers in the non-fissionable stream for the presence of hidden shielding placed to cloak diverted fissile material. The non-fissile stream would be checked in two steps for hidden fissile material to an agreed-upon sensitivity level, first using the EGRIS mode to check for the presence of uranium and plutonium, followed by inspection in the uncorrelated mode in conjunction with inspector-added moderator to enhance signals from Pu-239 or U-235, and to discriminate against U-238. The fissile containers would be checked for total amounts of fissile material to an agreed-upon sensitivity in a similar two-step process. The APSTNG could be equipped with coarse imaging capability, if specified under the protocol, to confirm declared changes in geometry from weapons-like configurations.

5.4.2.2 Checkpoint Monitoring for Smuggled Fissile Material

We consider a generic application in which a checkpoint inspection system is set up to monitor for undeclared fissile material. The APSTNG system is configured to inspect items simultaneously for unshielded U-235 and Pu-238 in a passive mode, and for the presence of shielding material in the EGRIS mode. An item that gives a positive response to the passive radiation inspection would be set aside for additional inspection, including high-resolution x-radiography, and APSTNG measurements to detect other materials. An item that gives a positive response for presence of shielding materials, but no passive measurement of gamma-ray signatures for U-235 or Pu-239 would be x-rayed and would be counted by the APSTNG for an extended period of time to compensate for extensive shielding.

The APSTNG system proposed for this application would employ an inspection volume with a radiation detector array on each of three sides. The reference inspection object is a closed cube 30 cm on a side. Each array would consist of 4 gamma-ray detectors, each of the present double-ended NaI type, with a total array active area of 40 cm × 40 cm. In order to avoid interference from neutron scattering, each array would be positioned 70 cm from the center of the interrogated object, and the neutron generator, running at ~ 10^8 n/s, would be placed 50 cm from the object center.

In a lightly shielded case (item surrounded by 1 cm Pb, sufficient to defeat passive detection of the 186-keV U-235 gamma), 750 g of Pu or U should be detected in the EGRIS mode within 30 seconds, or 15 g within 15 minutes. In a heavily shielded case (item surrounded by 5 cm Pb, sufficient to defeat passive gamma-ray detection of Pu-239 and U-235, plus 6 cm borated plastic, sufficient to cloak the material from active detection by a fission neutron source such as Cf-252, but insufficient to exclude 14-MeV neutrons), 750 g of Pu or U should be detected within 30 minutes. Conventional high explosives would be detected by the proposed APSTNG system in less time than required for the Pu and U. So the APSTNG system could provide a rather complete characterization of the object without opening the package.

The measurement times estimated for the heavily shielded case, include allowances for the difficulty in distinguishing the continuous fission gamma-ray spectrum from the accidental coincidence background and from spectra of other materials (see Sec. 4.2, particularly the last paragraph). We have not included potential improvements in sensitivity by optimizing analysis software and spectrum recognition algorithms, and by employing statistical criteria specific to types of interrogated objects expected. APSTNG hardware options to enhance fission signature recognition include use of coincident fission gamma-ray counts in the gamma detectors and use of neutron detectors in the ENIS mode (see Sec. 4.2, first two paragraphs).

The use of coincident fission gamma-ray counts to provide a more unique fission signature is based on the ~ 2.4 gamma rays emitted per fission in the EGRIS spectrum ROI, but it would result in a drastic reduction in the signal count rate and requires coincidence units to be procured and cabled between the gamma detectors in the array. The use of neutron detectors in the ENIS mode would require an array of large fast detectors capable of separating the neutron and gamma pulses and spectrum unfolding software to help distinguish fission neutrons from scattered APSTNG source neutrons. Source and/or detector collimation also might be needed. Additional study would probably be needed to determine whether either or both of these two hardware options would be appreciably more effective than detection of fission gammas by the standard EGRIS mode.

5.5 CW Munitions and Explosives Detection

ANL APSTNG experiments show that identifiable spectra can be obtained for the elements C, N, O, F, P, S, and Cl by inelastic scattering, and capture gamma rays can be observed for H, N, P, and Cl. These are the elements present in nerve and mustard CW agents. Indications are that an APSTNG system like that of the one used in this project would adequately discriminate CW and HE munitions. Measurements with CW surrogates having element compositions closer to the elemental ratios of real CW agents would be needed to clarify the ability of the NaI gamma-ray detector to identify specific CW agents loaded into steel shells. An HPGe detector has energy resolution more than sufficient to separate the gamma peaks, but it is more expensive, would have lower detection efficiency, and requires a supply of liquid nitrogen. Nevertheless, a supplemental HPGe detector might be useful to confirm identification, particularly if used with a stronger neutron source.

An APSTNG system has significant advantages over chemical sampling methods, including penetration through any intervening materials, no container opening (safe fast interrogation with minimal disruption), bulk quantification independent of sampling or leak rate, insensitivity to proprietary molecular bond information, and immediate analysis of results. Potential APSTNG on-site mobile and portal inspection roles include auditing inventory of chemical and munition storage facilities, checkpoint surveillance of transportation of CW agents and munitions, and monitoring CW agent-related chemical production. Shown in Fig. 38 is a schematic drawing depicting APSTNG identification and coarse imaging of CW munitions. This approach would make it possible to perform inspections on more than one item simultaneously; and thus would minimize the need to unpack and handle munitions.

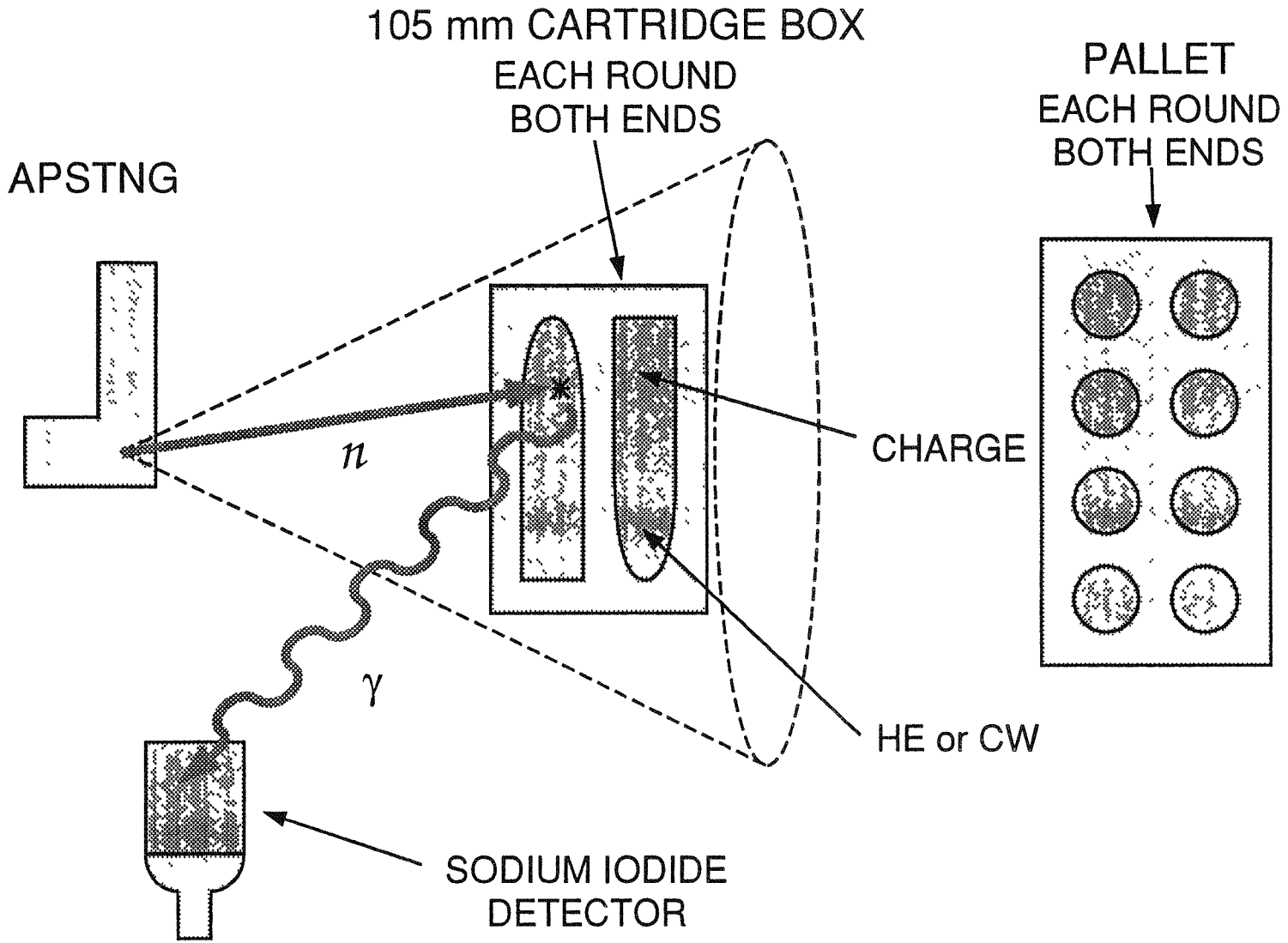

Figure 38. Identification and imaging of CW munitions with APSTNG system

APSTNG technology has considerable potential for detection of contraband explosives in applications of potential interest, such as airport and embassy portal surveillance of hand-carried luggage and shipments, and the detection of explosives concealed behind walls, beneath floors, above ceilings, and inside vehicles. The interrogation equipment could be located in panels, or walls and ceilings around portals, or even under shallow roadbeds. Appendix A (Ref. 1) predicts the capability of a APSTNG system to detect contraband for some simple cases, based on data from laboratory experiments. The APSTNG system model used for these calculations had a multipixel alpha detector and six large NaI detectors, in a configuration similar to that shown in Fig. 38. The detection algorithm used in these calculations utilized the density ratios of nitrogen to oxygen and carbon to nitrogen for various explosives and common materials. Computations indicated that short measurement times would be sufficient to distinguish drugs and explosives from other items. For example, a 4-second measurement would distinguish 1-kg C-4 explosive from materials common in luggage. See Appendix A.

For time-critical explosive surveillance applications, both false positives and false negatives must be considered, since the vast majority of objects inspected will not contain explosives but the consequences of one explosion can be large. This process can be facilitated by integrating complementary detection methods. For example, the APSTNG unit can be integrated with a dual-energy or tomographic x-ray unit. The x-ray data, which can distinguish relatively small density differences and provide fine spatial detail, is complementary to the APSTNG data, which provides relatively coarse spatial resolution but is highly specific to explosives materials. The x-ray data can be used to define suspicious volumes that might contain explosives or detonators. The APSTNG unit would interrogate only the suspicious volumes, which would reduce the measurement time required for positive identification.

5.6 Drug Detection

The ANL APSTNG experiments for the demonstration on detection of cocaine hidden inside a large liquid propane tank indicated that ~ 700 g of cocaine hydrochloride should be distinguished from propane within a few minutes measurement time by subtracting the EGRIS spectrum of the tank with cocaine from that of the tank with propane. The high-energy oxygen peaks provided the best cocaine identification, followed by chlorine and then nitrogen (all significant energy peaks were identified, and the carbon peaks approximately canceled out). For actual inspections, use of count rate ratios for specific elemental ratios (e.g., O/C, Cl/C, and N/C) probably is a better means of identification than subtraction of spectra obtained from a control configuration. The measurement time can be further shortened by using a gamma detector array or a stronger neutron source. In our measurements, the tank and propane were simulated by a steel cylinder and polyethylene, respectively, and rather accurate "nuclear" surrogates for cocaine and cocaine hydrochloride were developed for the measurements. These surrogates have the same element fractions as the real drugs and approximately the same density and consistency. The process used in making these surrogates can probably be applied to other drugs.

Calculations performed using the mapping technique discussed in the previous section[1], indicated that a 4-second measurement would be sufficient to obtain a possible identification of 1-kg cocaine hidden in fish.

A two-stage APSTNG-based inspection arrangement has been proposed for examination of large cargo containers for drugs, in which the first stage searches for "suspicious" cargo over the full container to identify cargo items for further inspection, and the second stage identifies contraband rather precisely for offloaded cargo. The proposed first stage is a gantry system of four EGRIS stations, each containing enough gamma detectors to cover a substantial cross-section of the container and each located at a different position along the drive path. The arrangement is designed to cover the full cross-section but to concentrate on the center, where sensitivity is generally worst. The proposed second stage is an EGRIS system similar to that shown in Fig. 38.

5.7 Waste Remediation

APSTNG radiation diagnostics are potentially useful for waste characterization, including active neutron interrogation that can detect plutonium and uranium even when heavily shielded, as well as nonradioactive toxic chemicals and water, and that can coarsely determine distribution of materials. Mixed waste and criticality issues can then be addressed. An APSTNG system probably would not require a separate passive radiation detection system. APSTNG technology was evaluated in detail by A. H. Aitken and C. W. Peters for bulk soil assay, barrel inspection, and decommissioning activities, with performance predictions based on calculations and laboratory experiment data.[5] Their report predicted favorable minimum detectable levels for radionuclides Cs-137, Co-60, Pu and U isotopes, and for elements Cl, Pb, Zn, As, Cr, Ni, Hg, and Cd.

For application to radioactive waste characterization, an APSTNG system must combine the capabilities of Sec. 5.3, detection of fissionable materials, and of Sec. 5.4, CW munitions and explosives detection, in the sense that the fission gamma-ray spectrum must be distinguished from the spectra of a range of elements, which must be individually identified. ANL data from radwaste benchmark experiments at RWMC and from preliminary laboratory measurements on the ANL radwaste calibration drum indicate that an APSTNG system similar to that shown in Fig. 38, should be able to detect uranium and plutonium and identify chlorinated chemicals and pockets of water inside 55-gallon radwaste drums within a few minutes measurement time. Identification of a wide range of toxic chemicals would require a supplemental large HPGe detector to obtain sufficient energy resolution.

5.8 Advanced APSTNG System

This project was completed by placement of a purchase order with a commercial firm, MF Physics, for procurement of a new higher-output longer-life welded metal-ceramic sealed-tube neutron generator and an improved control unit with HV supply. The specifications for this procurement reflected the lessons learned with the NDS APSTNG system during the course of this study project. These components will interface directly with the existing ANL single-pixel single-detector system (alpha detector, flight-time and detector electronics, gamma detector, and data acquisition system) to form a fully functional improved APSTNG system. This system will operate with either the large NaI detector used in this project or with a high-efficiency HPGe detector. This HPGe detector can be used in a high-resolution mode without flight-time (depth) discrimination, or it can be used in a low-resolution mode (256 energy channels) with flight-time discrimination.

MF Physics has substantial experience designing and fabricating complete neutron generator systems, including sealed tubes and one APSTNG system. Ceramic parts for the sealed tube are specified to pass drop tests to assure ruggedness. The tube is specified to contain two getters of an improved design, with one acting as a backup for the other.

MF Physics gives a warranty that the unit will provide a neutron output of 10^8 n/s without any target or ion source cooling, for a summed total operating time of at least 800 hours, and a maximum output of at least 10^9 n/s with externally supplied target water cooling (circulation of an externally supplied freon-like coolant around the ion source may also be required for 10^9 n/s). Thus, the maximum continuous output rate with no cooling is ~ 10 times that for the NDS APSTNG tubes used in this project, and the number of neutrons generated during the expected lifetime is 2.88×10^{14}, ~ 40 times that of life expectancy of the APSTNG tubes used in this project. This results in a life expectancy in excess of 8000-hour at the 10^7 n/s output rate adequate for most applications.

The alpha window scintillation material will be ZnO(Ga), which has a shorter emission duration than the ZnS of the C-10 and C-11 tubes, to accommodate higher neutron output.

The HV coupling unit for the new neutron tube will mate to a flange welded onto the accelerator tube with large machine screws, such that the coupling housing is the load bearing surface in a rigid mount. O-rings bear no structural loads and are used only for sealing in the pressurized SF_6 insulating gas. The coupling unit will have a pressure gage and a pressure switch that is cabled to the accelerator control unit to provide a low-pressure interlock and panel warning light. The accelerator HV cables and ion-source coolant pipes (if needed for neutron output exceeding 10^8 n/s) connect to the HV coupling unit housing, which also provides mounting surfaces for attaching a positioning system to orient the neutron correlation cone.

The new HV supply and control system will have circuits to limit output HV and current surges, and there will be a separate supply for each HV terminal. There will be a remote HV shutoff switch. The new control panel will have analog target, getter, and ion source current meters, instead of digital LCD meters.

5.9 Summary of Proposed APSTNG Applications

Table VI is a summary table of proposed APSTNG applications mentioned in this report. They have been grouped into six categories: Monitoring warhead dismantlement, monitoring at checkpoints for smuggled fissionable material, miscellaneous arms-control and nonproliferation, detecting contraband explosives, detecting illicit drugs, and waste remediation. These items are presented to illustrate the range of potential use of this technology, but Table VI is not intended to be a comprehensive list of specific, detailed applications.

Table VI. Summary of APSTNG Applications

As described in the text, APSTNG systems, operated in various modes, have the potential to be useful for the following purposes:

Monitoring warhead dismantlement

Input stream

- Assay the fissionable and fissile material
- Check for undeclared neutron and gamma-ray shielding
- Assay the chemical high explosive inside the incoming weapon
- Check that the configuration inside the weapon is acceptable

Fissionable output stream

- Check for moderator that might be there for concealment
- Assay fissionable material
- Assay fissile material
- Confirm declared changes in geometry

Nonfissionable output stream

- Check for hidden shielding
- Check for fissionable material
- Check for fissile material

Monitoring at checkpoints for smuggled fissionable material

Check for unshielded fissionable material
Check for shielding
Do extended counting of shielded items

Miscellaneous arms-control and nonproliferation

Inspect cruise missiles for undeclared warheads
Production control at SNM-producing facilities
IAEA use in monitoring reactor facilities
Fixed-portal monitoring of SNM at points of entry
Challenge inspections
Detect neutron shielding
Detect CW munitions
Detect HE munitions

Detecting contraband explosives

At airport and embassy portals
In hand-carried luggage
In vehicles
Behind walls; beneath floors; above ceilings

Detecting illicit drugs

Cocaine—concealed, for example, in propane tanks, luggage, or large cargo containers

Waste remediation

Characterizing waste by detecting

- Plutonium and uranium, even when heavily shielded
- Water
- Toxic, nonradioactive chemicals
- Coarse distribution of the above

6.0 ACKNOWLEDGEMENTS

The APSTNG project gratefully acknowledges the support extended to it by the U.S. Department of Energy, Office of Nonproliferation and National Security. It is a pleasure to recognize the guidance of M. F. O'Connell, Director of NN-21 On-site Systems, and discussions with K. Reinitz of NN-21. We also wish to acknowledge the continuing direction and support provided by ANL Arms Control and Nonproliferation Program Manager A. Travelli. Particular appreciation is due C. W. Peters, who developed the NDS APSTNG system and provided good advice. J. P. Regis provided valuable and timely operational support. We also thank A. B. Rothman for coordinating the Environmental Safety and Health reviews and the preparation of the surrogate materials. J. C. Demirgian prepared the CW simulants. D. Graczyk, K. Jensen, A. Essling, F. Smith, and I. Fox made and analyzed the cocaine Hcl surrogate. The visit to RWMC would not have been possible without the excellent cooperation extended by D. Akers, N. Kraft and their associates. G. S. Stanford provided valuable comments and assistance during the preparation of this report.

7.0 REFERENCES

1 E. Rhodes and C. W. Peters, "APSTNG: Neutron interrogation for Detection of Explosives and Drugs and Nuclear and CW Materials", Proc. Society of Photo-optical Instrumentation Engineers (SPIE), 1737, p. 160, 1992.

2. C. M. Gordon and C. W. Peters, "A Fast-neutron Probe for Tomography and Bulk Analysis", Int. J. Rad. Appl. Instr. Part A, 41 pp. 1111-1116, 1990.

3. C. W. Peters, private communication, September 15, 1989.

4. L. East, private communication.

5. A. H. Aitken and C. W. Peters, "Predicted Performance of Systems for Bulk Soil Assay Barrel Inspection and Decommissioning" DOE/CH-9210. Final Report, Contract No. 02112403, November 1991.

Appendices

APSTNG: Neutron Interrogation for Detection of Explosives and Drugs and Nuclear and CW Materials

E. Rhodes

Argonne National Laboratory, Reactor Engineering Division
9700 S. Cass Ave., Argonne, IL 60439

C. W. Peters

Nuclear Diagnostic Systems, Advanced Systems Division
PO Box 726, Springfield, VA 22150

Submitted to SPIE 1992 International Symposium on Optical Applied Science and Engineering 19-24 July 1992, San Diego, California, USA

Appendix A

APSTNG: neutron interrogation for detection of explosives and drugs and nuclear and CW materials*

E. Rhodes

Argonne National Laboratory, Reactor Engineering Division
9700 S. Cass Ave., Argonne, Illinois 60439

C. W. Peters

Nuclear Diagnostic Systems, Advanced Systems Division
PO Box 726, Springfield, Virginia 22150

ABSTRACT

A recently developed neutron diagnostic probe system has the potential to satisfy a significant number of van-mobile and fixed-portal requirements for nondestructive detection, including monitoring of contraband explosives, drugs, and weapon materials, and treaty verification of sealed munitions. The probe is based on a unique associated-particle sealed-tube neutron generator (APSTNG) that interrogates the object of interest with a low-intensity beam of 14-MeV neutrons generated from the deuterium-tritium reaction and that detects the alpha-particle associated with each neutron. Gamma-ray spectra of resulting neutron reactions identify nuclides associated with all major chemicals in explosives, drugs, and chemical warfare agents, as well as many pollutants and fissile and fertile special nuclear material. Flight times determined from detection times of the gamma-rays and alpha-particles yield a separate coarse tomographic image of each identified nuclide. The APSTNG also forms the basis for a compact fast-neutron transmission imaging system that can be used along with or instead of the emission imaging system. Proof-of-concept experiments have been performed under laboratory conditions for simulated nuclear and chemical warfare munitions and for explosives and drugs. The small and relatively inexpensive APSTNG exhibits high reliability and can be quickly replaced. Surveillance systems based on APSTNG technology can avoid the large physical size, high capital and operating expenses, and reliability problems associated with complex accelerators.

1. INTRODUCTION

Developments in hodoscope radiation detection and neutron diagnostic probe technologies offer some rather unique capabilities for a wide range of potential applications, including detection of explosives and drugs in aviation, customs, and physical security environments, arms control treaty verification, nonproliferation surveillance of SNM (special nuclear material) and CW (chemical warfare) agents, and remediation of radwaste and pollutants. In the hodoscope concept, an array of radiation detectors is used to image or detect objects inside opaque containers. Argonne interest stems from the fast-neutron hodoscope[1] in use at the Transient Reactor Test (TREAT) Facility for many years to image motion inside thick steel capsules of reactor fuel undergoing destructive testing that simulates hypothetical core-disruptive accidents.

Gamma-ray and neutron hodoscopes can be combined with a recently developed neutron diagnostic probe for a number of van-mobile and fixed-portal applications for NDA (nondestructive analysis). The probe is based on a unique associated-particle sealed-tube neutron generator (APSTNG) that interrogates the object of interest with a low-intensity beam of 14-MeV neutrons generated from the deuterium-tritium reaction and detects the alpha-

*Argonne National Laboratory is owned by the U. S. government and operated by the University of Chicago under the provisions of a contract with the Department of Energy. This work was performed partly under sponsorship of the U. S. Department of Energy Office of Arms Control and Office of Environmental Restoration and Waste Management as part of a research and development program and does not imply current or future policy decisions or technical preferences of any agency of the U. S. government.

particle associated with each neutron. Gamma-ray spectra of resulting neutron reactions identify nuclides associated with all major chemicals in explosives, drugs, and CW agents, as well as many pollutants and fissile and fertile SNM. Flight times determined from detection times of the gamma-rays and alpha-particles yield a separate low-resolution tomographic image of each nuclide identified in the time-correlated gamma-ray spectrum. By detecting only neutrons that have the proper flight-time to be uncollided, the APSTNG can also form the basis for a compact fast-neutron transmission imaging system with no collimator that can be used along with or instead of the emission imaging system.

2. APSTNG SYSTEM CHARACTERISTICS

The diagnostic probe which Argonne has recently been supporting was developed by the Advanced Systems Division of Nuclear Diagnostic Systems (NDS).[2,3] Its operation can be understood from Fig. 1. The object to be interrogated might be baggage or a TLI (Treaty Limited Item: item to be inspected under arms control treaty provisions), that could contain explosives or drugs or CW or fissile material. In the APSTNG, deuterons are accelerated into a tritium target, producing 14-MeV neutrons isotropically. Each neutron is accompanied by an associated alpha-particle travelling in the opposite direction. The gamma-ray and neutron detectors are time-gated by pulses from the alpha detector, forming a cone of flight-time-correlated neutrons through the object. Detector pulses are time-resolved by CFD's (constant-fraction discriminators). Flight times are determined by a TAC (time-to-amplitude converter), digitized by an ADC (analog-to-digital converter), and recorded.

When a reaction occurs in the object along the cone that results in a detected gamma-ray, the time-delay from the alpha pulse yields the position (depth) along the cone where the reaction occurred, since the source neutron and gamma-ray speeds are known (5 cm/ns and 30 cm/ns, respectively). By scanning the alpha detector horizontally and vertically, or by using a two-dimensional (2D) position-sensitive multipixel alpha detector, transverse and depth coordinates of reaction sites can be mapped, providing three-dimensional (3D) emission imaging of reaction densities from measurements at a single orientation. In most applications, systems would probably include a 2D alpha detector, as well as an array of gamma-ray reaction detectors, so as to maximize information obtained from each interacting neutron and sufficiently minimize measurement time.

Figure 2 illustrates the electronics and information flow for a basic multipixel system containing a 2D position-sensitive alpha detector and one gamma-ray reaction detector. In Fig. 2, the vectors involved in the reaction location are "Rt", "Rd", and "Rs". The transverse "X" and "Y" coordinates of "Rt" are digitized and stored in the PC computer in list mode, along with "TOF" (time-of-flight = "t" - "T") and gamma-ray energy "Eg". Not shown in Fig. 2 is an alpha-gamma coincidence circuit that ensures the TAC receives only start pulses that are followed by stop pulses. The PC controls the experiment, calculates positions, and displays data and images. Software can be developed for specific applications that will allow the PC to perform intelligent data analysis and interact with the operator to determine which items are sufficiently suspect to require further examination.

2.1 Different operational modes

Fast-neutron inelastic scattering reactions in the object provide prompt gamma-ray spectra that can identify many nuclides. By choosing gamma lines of specific nuclides, a 3D image of each identifiable nuclide in the time-correlated spectrum can be mapped. By choosing appropriate nuclide intensity ratios, 3D images of compounds can be made (molecular bonds are not identified). The use of the time-correlated gamma-ray spectra is denoted the EGRIS (emissive gamma-ray imaging and spectroscopy) mode. Slow-neutron capture is not time-correlated with the alpha pulses, but provides nonimaging gamma-ray spectra that can aid nuclide identification. The use of non-correlated gamma-ray spectra is termed the CGRS (capture gamma-ray spectroscopy) mode; neutron moderation may be required to get sufficient intensity. (If fissionable materials are present, neutron reaction detectors may be used to detect emitted fission neutrons).

As shown in Fig. 1, by discarding detected neutrons not having the proper flight time to be uncollided, one can perform fast-neutron 2D transmission imaging without a collimator (by scanning, using a neutron detector hodoscope array, or using 2D neutron detectors), since scattered neutrons are removed by "electronic collimation". This is called the FNTI (fast-neutron transmission imaging) mode. By measuring at a sufficient number of views around 180 degrees, 3D tomography is feasible. Transmission imaging (FNTI) can be done along with or instead of emissive reaction-density imaging (EGRIS).

2.2 Sealed-tube neutron generator

The use of the associated-particle method in arms control treaty verification and contraband detection research and development is recent. However the application of this method to NDA for neutron inelastic scattering is not new, although it has been relatively undeveloped and confined to the laboratory because of the bulk, complexity, and reliability and maintenance problems of the accelerator equipment previously required. The replacement of the accelerator in this neutron diagnostic probe system by the sealed-tube APSTNG brings new flexibility to the method and allows it to become a tool for field use. The state-of-the-art APSTNG was developed by the Advanced Systems Division of NDS, after considerable experience.

As diagrammed in Fig. 3, a Penning ion source inside the APSTNG emits a continuous mixed beam of deuterium and tritium ions that is accelerated and focused on a small spot (~ 1 mm diameter) on the target, tritiating the target and producing neutrons and alpha particles. A getter controls the mixture of deuterium and tritium. The ions are accelerated by a high voltage of 95 kV and focused by a variable extraction voltage, nominally 15 kV. The ion beam current (~ 1 μA to get 10^6 n/s) is controlled by varying the getter heating current. All operating voltages and currents are furnished and monitored by a high-voltage control system. Internal pressure is ~ 10^{-9} Torr without getter heating and ~ 10^{-5} Torr under normal operating conditions. The single-pixel alpha detector consists of a ZnS screen inside the tube, with a photomultiplier outside interfaced to a window. (In the case of a multipixel 2D alpha detector, the photomultiplier can be replaced by a microchannel plate and resistive anode readout.) The tube contains 0.4 Ci tritium at low pressure compared to the atmosphere, and the tritium is contained in the getter when the tube is not operating. A 1.6 mm lead shield reduces operator exposure to x-rays from the ion source.

The operating history of each APSTNG made by NDS has been maintained and is available. Initial maximum output of a typical APSTNG is around 3×10^7 n/s, but the maximum output soon falls to about the level of 10^7 n/s, as the cathode target is sputtered away, and slowly decreases thereafter. An output of ~ 10^6 n/s can be maintained for ~ 2000 hours by increasing the ion current to compensate for sputtering. Eighteen ceramic tubes have been made, fourteen of which passed quality control tests (a 78% yield). Eleven of these tubes were put in operation (three are in stock), of which six are still operating. Three tubes failed in normal operation; two were failed by continuous operation at excessive voltage. For the nine tubes which were operated normally, the average lifetime output is 7.35×10^{12} neutrons, if end of life is defined as being reached when the maximum output becomes less than 10^6 n/s.

The design of the APSTNG differs substantially from the current well-logging neutron generator tubes, which cannot be used for associated-particle operation. The APSTNG is an inexpensive small sealed module with low-bulk support equipment. It has a long mean-time-between-failures (around 2000 hours at 10^6 n/s or 200 hours at 10^7 n/s), is easily replaced (allowing simple field operation), presents low radiation exposure, and the sealed-tube design prevents tritium contamination. APSTNG tubes are commercially available from NDS.

2.3 Proof of principle

A proof-of-principle experiment on gamma-ray emission reaction-density imaging was performed on an interrogation volume containing a carbon block and an aluminum block and plate. Shown in Fig. 4 are the

gamma-ray energy spectra for APSTNG neutron inelastic scattering in C and Al obtained from a relatively large NaI detector (in Fig. 4, "SE" and "DE" denote single and double escape peaks, respectively). By using a multi-pixel 2D alpha detector (containing a microchannel plate with resistive anode readout and analog position computer), transverse x and y coordinates of reaction locations in the carbon and aluminum objects along the correlation cone were simultaneously obtained. By mapping reaction locations from flight-time along the correlation cone (z, or depth, coordinate) for energy windows enclosing C and Al gamma lines, the objects were correctly identified and 3D-imaged, as shown in Fig. 5.

3. APSTNG APPLICATIONS

APSTNG technology has the capabilities for identification and 3D imaging of many individual nuclides and compounds, with flexible positioning of reaction detectors with respect to the neutron source (on the same side, perpendicular, or opposite side), as well as capability for fast-neutron transmission imaging. The source and emitted radiation are high-energy and penetrate highly absorbing objects. Proof-of-concept laboratory experiments have been successfully done for a number of applications: nuclear warhead detection, chemical ordnance identification, explosive detection and identification, contraband drug detection, uranium borehole logging, corrodent detection on steam-turbine blades, kerogen analysis of shale,[4] on-line assay of coals, and bulk soil remediation of radwaste and pollutants.[5]

3.1 Treaty verification roles

For the proof-of-concept experiment on nuclear warhead detection in the FNTI mode, a mockup was made consisting of two hollow Pb spheres (20 cm OD, 10 cm ID) separated by ~ 3 cm (simulating SNM) embedded in dry sand (simulating high explosive or propellant) in a 50-cm diameter container. Measurements were taken using a plastic neutron detector and a single-pixel APSTNG, with the alpha detector masked so the pixel diameter was ~ 2.5 cm at the mockup position. The experiment setup is shown in Fig. 6 (the detector is located far enough from the interrogated object that forward-peaked scattering is negligible). The resulting signal transmission given in Fig. 7 shows the Pb spheres, their hollow nature, and the sand. The transmission profile data is in good agreement with a simple convolution of the pixel diameter and the expected attenuated projection of the mockup from known cross-section data for 14-MeV neutrons, indicating that for a 2D detector or hodoscope array, image spatial resolution will be limited by spatial resolution of the neutron detection system, rather than by flight-time resolution. These experiments and other experiments on transmission through thick depleted-U blocks demonstrate high penetration yet adequate contrast, for treaty verification roles.

For the proof-of-concept experiment on nuclear warhead detection in the EGRIS mode, a mockup was made consisting of two 12.7 cm × 15.2 cm × 15.2 cm solid blocks of depleted U (simulating SNM) separated by 10.2 cm and surrounded on all sides by 15.2 cm NH_4HCO_3 (simulating conventional high explosive or propellant). Measurements were taken using an APSTNG containing a single-pixel alpha-particle detector and a 15.2 cm × 35.6 cm NaI gamma-ray detector. The experiment setup is shown in Fig. 8 for the case where the two blocks were aligned along the axis of the APSTNG correlated neutron beam. The overall energy spectrum shown in Fig. 9 was obtained. The energy bands shown were used to separately image uranium (fission gamma-ray spectrum) and ammonium bicarbonate (oxygen inelastic scattering lines) along the beam axis, leading to the results shown in Fig. 10. Although the signal amplitudes are smeared out by the finite system time resolution (caused primarily by the large NaI detector), the U blocks and ammonium bicarbonate regions are correctly identified. The signal from the block farthest from the APSTNG is readily apparent, despite substantial attenuation by the closest block and by the ammonium bicarbonate.

An investigation of chemical ordnance configurations, gamma-ray energies and cross-sections for neutron inelastic scattering, and element structure of CW agents and explosives indicates that the EGRIS mode should be capable of detecting and distinguishing nearly all CW agents, by using ratios of element gamma-line intensities.

For a very early version of an EGRIS system, measurements were taken of 155-mm shells filled to the proper levels with CW simulants. Resulting spectra (yielding oxygen, phosphorus, and sulfur peaks of various magnitudes) are shown in Figs. 11-13 for VX, GB, and mustard simulants, with shell spectrum subtracted. The spectra are different enough to be distinguished by eye, without quantitative analysis.

3.2 Detection of explosives and drugs

Based on data from APSTNG laboratory experiments on explosives and drugs, it is interesting to estimate the measurement times required for detection of contraband items in some simple idealized cases using a fielded APSTNG system, in this case, one having a multipixel alpha-particle detector and six relatively large NaI gamma-ray detectors. The laboratory data consists of EGRIS gamma-ray spectra for nitrogen, oxygen, and carbon, for specific amounts of explosives (C-4, PBX, Octol, Composition B, TNT, Pentolite, Dynamite, and Deta sheet), and for cocaine and heroin simulants. A spectrum for a typical explosive, such as C-4 shown in Fig. 14, exhibits a number of principal peaks (mostly from neutron inelastic scattering) characteristic of nitrogen, oxygen, and carbon, along with a number of escape peaks, with a number of peaks overlapping. (In Fig. 14, "SE" and "DE" refer to single and double escape peaks, respectively.)

By a judicious choice of energy windows and knowledge of the basic nitrogen, oxygen, and carbon spectra, a "detection" algorithm was obtained that correctly reproduces the density ratios of nitrogen to oxygen and carbon to oxygen for the explosives and for other materials that might be present. It was found that a plot of these ratios is useful for differentiating contraband drugs or explosives from ordinary items expected to be seen, such as Fig. 15. Materials that would normally appear in luggage or foodstuffs are separated from explosives (open squares) and cocaine.

The boxes shown in Fig. 15 represent count statistics for a 15-second measurement of 1 kg C-4 explosive, the larger box enveloping five standard deviations (5 sigma), the smaller box enveloping two standard deviations. (The C-4 is assumed to be located in one volume element, rather than being spread out in a sheet.) The C-4 is definitely identified as an explosive. In fact, even a 4-second measurement would distinguish the C-4 from items normally found in luggage, so if luggage is being examined, suspicion is indicated. In 480 seconds of measurement time, the C-4 would be differentiated from other common explosives.

In Fig. 16, boxes are drawn for two and five standard deviations of count statistics for a 2-second measurement of 1 kg of meat. With high probability, the meat is identified as a foodstuff rather than explosives or contraband, indicating a very low false alarm rate for monitoring foodstuffs. In Fig. 17, a two-standard-deviation box is shown for a 4-second measurement of 1 kg of cocaine in fish. (The cocaine is assumed to occupy only one volume element.) The item is identified as suspicious, since it is not just fish, and is thought probably to be cocaine, since it is not amphetamines (it could be plastic, but why would plastic appear in fish?).

These simple computations and the underlying laboratory data can be considered as comprising a feasibility study for the application of an APSTNG system to monitoring contraband explosives and drugs, but are of course no substitute for analysis of laboratory measurement of realistic mockups and actual field trials of prototype units. Attenuation effects, the complex arrangements of many diverse items that may appear in luggage, and deception attempts have not been considered. On the other hand, much more powerful detection algorithms that utilize material densities directly along with full spectral regression fitting, adaptive learning processes, and external information from other surveillance methods can be developed.

3.3 Use of different modes

For the most part, the proof-of-concept experiments have been conducted using only time-correlated, or imaging, reaction gamma-ray spectra (from neutron inelastic scattering for nearly all applications), in the EGRIS

mode. Analysis of the soil remediation experiments included the uncorrelated gamma-ray spectrum, called the CGRS mode. The FNTI mode has so far not been much used, but it may find use in the future for simultaneous mode measurements, to correct EGRIS images for neutron attenuation or for multimode image analysis, or in a separate system for imaging extended or highly absorbing objects.

The EGRIS mode is not very suitable for imaging extended objects much over a meter or so in all three dimensions or highly absorbing objects. For large objects, the double solid angle reduction (source-to-object and object-to-detector) substantially reduces signal count rate. For large objects, accidental counts become limiting, and the raw images exhibit amplitude reductions and increased fluctuations in regions where neutron or gamma-ray attenuation are significant.

In the FNTI mode, the signal is proportional to the source-to-detector solid angle alone. It may be feasible to combine FNTI hodoscope arrays with GRTI (gamma-ray transmission imaging) hodoscope arrays so as to obtain Z-sensitive images of large volumes, such as a truck or cargo container, by employing the differences in attenuation Z-dependence (tomographic imaging may be necessary to do this). In some applications, this combination of FNTI and GRTI may allow determination of suspicious regions inside the volume, with a low false alarm rate. Then a two-stage interrogation process could be applied, in which the suspicious region would be offloaded and examined using a separate system based on the EGRIS mode.

3.4 Complementary systems approach

It has been pointed out that more effective surveillance of explosives in the aviation security environment would result from integration of different types of sensors and detection methods in a sequential and/or logic arrangement.[6] Another option is to directly use complementary information to maximize detection probability while minimizing false-alarm rates and inspection times. For example, rather than using sequential measurement, which can tend to minimize false-alarm rates at the expense of lowered detection probability (or vice-versa), the actual integration of the data from a dual-energy or tomographic x-ray unit linked to an APSTNG system could be done. In a piece of luggage, a suspicious object imaged by x-rays would be probed for high-explosives by the APSTNG unit, substantially increasing the detection confidence of the combined system, while reducing the overall false-alarm rate.

The x-ray data, which can distinguish density differences and provide fine spatial detail, is complementary to the APSTNG data, which provides relatively coarse spatial resolution but is highly specific to explosives materials. The x-ray data can be used to define suspicious shapes and densities that might indicate explosives or detonators. This data would be passed on to the APSTNG unit, which would measure only the suspect volume, at the most advantageous orientation for detection as determined from the x-ray data. This would reduce the measurement time required by the APSTNG unit for positive identification. A computer would integrate the data from both systems for final determination. The complementary x-ray/APSTNG system could be fine-tuned for the desired high detection probability and low false-alarm rate. For the aviation security environment and other surveillance applications, the vast majority of objects interrogated will not contain items being screened for, so the occurrences of both false positives and false negatives should be minimized. The complementary systems approach is a means of accomplishing this goal.

4. CONCLUSIONS

The proof-of-concept experiments for nuclear warhead detection show a potential for high-confidence measurements in treaty verification applications for detection, counting, and dismantlement of nuclear weapons. The proof-of-concept experiments for CW agents indicate a means other than chemical sampling is available and should be effective for verification of these agents, a method that requires no opening of sealed containers, penetrates intervening materials, and is nonintrusive regarding sensitive molecular bond information. The treaty

verification instrumentation criteria of transportability, reliability, easy operation and maintenance, personnel safety, and relatively low cost, would be met in these applications. Intrusion can be limited by limiting allowed output, measurement time, or time, space, or energy resolution, or by encryption of data.

Combining hodoscope technology with APSTNG technology opens avenues to a wide range of applications, not only for treaty verification, but also for nonproliferation surveillance of weapon materials, detection of contraband drugs and explosives, and remediation of radwaste and pollutants. A feasibility study indicates strong potential for success in detecting contraband explosives and drugs with APSTNG technology. However much remains to be done before any applications can be fully realized. For each specific application, realistic laboratory mockup experiments, development of deception-resistant detection algorithms, and fabrication and field testing of prototypes will be required. For surveillance applications, the direct combination of an APSTNG system and a complementary detection system (such as a dual-energy or tomographic x-ray unit) would be advantageous for reducing occurrences of both false positives and false negatives.

There are some limitations in the EGRIS mode of the present APSTNG system that can be significant for many applications, even for interrogation of volumes that are not large. Presently attainable depth resolution is limited, for a small gamma-ray detector, to about 5 cm (because the system has an overall time resolution of ~ 1 ns and a 14-MeV neutron travels 5 cm in 1 ns), and measurement times can be lengthy to obtain sufficient gamma-ray counts from a single gamma-ray detector. The gamma-ray signal count rate is limited by reaction cross-sections, solid angles subtended by the alpha detector and gamma-ray detectors, gamma-ray detector efficiency, and neutron source strength, but usable source strength is limited by accidental counts and pileup.

A gamma-ray hodoscope detector array can be used to substantially increase the signal count rate to lower measurement times, when necessary. However, small detectors will have a small energy-peak efficiency for the high-energy gamma-rays detected, while large detectors of the standard form will degrade the time resolution (and thus the depth resolution) substantially. Detector configurations are being investigated that will substantially improve the signal count statistics, while retaining as much time and energy resolution as possible. One configuration being investigated is a long NaI detector with two photomultipliers, one at each end; encouraging results are being obtained by combining the timing and energy data from the two ends.

For most applications (including physical and aviation security), the usable neutron source strength is expected to be limited to the range of 10^6 to 10^7 n/s for the associated particle method, for which the present APSTNG tube has adequate output and lifetime. There may be some incentive to develop an APSTNG with higher output and longer lifetime for some applications, but the development will likely be difficult and uncertain. A faster, less expensive, and more certain development path is to increase the number of gamma-ray detectors. Even a large array of detectors can be made to be fairly compact and to operate reliably, with little maintenance required.[1] In this way, the present APSTNG, which exhibits high reliability and can be quickly replaced, can be used in many applications. Surveillance systems based on APSTNG technology can avoid the large physical size, high capital and operating expenses, and reliability problems associated with complex accelerators.

5. ACKNOWLEDGMENTS

The support and direction of M. F. O'Connell, Project Manager for the Office of Arms Control, U. S. Department of Energy are greatly appreciated. We acknowledge, with many thanks, the continuing cooperation and support of the NDS staff, A. H. Aitken, C. C. Blackmon, and C. J. Henderson. We also appreciate the continuing direction and support provided by Argonne Arms Control Program Manager A. Travelli and by A. DeVolpi and C. E. Dickerman.

6. REFERENCES

1. A. DeVolpi, C. L. Fink, G. E. Marsh, E. A. Rhodes, and G. S. Stanford, "Fast-Neutron Hodoscope at TREAT: Methods for Quantitative Determination of Fuel Dispersal", *Nucl. Tech.*, vol. 56, pp. 141-188, Jan. 1982.

2. C. M. Gordon and C. W. Peters, "A Fast-neutron Probe for Tomography and Bulk Analysis", *Int. J. Radiat. Appl. Instrum. Part A*, vol. 41, pp. 1111-1116, 1990.

3. C. M. Gordon and C. W. Peters, "A Fast-neutron Probe for Tomography and Bulk Analysis", *Trans. Amer. Nucl. Soc.*, vol. 56 (Suppl. 3), pp. 1-86, 1988.

4. C. M. Gordon and C. W. Peters, "Instrumental Assay of Kerogen in Shale Using Fast Neutrons", *Int. J. Radiat. Appl. Instrum. Part E*, vol. 2, pp. 123-128, 1988.

5. Mitchell D. Erickson, Jas. S. Devgun, Jeffry J. Brown, and Nicholas J. Beskid, "R&D Activities at DOE Applicable to Mixed Waste", submitted for publication in proceedings of the Hazardous Materials Conference/South (Atlanta, Georgia USA, October 2-4, 1991).

6. A. Fainberg, "Explosives Detection for Aviation Security", *Science*, vol. 255, pp. 1531-1537, 20 March 1992.

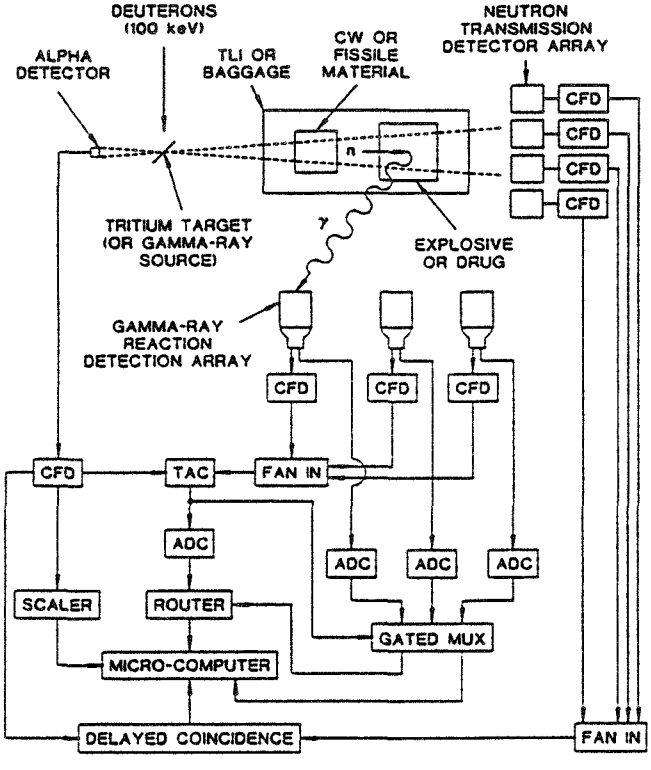

Fig. 1. Schematic layout of APSTNG-based interrogation system.

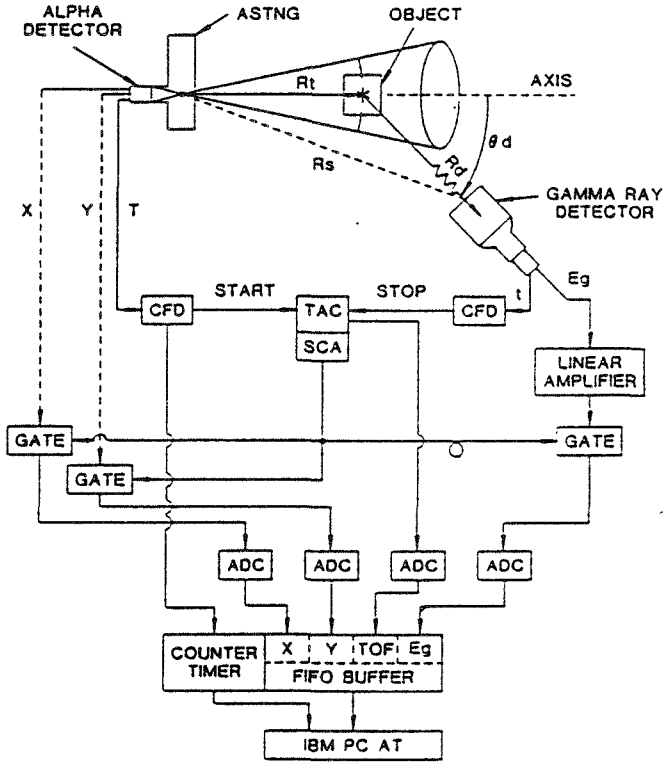

Fig. 2. Electronics and information flow for basic multipixel APSTNG-based system with 2D position-sensitive alpha-particle detector and one gamma-ray detector.

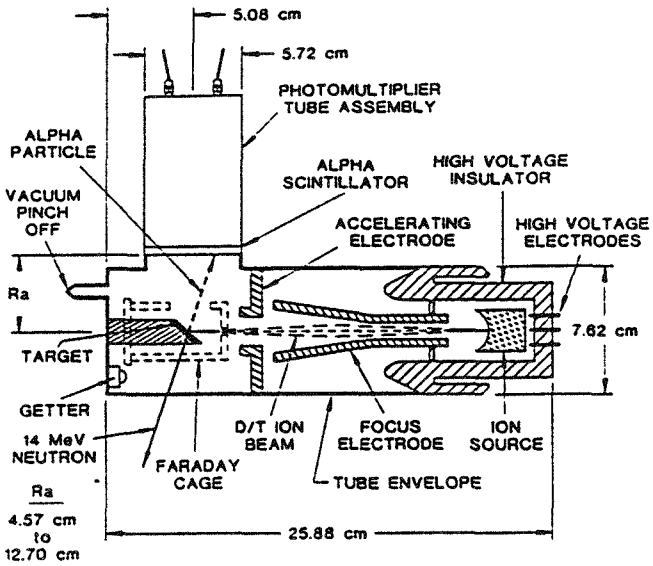

Fig. 3. Cross-section of interior of APSTNG tube.

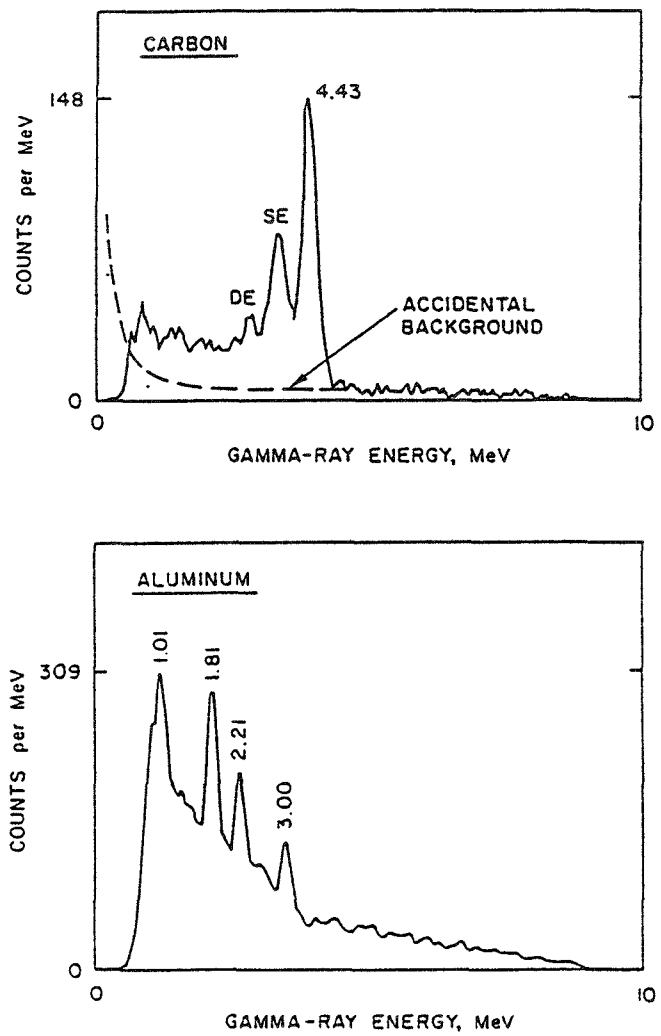

Fig. 4. EGRIS gamma-ray energy spectra of C and Al.

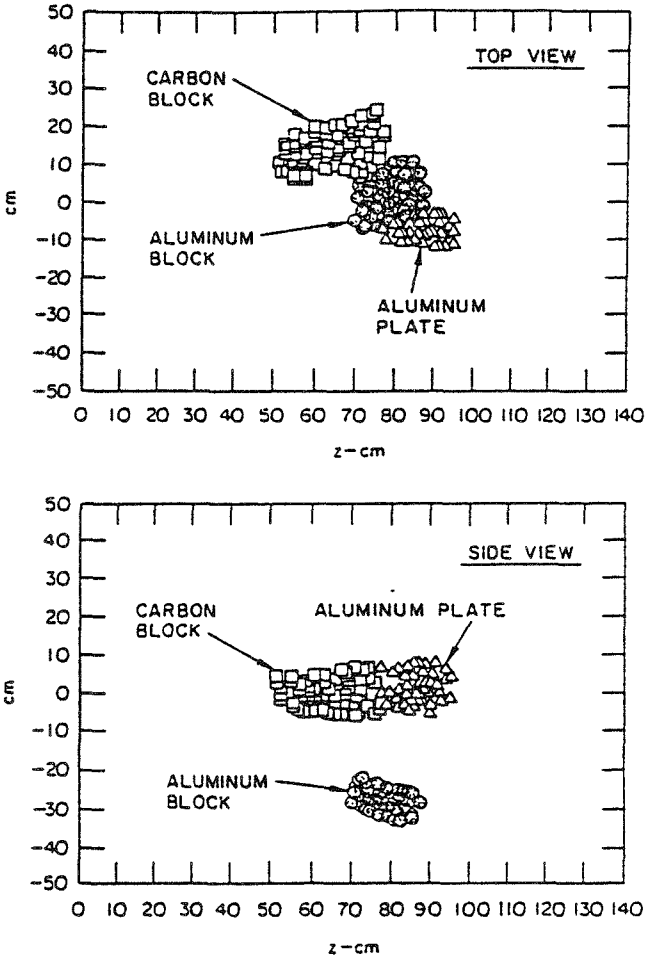

Fig. 5. Top and side views of 3D location of C and Al objects as mapped from EGRIS data. Points indicate mapped reaction locations.

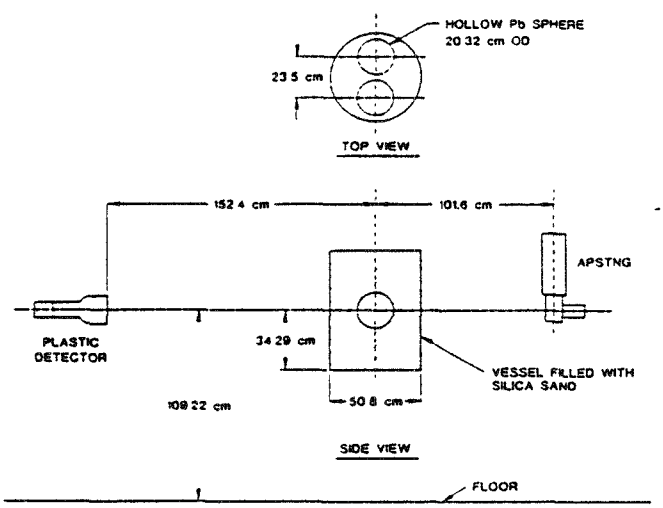

Fig. 6. Experiment setup for FNTI measurement of Pb spheres in sand, perpendicular to neutron beam.

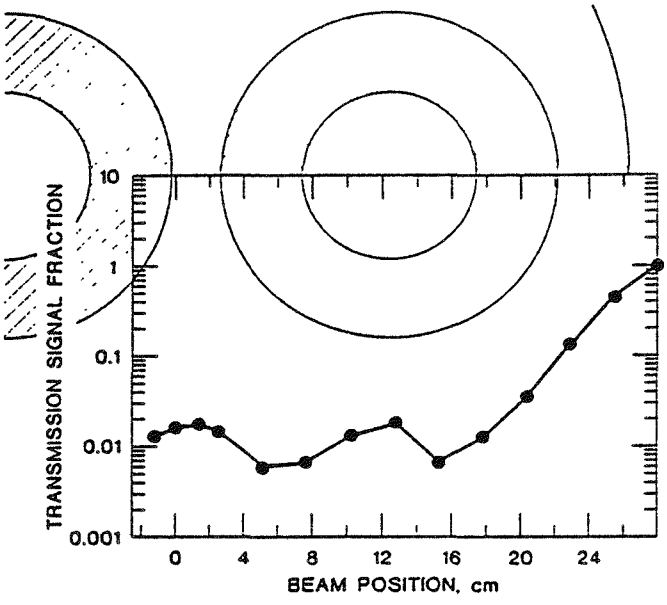

Fig. 7. FNTI signal transmission for hollow Pb spheres embedded in dry sand, perpendicular to neutron beam.

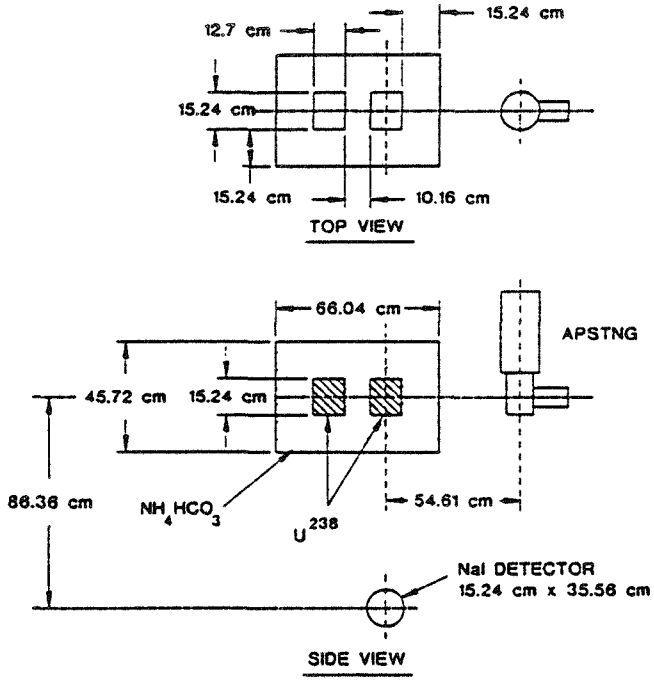

Fig. 8. Top and side views of experiment setup for EGRIS measurement of depleted-U blocks in ammonium bicarbonate, blocks aligned along correlated neutron beam.

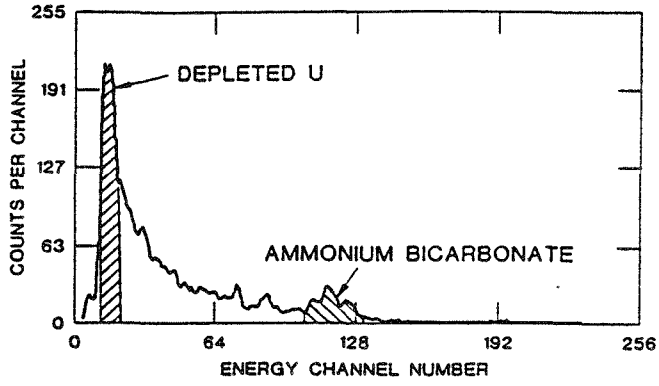

Fig. 9. Energy bands used for selection of EGRIS events primarily due to depleted-U and ammonium bicarbonate.

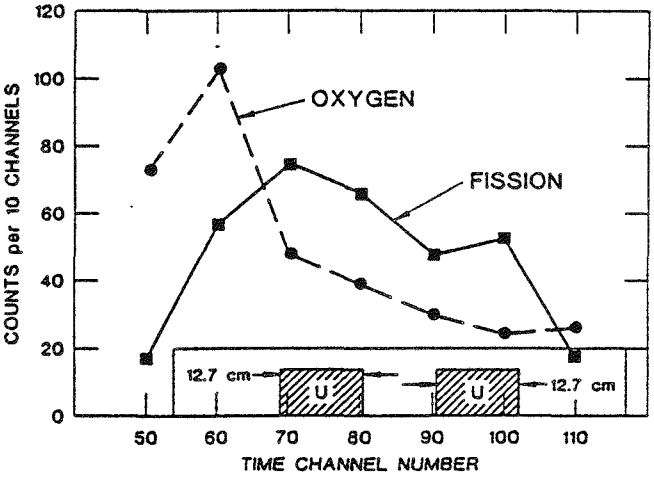

Fig. 10. EGRIS energy band signals for depleted-U and ammonium bicarbonate vs. flight time.

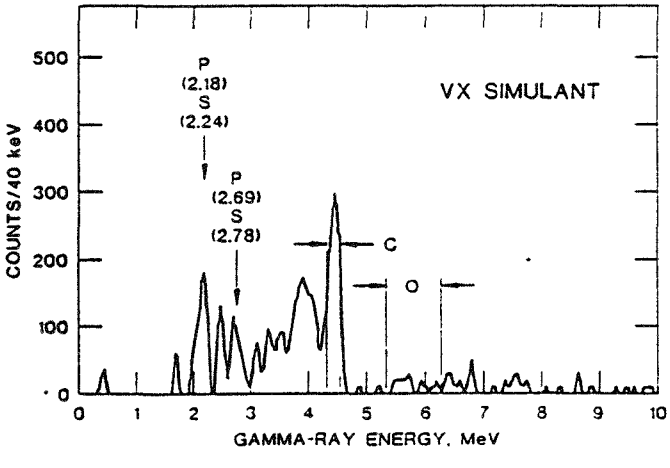

Fig. 11. Inelastic gamma-ray spectrum of 155-mm shell filled with bensulfide-xylene (54%) as VX simulant.

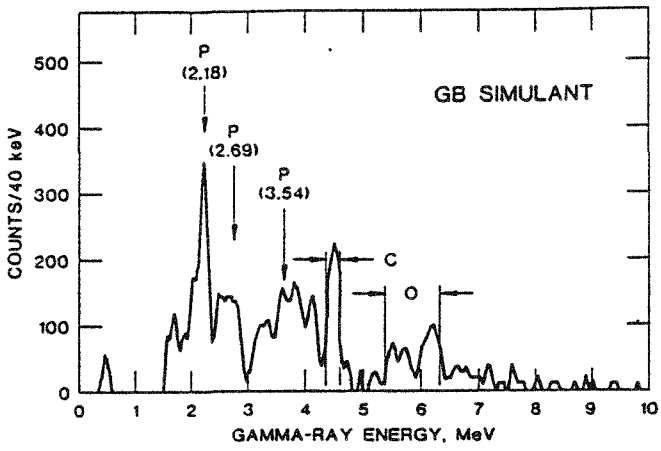

Fig. 12. Inelastic gamma-ray spectrum of 155-mm shell filled with dimethyl methyl phosphonate as GB simulant.

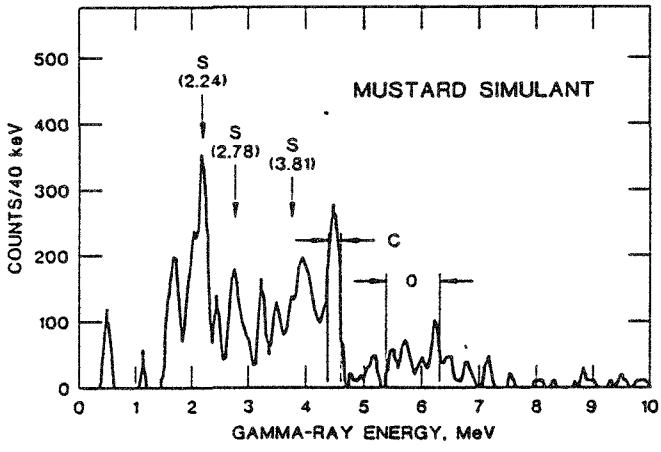

Fig. 13. Inelastic gamma-ray spectrum of 155-mm shell filled with thiodiglycol as mustard simulant.

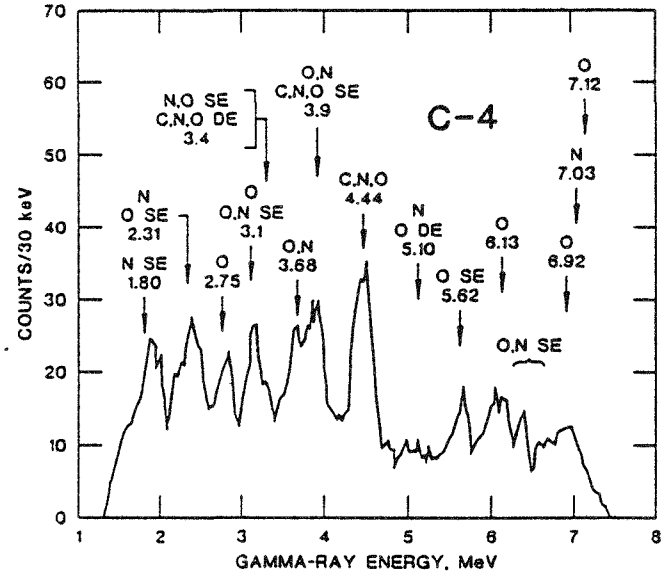

Fig. 14. EGRIS gamma-ray spectrum of C-4 explosive.

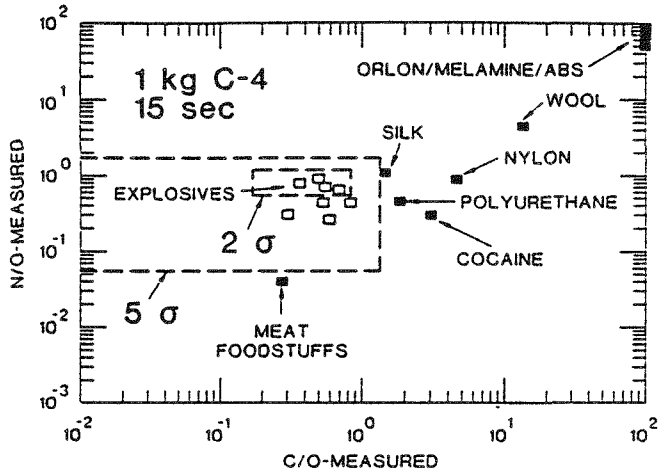

Fig. 15. N/O vs. C/O for 15-s measurement of 1 kg C-4. Large box envelops 5-σ statistics; small box envelops 2-σ.

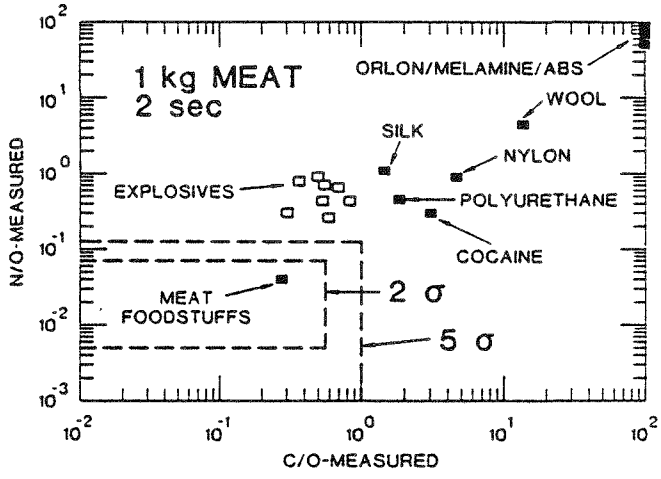

Fig. 16. N/O vs. C/O for 2-s measurement of 1 kg of meat. Large box envelops 5-σ statistics; small box envelops 2-σ.

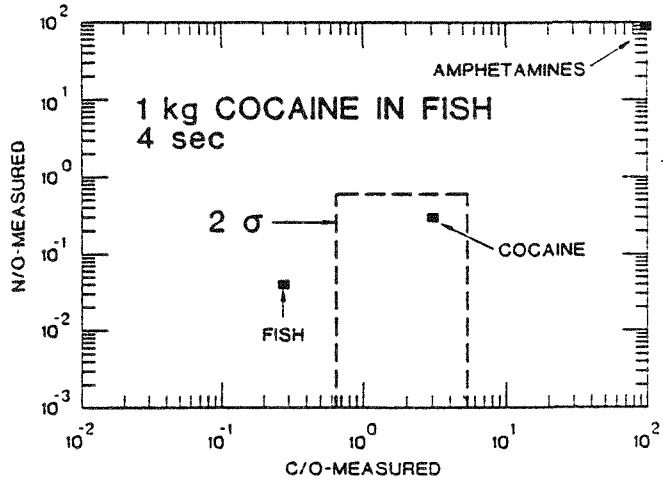

Fig. 17. APSTNG N/O vs. C/O for 4-s measurement of 1 kg of cocaine in fish. Box envelops 2-σ statistics.

Appendix B

ANL APSTNG Radwaste Calibration Drum

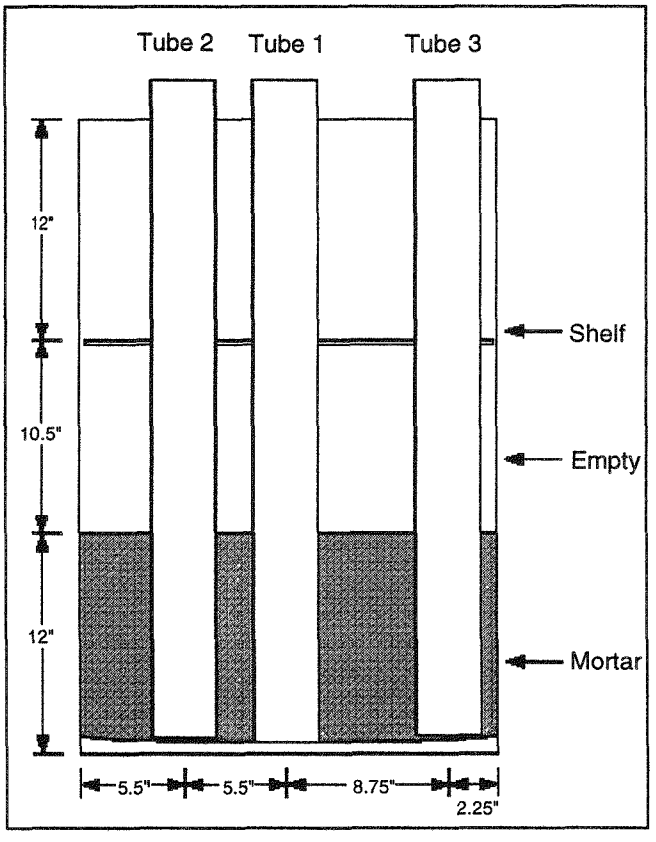

Fig. B1 APSTNG Calibration Drum Side View

The ANL APSTNG calibration drum was constructed in the spring of 1994 and was used in laboratory experiments at ANL in preparation for measurements on the SWEPP site at INEL. The 55 gallon drum used for the APSTNG calibration drum has on it these markings: UN/1A2/X400/S/94, USA//SDCC+AB0526, 1.5 MM, SDCC, 16 55 94, DOT 17C, STC. Figure B1 is the side view of this drum. The drum was divided into three axial parts to accommodate three simulations. The upper third of the drum simulates the SWEPP heterogeneous mixed metals calibration drum. There are various metal objects, all 10 inches tall, supported by a removable shelf as shown in Figure B2. This simulation replicates the positions of the mixed metals in the SWEPP drum, but is reduced in height to fit within the top third of the simulation drum. The middle third of the drum was left void to allow for any arrangement later required. The lower third of the drum was filled with approximately 100 kg of mortar to simulate a SWEPP concrete sludge calibration drum.

Appendix B

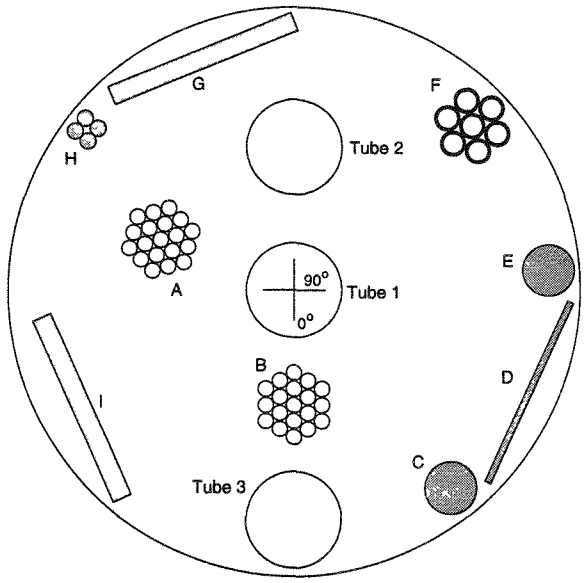

Fig. B2 APSTNG Calibration Drum Top View

Shelf - 22" diam, 1/4" thick. Three large holes, 3 11/16" in diameter. (Located in center, 5.5" from center, and 8 3/4" from center.) 4.045 kg total mass.

A. **Copper Tubing Bundle 1** - 19 tubes, .625" OD, .562" ID, 10" tall. 1.882 kg with clamps and brackets, 1.793 kg Cu only. (5.5", 249°).

B. **Copper Tubing Bundle 2** - 19 tubes, .625" OD, .562" ID, 10" tall. 1.884 kg with clamps and brackets, 1.795 kg Cu only. (4.5", 0°).

C. **Lead Cylinder** - 2" diameter, 10" tall. 5.630 kg with clamp and brackets, 5.585 kg Pb only. (9.75", 38°).

D. **Carbon Steel Plate** - 11/32" × 7 9/16" × 10". 3.606 kg with brackets, 3.579 kg Fe only. (9.9", 66°).

E. **Carbon Steel Cylinder** - 2" diameter, 10" tall. 4.056 kg with clamp and brackets, 4.011 kg Fe only. (9.75", 94°).

F. **Carbon Steel Pipe Bundle** - 7 pipes, 1" OD, .75" ID, 10" tall. 3.856 kg with clamps and brackets, 3.759 kg Fe only. (9.3", 133°).

G. **Aluminum Plate 1** - 3/4" × 7 5/8" × 10". 2.440 kg with brackets, 2.413 kg Al only. (9.6", 201°).

H. **Stainless Steel Rods** - 4 rods, 5/8" diameter, 10" tall. 1.677 kg with clamps and brackets, 1.580 kg stainless steel only. (10", 232°).

I. **Aluminum Plate 2** - 3/4" × 7 5/8" × 10". 2.462 kg with brackets, 2.435 kg Al only. (9.4", 299°).

The locations listed as polar coordinates, with the center of the shelf as the origin (distance to center of object, angle). The coordinates are only accurate to within a 1/2". The tubes, pipes, and rods are held together with two stainless steel hose clamps. Two 1" aluminum angles are attached to each object. These brackets hold the object on the shelf.

Appendix B

There are three aluminum tubes which run the length of the drum. These tubes are 84 mm i.d. The three aluminum tubes are of different lengths because the bottom of the drum is concave. The tube dimensions are listed below.

	Distance from Center	Outer Diameter	Inner Diameter	Length
Tube 1, Aluminum	0"	3.5"	3 3/8"	36"
Tube 2, Aluminum	5 1/2"	3.5"	3 3/8"	35 3/4"
Tube 3, Aluminum	8 3/4"	3.5"	3 3/8"	35 5/8"

The original SWEPP calibration drums have 40 mm i.d. tubes just large enough to hold inserts containing standard Nuclear Accident Dosimeter (NAD) sources. For ANL's research, it was beneficial to have the capability to accommodate larger inserts that could hold larger objects. These tube inserts were made by attaching two 1/8" x 7/8" x 30" strips of aluminum to two 1/8" x 7/8" x 3" strips to create a rectangular insert. Holes were drilled along the length of each strip every 1/2" which were then used to attach brackets to the aluminum strips. These brackets can hold a can, bottle, or other object in the tube. The position of the can or bottle is adjustable by moving the brackets up or down. At the top of each aluminum tube, notches were cut at an angular spacing of every 45°. This allows objects placed in the tubes to be located at specific angles with respect to the APSTNG neutron cone axis.

Distribution

Internal:

R. E. Boyar
L. W. Deitrich
C. E. Dickerman (10)
L. L. Gaines
R. G. Palm
J. P. Regis
T. Brunner (5)
A. Hess (5)
S. Tylinski (5)
E. A. Rhodes (10)
G. S. Stanford
A. Travelli
D. P. Weber
RE Experimental Physics Files: C
RE Files: 23672, A15
TIS Files

External:

DOE/OSTI (2)
ANL-E Library (2)
ANL-W Library
Manager, Chicago Operations Office, DOE
M. F. O'Connell, Office of Nonproliferation and National Security, U.S. Department of Energy, Washington, DC (10)
J. D. Cole, INEL
L. R. Franks, STL
D. M. Gordon, BNL
T. B. Gosnell, LLNL
R. B. James, SNL-L
M. W. Johnson, LANL
J. T. Mihalczo, ORNL
R. A. Warner, PNL
D. R. Waymire, SNL
W. G. Winn, SRTC